Synthesis of amphiphilic antimicrobial polymer-antibiotic conjugates and particle networks

Zur Erlangung des akademischen Grades eines

Dr. rer. nat.

von der Fakultät Bio- und Chemieingenieurwesen
der Technischen Universität Dortmund
genehmigte Dissertation

vorgelegt von

M. Sc. Alina Romanovska

aus

Nikopol, Ukraine

Tag der mündlichen Prüfung: 31.10.2023

1. Gutachter: Prof. Dr. Jörg C. Tiller
2. Gutachter: Prof. Dr. Markus Nett

Dortmund 2023

Danksagung

An dieser Stelle möchte ich mich herzlich bei allen bedanken, die zur Entstehung dieser Doktorarbeit beigetragen haben.

In erster Linie möchte ich mich bei Prof. Dr. Jörg C. Tiller, für die Möglichkeit an einem sehr interessanten Thema promovieren zu können, bedanken. Außerdem danke ich vielmals Prof. Dr. Markus Nett für die Übernahme des Zweitgutachtens und der fachlichen Beurteilung meiner Arbeit. Zu guter Letzt möchte ich mich auch bei den verbliebenen beiden Mitgliedern der Prüfungskommission Prof. Dr. Stephan Lütz und Prof. Dr. Oliver Kayser bedanken.

Für die didaktische, fachliche und persönliche Unterstützung möchte ich mich bei Dr. Frank Katzenberg bedanken. Herr Thorsten Moll danke ich für die technische Unterstützung im Labor und bei allen Chemikalienbestellungen. Vom Zentrum für Elektronenmikroskopie möchte ich mich herzlich bei Frau Monika Meuris und Herr Volker Brandt für deren analytische Unterstützung danken. Ich bedanke mich auch herzlich bei Frau Alexandra Riedel für die Hilfestellung bei bürokratischen Fragestellungen und die tollen Gespräche.

Von den ehemaligen Mitgliedern des Arbeitskreises möchte ich mich zu allererst bei Dr. Martin Schmidt bedanken. Durch ihn habe ich mein Interesse an der Polymerwissenschaft und Pharmazie entdeckt. Die tolle Arbeitsatmosphäre und eine hervorragende Zusammenarbeit war möglich dank: Dr. Christian Krumm, Dr. Montasser Hijazi, Dr. Marko Milovanovic, Lena Richter, Sascha Wilhelm, Dr. Dominik Segiet, Paola Benitez Rengifo, Robert Jerusalem, Michail Maricanov und Jonas Tophoven. Dank euch war ich steht’s motiviert und hatte immer sehr große Freund an meiner Arbeit und auch an unserer gemeinsamen Zeit.

Ich möchte natürlich auch allen Studierenden und zahlreichen Praktikanten danken, welche mich bei der praktischen Durchführung meiner Doktorarbeit unterstützt haben: Elif Cagri, Johanna Keil, Jonas Tophoven, Nicole Hugo, Elpida Pohlkötter, Kai Oset, Maeein Ahmed, Murat Furkan Oruc, Tristan Mairath, Sümeyra Gürbüz, Simon Schumann, Shaian Afshar, Rajeha Perinbarajah, Justus Reitz, Julian Hauda, Janick Weßelmann, Gonca Sevingen, Patronas Dimitrios-Paoulo, Daniel Luft, Armin Kamali und Andreas Rumpel. Euch in meinem Team gehabt zu haben, hat meine Doktorzeit sehr bereichert und ich hatte immer sehr großen Spaß an eurer Betreuung.

Danksagung

Zum Schluss möchte ich den wichtigsten Menschen in meinem Leben für ihre Unterstützung und Zuspruch in schwierigen Phasen meines Lebens Danken, meiner Mutter Liliya Ramonovska, meinem Bruder Ilija Vasylenko und meinem Partner Lucas Humburg sowie zahlreichen weiteren Mitgliedern die hier nicht explizit namentlich erwähnt wurden. Ich danke euch von Herzen, dass ihr immer an mich und meinen Weg geglaubt habt und mir immer zur Seite standet.

The present work was carried out in the period November 2018 to June 2023 under the supervision of Prof. Dr. Jörg C. Tiller at the Chair of Biomaterials and Polymer Sciences at the Faculty of Bio- and Chemical Engineering at the Technical University of Dortmund.

Publications

M. Schmidt, A. Romanovska, Y. Wolf, T.-D. Nguyen, A. Krupp, H. L. Tumbrink, J. Lategahn, J. Volmer, D. Rauh, S. Luetz, C. Krumm, J. C. Tiller; Insights into the Kinetics of the Resistance Formation of Bacteria against Ciprofloxacin Poly(2-methyl-2-oxazoline) Conjugates, *Bioconjugate Chem.*, **2018**, 29, 8.

A. Romanovska, J. Keil, J. Tophoven, M. F. Oruc, M. Schmidt, M. Breisch, C. Sengstock, D. Weidlich, D. Klostermeier, J. C. Tiller; Conjugates of Ciprofloxacin and Amphiphilic Block Copoly(2-alkyl-2-oxazolines)s Overcome Efflux Pumps and Are Active against CIP-Resistant Bacteria, *Mol. Pharmaceutics*, **2021**, 18, 3532−3543.

Presentations

A. Romanovska, M. Schmidt, C. Krumm, J. C. Tiller; Poly(2-oxazoline) Conjugates with Antibiotics, American Chemical Society, Orlando, Florida, USA, **April 2019**.

Abstract

In previous work by MARTIN SCHMIDT[1] in 2018, it was found that amphiphilic polymer systems based on poly(2-oxazolines) (POx) could be successfully conjugated to the antibiotic ciprofloxacin (CIP). These amphiphilic polymer-antibiotic conjugates (PACs) led to the enhanced activity of the antibiotic CIP. In this work, these amphiphilic PAHs were taken up and further investigated for their exact mode of action. Thus, the mode of action of the additional induced membrane activity by the amphiphilic polymer system on the activity of the antibiotic was investigated. A crucial factor is the dependence of the amphiphilic PACs on the hydrophobic/hydrophilic balance (HHG) of the POx tail.

Continuation of the mechanistic investigations led to the consideration of replacing the hydrophobic part of the amphiphilic poly(2-oxazoline) block copolymers with a biocompatible naturally occurring substance. In doing so, poly(2-methyl-2oxazoline) (PMOx) should remain as the hydrophobic moiety. The purpose of this consideration is to improve the biocompatibility of amphiphilic PACs and lower blood and cell toxicity.

Furthermore, also based on the results of MARTIN SCHMIDT[1], the reversible crosslinking of polymer-antibiotic conjugates with amphiphilic ABA triblock copolymers was investigated at the molecular level. It was already known that PACs based on hydrophilic and hydrophobic poly(2-oxazolines) form worm micelles that are very stable and strongly activate the conjugated antibiotic. Further, the exact interaction of the PACs with the ABA triblock copolymers should be investigated and explored to understand the exact background for the controlled and switchable antimicrobial effect of the antibiotic.

Zusammenfassung

In der vorhergehenden Arbeit von MARTIN SCHMIDT[1] im Jahr 2018 wurde festgestellt, dass amphiphile Polymersysteme basierend auf Poly(2-oxazolinen) (POx) erfolgreich mit dem Antibiotikum Ciprofloxacin (CIP) konjugiert werden konnten. Diese amphiphilen Polymer-Antibiotikum Konjugate (PAKs) haben zur erhöhten Aktivität des Antibiotikums CIP geführt. In dieser Arbeit wurden diese amphiphile PAKs aufgegriffen und weitergehend auf ihr genaues Wirkprinzip hin untersucht. Somit wurde die Wirkungsweise der zusätzlich induzierte Membranaktivität durch das amphiphile Polymersystem auf die Aktivität des Antibiotikums untersucht. Ein entscheidender Faktor ist die Abhängigkeit der amphiphilen PAKs von dem hydrophoben/hydrophilen Gleichgewicht (HHG) des POx-Schwanzes.

Die Fortsetzung der mechanistischen Untersuchungen führte zu der Überlegung, den hydrophoben Teil der amphiphilen Poly(2-oxazolin)-Blockcopolymere durch eine biokompatible natürlich vorkommende Substanz zu ersetzen. Dabei sollte Poly(2-methyl-2oxazolin) (PMOx) als hydrophobe Einheit bestehen bleiben. Zweck dieser Überlegung ist die Verbesserung der Biokompatibilität der amphiphilen PAKs und Erniedrigung der Blut- und Zelltoxizität.

Im Weiteren wurde ebenfalls basierend auf den Ergebnissen von MARTIN SCHMIDT[1] die reversible Vernetzung von Polymer-Antibiotikum Konjugaten mit amphiphilen ABA-Triblockcopolymeren auf molekularer Ebene untersucht. Es war bereits bekannt, dass PAKs auf der Basis von hydrophilen und hydrophoben Poly(2-oxazolinen) Wurm-Mizellen ausbilden, die sehr stabil sind und das konjugierte Antibiotikum stark aktivieren. Im Weiteren sollte das genaue Zusammenspiel der PAKs mit den ABA-Triblockcopolymeren untersucht und erforscht werden, um die genauen Hintergründe für die kontrollierte und schaltbare antimikrobielle Wirkung des Antibiotikums zu verstehen.

Romanovska, Alina:

Synthesis of amphiphilic antimicrobial polymer-antibiotic conjugates and particle networks:

Declaration (Affidavit)

I declare in lieu of oath that I have completed the present doctoral thesis with the following title independently and without any unauthorized assistance. I have not used any other sources or aids than the ones listed and have documented quotations and paraphrases as such. The thesis in its current or similar version has not been submitted to an auditing institution.
I declare in lieu of oath that I have not attempted to graduate in any doctoral procedure before.

Confirmation virtual reviewer/examiner

Hereby I confirm, that one member of the examination board is allowed to join the examination virtually using conferencing service like Zoom or Webex. This option particularly applies to external reviewers in accordance to the “Promotionsordnung of 2022” § 15 (5). The working group of the supervisor will deal with the technical details.

Recklinghausen, 06.07.2023

Declaration on the reproduction of previously published content

Parts of this work were previously published by the author of this thesis ([A]) and parts of this work were based on data which were obtained in bachelor and master theses performed at the Chair of Biomaterials and Polymer Science ([B]-[E]) under the supervision of the author.

This is a comprehensive list of the individual contributions to this work's chapters:

Chapter 4.1: in parts based on [A]

Chapter 4.1: in parts based on data from [B], [C], [D]

Chapter 4.3: in parts based on data from [E]

[A] A. Romanovska, J. Keil, J. Tophoven, M. F. Oruc, M. Schmidt, M. Breisch, C. Sengstock, D. Weidlich, D. Klostermeier, J. C. Tiller; Conjugates of Ciprofloxacin and Amphiphilic Block Copoly(2-alkyl-2-oxazolines)s Overcome Efflux Pumps and Are Active against CIP-Resistant Bacteria, *Mol. Pharmaceutics*, **2021**, 18, 3532−3543.

[B] Tophoven, J., Synthese und Charakterisierung amphiphiler Blockcopolymere, *Chair of Biomaterials and Polymer Science, TU Dortmund University*, **2019**.

[C] Oruc, M., F., Untersuchung der antimikrobiellen Wirkung von amphiphilen Blockcopolymeren, *Chair of Biomaterials and Polymer Science, TU Dortmund University*, **2019**.

[D] Keil, J., Synthese und Untersuchung des Seitenketteneinflusses amphiphiler Blockcopolymere auf deren antimikrobielle Wirkung, *Chair of Biomaterials and Polymer Science, TU Dortmund University*, **2020**.

[E] Tophoven, J., Synthese und Charakterisierung von Triblockcopolymeren zur kontrollierten Deaktivierung von Polymer-Antibiotika-Konjugaten, *Chair of Biomaterials and Polymer Science, TU Dortmund University*, **2022**.

List of Abbreviations and Symbols

AM/NR8383	rat alveolar macrophages
APCN	amphiphilic polymer connetwork
BA	butyl acrylate
Bidest.	Double distilled water
BMB	4-bromomethylbenzoyl bromide
BuOx	2-Butyl-2-oxazoline
CIP	Ciprofloxacin
CMC	critical micelle formation concentration
DBB	*Trans*-1,4-Dibromo-2-butene
DCM	Dichlormethane
DCX	*α,α'*-Dichloro-*p*-xylene
DDA	*N,N*-Dimethylaminododecan
DMAEAMC	2-(dimethylamino)ethyl acrylate methyl chloride
DNA	Deoxyribunucleic acid
DP	Degree of Polymerization
DTAC	Dodecyltrimethylammonium chloride
E. coli	*Escherichia coli*
EDA	1,2-Ethylendiamine
ESI-MS	Electrospray Ionisation Mass Spectrometry
EtOx	2-Ethyl-2-oxazoline
Fc	fragment crystallizable
Fd	Degree of functionalization
FDA	Food and Drug Administration
FT-IR	Fourier Transform Infrared Spectroscopy
GL	Gelatine

GMA	glycidyl methacrylate
GPC	Gel permeation chromatography
GTP	group transfer polymerization
HC_{50}	Hemocompatibility concentration 50
HeptOx	2-Heptyl-2-oxazoline
HexOx	2-Hexyl-2-oxazolin
HHB	hydrophobic/hydrophilic balance
HHR	hydrophilic and hydrophobic repeating units
hMSC	human mesenchymal stem cells
K. pneumoniae	*Klebsiella pneumoniae*
MALDI	Matrix-assisted Laser Desorption/Ionization
MIC	Minimal inhibitory concentration
MOx	2-Methyl-2-oxazoline
MRSA	Methicillin-resistant *Staphylococcus aureus*
NCS	Neocarzinostatin
NMR	Nuclear magnetic resonance
NonOx	2-Nonyl-2-oxazoline
OctOx	2-Octyl-2-oxazoline
P. aeruginosa	*Pseudomonas aeruginosa*
PAC	Polymer-Antibiotic Conjugate
PBuOx	Poly(2-butyl-2-oxazoline)
PDMS	Poly(dimethylsiloxane)
PEG	Poly(ethylene glycol)
PEtOx	Poly(2-ethyl-2-oxazoline)
PGLA	Poly(lactid-co-glycolid)
PHeptOx	Poly(2-heptyl-2-oxazoline)

PHexOx	Poly(2-hexyl-2-oxazoline)
PhOx	2-Phenyl-2-oxazoline
PHPMA	Poly(2-hydroxypropyl)methacrylamid
PIB	Poly(isobutylene)
PMMA	Poly(methyl methacrylate)
PMOx	Poly(2-methyl-2-oxazoline)
PNIPAM	Poly(N-isopropylacrylamide)
PNonOx	Poly(2-nonyl-2-oxazoline)
POctOx	Poly(2-octyl-2-oxazoline)
POx	Poly(2-oxazoline)
S. aureus	*Staphylococcus aureus*
SG	Satellite Group
SMA	Styrene maleic anhydride
SMZ	Sulfamethoxazole
TEA	Triethylamine
TEM	Transmission electron microscopy
TG100-115	6,7-Bis(3-hydroxyphenyl)pteridine-2,4-diamine
TLN	Triple-Layered Nanogel
TMP	Trimethoprim
TOF	time of flight
TU	Technical University
UCST	upper critical solution temperature
VitE	Vitamin E or *α*-tocopherol
VitE-BMB	vitamine E 4-(bromomethyl)benzoate
wt%	Percentage by weight
xCIP	*N*-(4-(Chloromethyl)benzyl-ciprofloxacin

Table of contents

1 Preface

Both humans and nature are surrounded by the oldest living creatures on earth, bacteria.[2-4] Of course, there are many harmless bacteria that have a positive effect on humans and their development. But in addition to these seemingly harmless bacteria, harmful pathogenic bacteria also exist.[5-6] Only the discovery of penicillin in 1929 by Alexander Fleming allowed to specifically and effectively stop bacterial infections.[7-8] After the first successful medications against bacterial diseases using penicillin or other antibiotics, the downside of this treatment method also became apparent, the development of resistant strains of bacteria.[9] For this reason, there are a large number of bacteria that are resistant to the effects of the antibiotics available on the market.[10] These may include multi-resistant bacteria, which are also potential triggers for hospital infections, such as methicillin-resistant *Staphylococcus aureus* (MRSA).[11] This is exactly where the problem lies, as fewer and fewer new antibiotics are being developed and approved for the market, yet the number of resistant strains of bacteria continues to rise (Figure 1).[12-13]

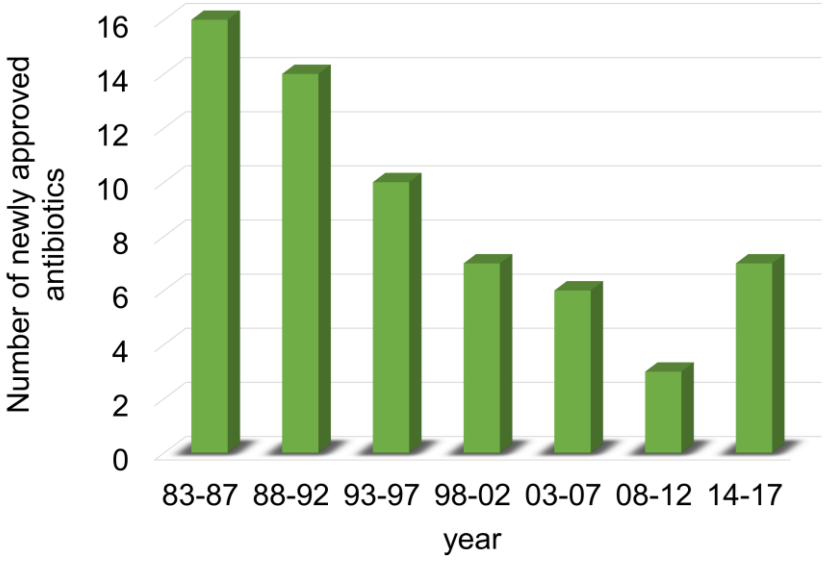

Figure 1: *Novel FDA-approved antibiotics by year.*[12]

The solution lies in developing new antibiotics or improving existing ones to avoid, at best, rapid development of resistance.[14]

A promising alternative to slow down antibiotic resistance and thus fight bacterial infections more efficiently is the conjugation of antibiotics with amphiphilic polymers.[1,

[15-17] This derivatization opens many new properties to polymer-antibiotic conjugates (PACs), such as lower toxicity, better solubility, improved permeability, and retention efficiency.[18-19] Moreover, the mechanistic study of the exact mode of action of these PACs seems to be of particular interest. Thus, elucidation of the mode of action may not only contribute to the understanding of the actual advantage of modification with polymers, but also open new perspectives.

In addition, the control of antimicrobial activity by cleavable groups is another interesting approach that will be discussed in detail. Here, the non-covalent crosslinking of amphiphilic PACs with ABA triblock copolymers will be investigated at the molecular level to better understand the interrelationships and dependencies of this interaction.

2 State of the Art

2.1 Synergistic Effects

The addition of additives to antibiotics can increase their antimicrobial effect or circumvent the resistance mechanisms.[20] However, it is also possible to kill airborne germs efficiently with the combination of UV indirect irradiation and an evaporation of triaethylene glycol.[21] Clinical indications for combination therapy can be: Foreign body infections, endocarditis, high-grade immune deficiency, mixed infections, or initial chemotherapy.[22] Basically, often the combination of different classes of antibiotic substances shows a synergistic effect and thus an enhancing killing effect against different bacterial species.[23] One study deals with the influence of the addition of pipemidic acid as well as minocycline, gentamicin, cefazolin, mezlocillin, or ampicillin on the antimicrobial effect of ciprofloxacin. It was found that there was usually a synergistic or additive effect.[24] The combination of ciprofloxacin and an antipseudomonal penicillin in Figure 2 has shown synergistic effects in 20-50% of *Pseudomonas aeruginosa* (*P. aeruginosa*) isolates. A similar effect has been reported for the combination of ciprofloxacin and fosfomycin.[25] Both cotrimoxazole and β-lactam antibiotics plus aminoglycosides may be useful for spectrum expansion and to prevent rapid development of resistance.[26-28]

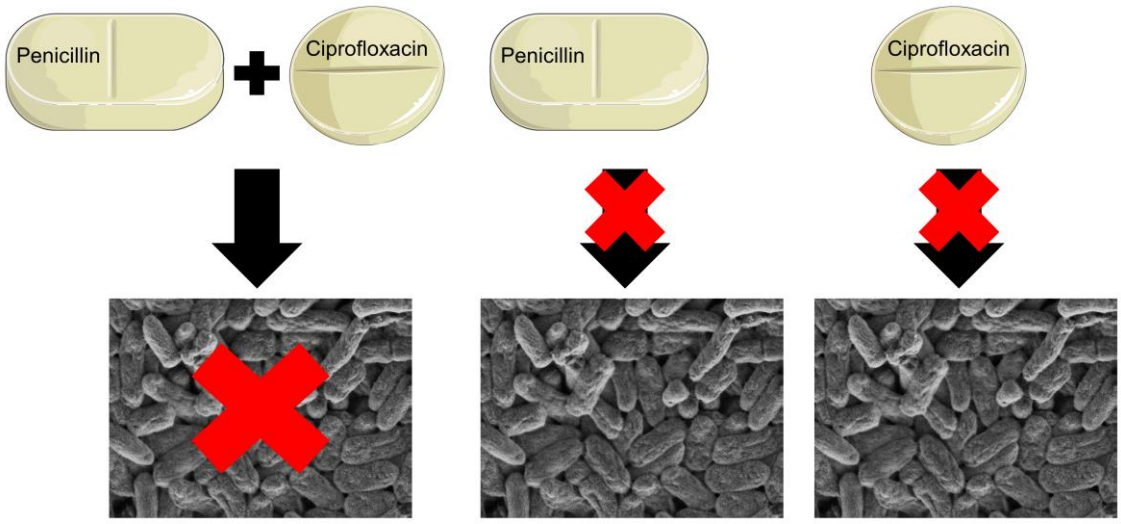

Figure 2: *Schematic representation of the combination therapy of ciprofloxacin and an antipseudomonal penicillin, which shows synergistic effects against P. aeruginosa.*[25]

In dermatology, glucocorticoids are often administered together with a local antibiotic or an antiseptic in order to be able to treat chronic infections or superinfections in a more targeted manner.[29] However, only a few substance combinations show a synergistic or additive effect. For example, a synergistic effect is seen with the additive addition of octenidine to the antibiotic gentamicin.[30] To combat recurrent urinary tract infections, taking a combination of selected probiotics and cranberry fruit powder can provide relief. Both lactobacilli and proanthocyanidins have bacteriostatic effects on pathogens such as *Escherichia coli* (*E. coli*), preventing bacterial adhesion and thus maintaining a healthy intestinal flora.[31]

Clavulanic acid enhances the antimicrobial effect of amoxicillin by making the most β-lactamase-producing isolates sensitive to the drug.[32] This is the most common drug combination used to combat resistant bacterial infections.[33-34] In general, combining a β-lactamase inhibitor such as clavulanic acid, sulbactam, or tazobactam with a penicillin prevents inactivation by β-lactamase-producing pathogens.[35] Combining imipenem with cilastatin blocks dehydropeptidase I in the renal brush border, increasing efficacy while decreasing nephrotoxicity.[36-37] In mixed infections with aerobic and anaerobic germs, β-lactam antibiotics can be combined with metronidazole.[38-39] In the presence of carbapenem-resistant *Klebsiella pneumoniae* (*K. pneumoniae*), a favorable synergistic effect of colistin with tigecycline has been demonstrated.[40] Similarly, data exist on the synergistic effect of plazomicin with colistin, meropenem, or fosfomycin against *K. pneumoniae* bacteria.[41] Triple therapy of aztreonam with colistin or meropenem against highly resistant *K. pneumoniae* isolates producing metallo-β-lactamases showed synergistic and bactericidal effects, respectively.[42]

2.2 Specific Transportation

The definition of drug delivery systems is the transport of pharmaceutical compounds to their target site in order to achieve the desired therapeutic effect.[43] This enables controlled, targeted and local therapy, a longer duration of action and, for example, reduces toxicity or resistance mechanisms.[44-45] There are numerous and different drug delivery systems, such as liposomes, polymersomes, gels, nanoparticles, micelles, biodegradable polymers and various other polymer-based systems.[45] In the following, some drug delivery systems will be presented and discussed (Figure 3).

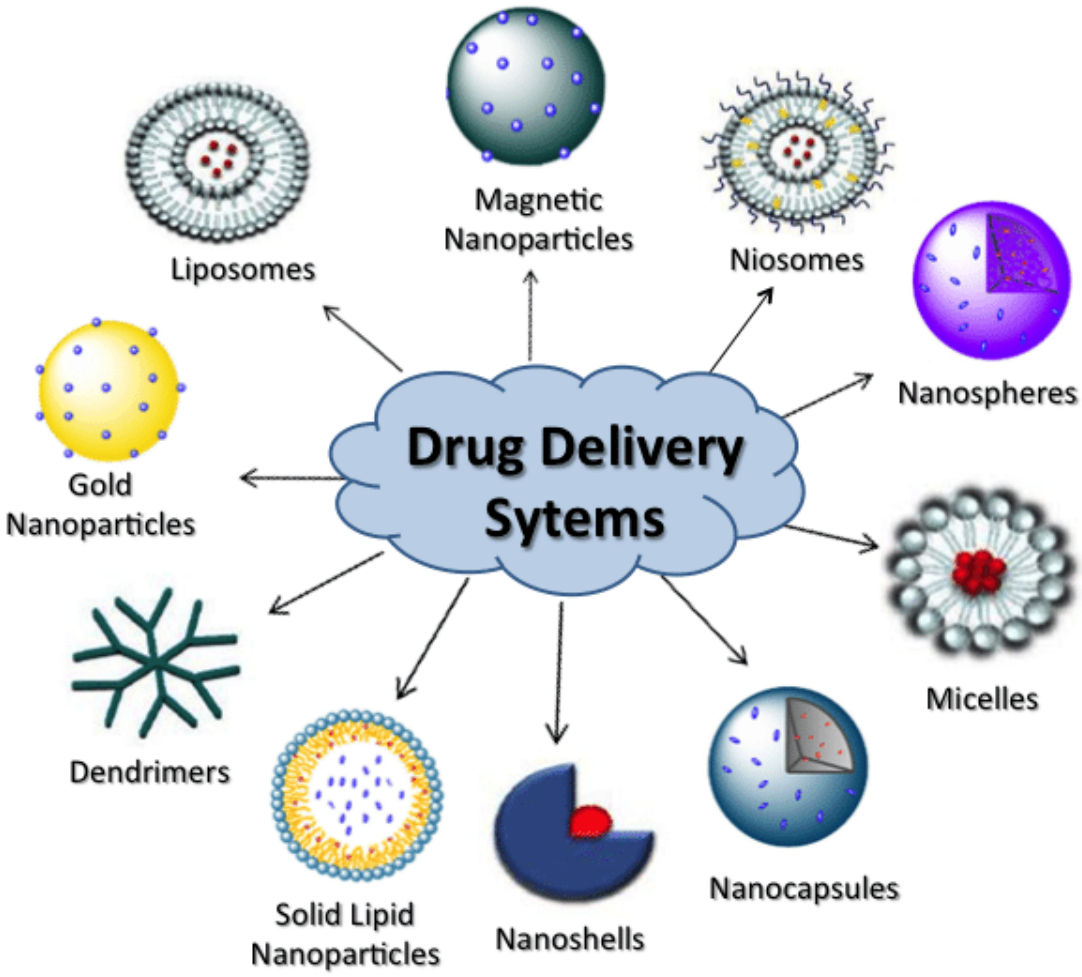

Figure 3: *Drug delivery systems for the administration of drugs.*[46-47]

2.2.1 Liposomes and Polymersomes

Liposomes (Figure 4) and polymersomes (Figure 5) are frequently used drug delivery vesicles that, in principle, improve drug efficacy in a simple and cost-effective manner, as well as reduce toxicities.[48-49] Typically, natural and synthetic lipids, as well as surfactants, are used in the synthesis of liposomal drug delivery vesicles. Because of this diversity, systems with a wide variety of functions can be produced, such as a pH response or prolonged blood circulation (Figure 4).[50-51]

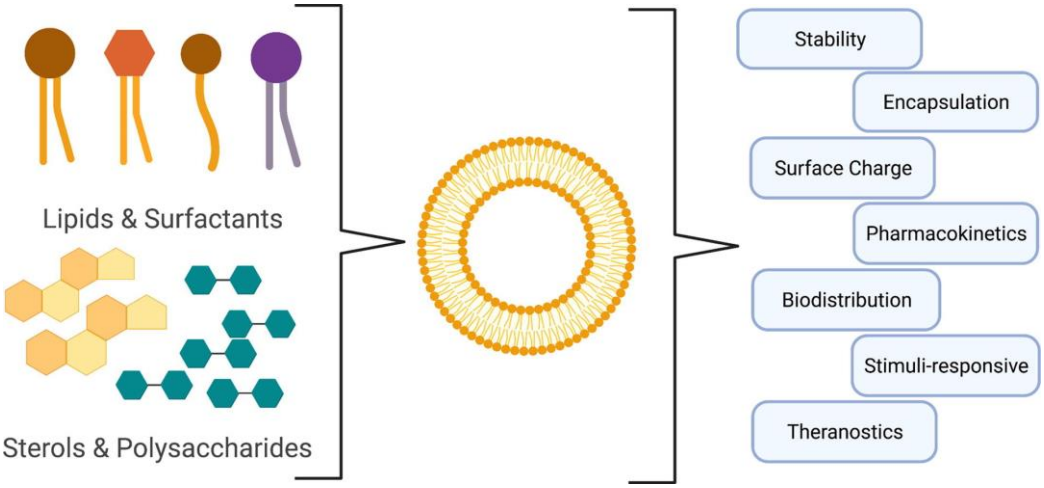

Figure 4: *Schematic structure of liposomes and the resulting advantages.*[50]

To extend the blood circulation time of liposomes, they have been modified with glycoproteins, oligosaccharides, polysaccharides, and synthetic polymers, such as PEG, on the surface.[52-54] In addition, the surface can be modified for active targeting, with, for example, ligands such as peptides and antibodies, or passive targeting.[55-56] In principle, liposomes have multiple environments in which a drug can be encapsulated, such as the hydrophilic aqueous core, the lipophilic phospholipid membrane bilayer, and the surface for direct drug conjugation/association.[57-58] Due to these many aforementioned advantages and their biodegradability and biocompatibility, liposomal systems are ideally suited for the delivery of various anticancer drugs.[59] Some well-known therapeutics on the market are Doxil™, Onivyde™, and Marqibo®.[60] The drug paclitaxel became less toxic and could be administered at higher doses using liposomal encapsulation.[61] Selective release to peptidase secreting cells was made possible by combining liposomes and peptide-

lipid conjugates. Thus, the liposomes remained intact until they encountered the target cells secreting peptidase and the peptide moiety was degraded from the lipid, resulting in destabilization of the liposomes.[62] Cross-linked liposomes consisting of lipoic acid and glycerophosphorylcholine cross-linked by dithiothreitol are capable of delivering drugs with intracellular reduction of disulfide bonds.[63-64] Mimicking the expression of surface-oriented proteins by *Staphylococcus aureus* (*S. aureus*) was investigated using antibody-liposome conjugation. Here, the fragment crystallizable (Fc) binding peptide was attached to the liposomes via an amide bond. Subsequently, the prepared liposome was incubated with antibodies to prevent the Fc binding peptide from covalently binding to the Fc region of the antibody. This produced orientation-controlled, antibody-labeled liposomes.[65] One of the most recently approved liposomal therapeutics is Onpattro®; this has been used to treat transthyretin-mediated amyloidosis. After liposomal treatment, an 81% reduction in transthyretin production and improved muscle strength, sensation, reflexes, and heart rate were observed.[66-67]

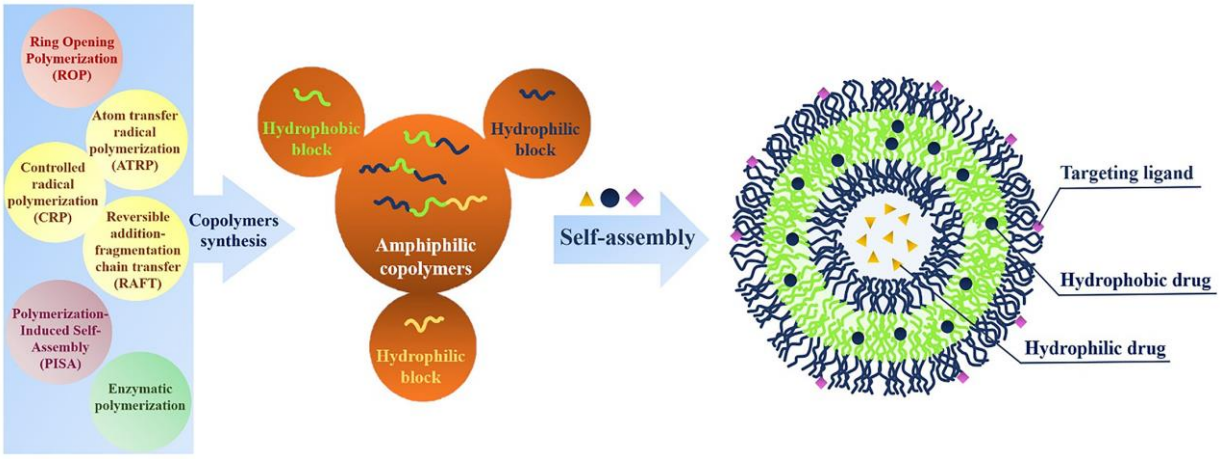

Figure 5: *Different synthetic routes for the production of amphiphilic block copolymers and subsequent self-assembly into polymersomes.*[68]

Self-assembling polymersomes consisting of amphiphilic block copolymers have the same structure as liposomes but are a promising alternative due to several advantages. The chemical versatility of the polymer structure, its ease of synthesis, the possibility of adding more functions, and the increased stability to several months are some of the advantages mentioned (Figure 5).[68-73] Commonly used hydrophobic blocks in polymersome-forming block copolymers are poly((meth)acrylates) and

polydimethylsiloxane (PDMS), and the commonly used hydrophilic polymers are poly(ethylene glycol) (PEG), hydrophilic poly(meth)acrylates, or poly(2-methyl-2-oxazoline).[74-77] However, a major disadvantage of polymersomes is the often unknown toxicological information of the polymers used.

Polymersomes degradable by hydrolysis or other enzymatic processes are of particular interest.[78] Biocompatible and biodegradable polymers, such as poly(DL-lactide), poly(trimethylene carbonate), and poly(caprolactone), are often used for this purpose.[79-81] One of the first biodegradable polymersomes consisted of hydrophobic poly(DL-lactide), poly(ε-caprolactone), or poly(trimethylene carbonate) and PEG as a hydrophilic block.[82] Polymersomes consisting of three-armed $(PEG)_3$-*b*-poly(DL-lactide) copolymers linked to a citric acid linker were loaded with doxorubicin. These polymersomes were shown not only to form polymersomes even under variable copolymer composition, but also to achieve significantly faster and more specific doxorubicin concentrations in tumors.[83-84]

Replacement of PEG with poly(amino acids) allows complete biodegradation of the hydrophilic polymer component and lower toxicities.[85-86] The response of polymersomes to external stimuli is also a four-promising route to release bound component. Here, enzymatic hydrolysis with, for example, lipase within 40 hours shows successful release of bound active compounds.[87-91] ABA triblock copolymers composed entirely of poly(amino acids) can also form polymersomes. These polymersomes have also been loaded with doxorubicin and show similar efficacy to the liposomal anticancer drug Myocet.[92] Controlled degradation of polymersomes can be achieved by enzyme-cleavable blocklinkers. For this purpose, PEG-*b*-poly(lactic acid) block copolymers were prepared in which the two blocks were linked by a synthetic peptide that can be cleaved by matrix metalloproteinase 2.[93-94] Polyethylene glycol (PEG) was linked to polylactide (PLA) via the synthetic peptide PVGLIG to form self-assembling chimeric polymersomes at the nanoscale. These can be selectively cleaved by the tumor-associated matrix metalloproteinase-2 enzyme to release the topoisomerase I inhibitor SN38. Even more targeted release of the drug can be achieved by modification at the polymersome surface by a targeted ligand. Thus, the highest therapeutic index is achieved compared to non-responsive formulations.[95]

The synthesis of polymersomes that respond to external stimuli are sensitive but efficient systems. The combined use of photosensitizers and oxidation of stimuli-responsive blocks resulted in promising biocompatible polymersomes. A synergistic effect on tumors was observed, through the release of the drug doxorubicin and the near-infrared light used to induce its release.[96] Most of the methods for the preparation of polymersomes were derived and transferred from liposomes. Polymerization-induced self-assembly is a new technique. For this self-assembling technique, water-soluble macrochain transfer agents or hydrophilic macromolecular initiators were used.[97-98] Thus, this principle combines two steps in one, polymer synthesis and assembly into polymersomes. As a result, a protein encapsulation efficiency of up to 79% was achieved.[99]

2.2.2 Nanoparticles

Nanoparticles classically have a size of up to 100 nm and can assume different morphologies. Figure 6 shows a comparison of different release systems, with the focus of this chapter being on nanoparticles. The potential applications for nanoparticles are numerous, ranging from improving various materials in the home to mass transfer in medicine.[100-101] For example, nanoparticles are being used to compensate for or even improve problems in the treatment with antibiotics. This is achieved, for example, through targeted or environmentally friendly antibiotic delivery, combinatorial antibiotic delivery, or antibacterial vaccination enabled by nanoparticles.[102]

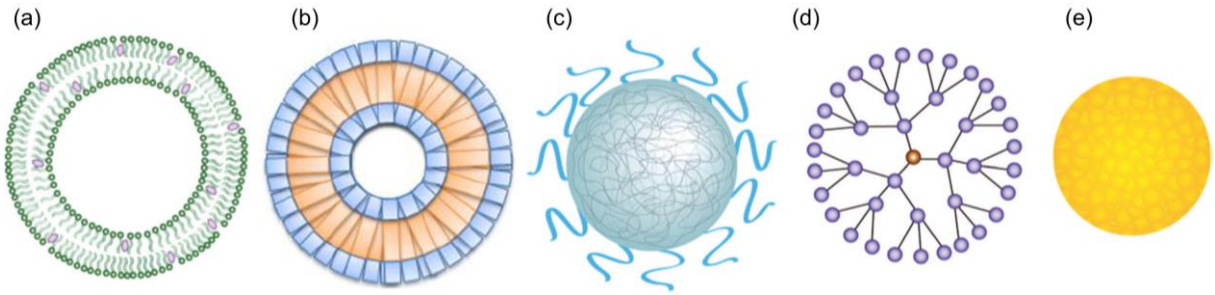

Figure 6: *Schematic representation of: (a) liposome, (b) polymersome, (c) polymeric nanoparticle, (d) dendrimer, and (e) inorganic nanoparticle.*[102-103]

By self-assembly, a polymer network consisting of PEI conjugated with methoxy poly(ethylene glycol) aldehyde, poly(ε-caprolactone) aldehyde and pyrene-1-carboxaldehyde was transformed into pH-sensitive nanoparticles. These nanoparticles were loaded with doxorubicin and coated with hyaluronic acid for targeted tumor control. This allowed for more efficient treatment and faster release of the drug.[104] Inorganic nanoparticles can be controlled in size and shape using block copolymers that form micelles or star polymers by self-assembly. The main advantage of such nanoparticles is their stability, as well as the variation of properties by external polymer chains. The areas of application are in catalysis, solar cells and lithium ion batteries.[105]

SiO_2 nanoparticles were functionalized with 3-(trimethoxysilyl)-propyldimethyloctadecyl ammonium chloride to produce antimicrobial hydrophobic surfaces. These nanoparticles are applied to a silicone surface and exhibit self-assembling micro- and nanostructures and a lotus effect, combined with contact-active antimicrobial properties.[106] The poor intracellular bioavailability of antibiotics and the associated development of resistance makes the use of nanoparticles coupled with antibiotics for targeted release a promising approach. Self-assembly into nanoparticles of the two terpenes farnesyl and geranyl, which were coupled to penicillin G via environmentally sensitive binding, allowed efficient antibacterial activity against *S. aureus*.[102] Rapid antibiotic release within 48 h and subsequent sustained release of 21 days was achieved by loading amoxicillin onto laponite nanoplatelets and then immobilizing them on the surface of electrospun polylactic acid nanofibers.[107] An effective method to treat skin infections caused by methicillin-resistant *S. aureus* (MRSA) is the use of synergistically acting allicin, silver nanoparticles.[108]

2.2.3 Nanogels

Nanogels are crosslinked hydrogel particles and thus form the interface between nanoparticles and hydrogels. In principle, they exhibit very many similar positive properties to hydrogels.[109] Hybrid nanogels, i.e. complexes of nanoparticles that disperse in organic as well as inorganic media, show very good interactions with various drug molecules, proteins and DNA. For this purpose, cholesterol branches

were physically crosslinked together with the pullulan backbone via hydrophobic groups to be able to produce nanogels by self-assembly. During self-assembly, insulin was encapsulated in the nanogels using van-der-Waals forces and hydrogen bonding.[110-111] Temperature-induced gelation was performed with the oppositely charged proteins ovalbumin and ovotransferrin or lysozyme, to produce nanogels.[112]

Hybrid nanogels of hydroxypropyl-β-cyclodextrin were prepared to improve the solubility of the drug dexibuprofen. Thus, compared to tablet administration, the solubilization of dexibuprofen can be significantly improved due to the nano size and hydrophilicity of the nanogels.[113] pH sensitive nanogels was prepared from carbopol and methacrylic acid and showed gastroprotective drug release of gastric irritant ketoprofen. Here, the change in pH affects the swelling behavior of the nanogel, resulting in the release of the drug by an external stimulus. The maximum swelling index was at a pH of 7.4 as well as the maximum drug release.[114]

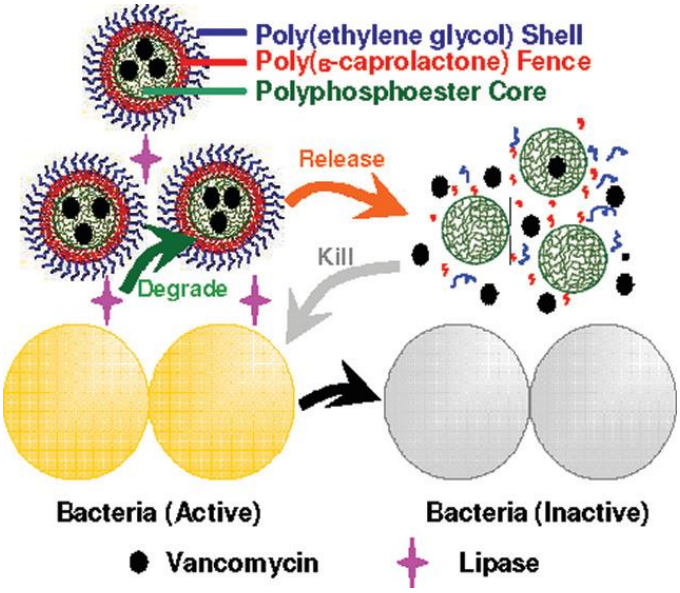

Figure 7: *Lipase-sensitive trilayer polymer nanogel for smart drug delivery.*[115]

A lipase-sensitive polymer triple-layered nanogel (TLN) was prepared to transport antibiotics. The nanogel has a polyphosphoester core, which was enclosed by a hydrophobic poly(ε-caprolactone) segment. This segment prevented the release of the antibiotic from the polyphosphoester core before it reached the bacterial infection sites. However, as soon as the TLN sensed the lipase-secreting bacteria, the poly(ε-

caprolactone) barrier of the TLN disintegrated and released the antibiotic (Figure 7).[115]

PEG-functionalized poly(methacrylic acid) nanogels respond to multiple stimuli, enzymes, pH, and reduction, and have been used for simultaneous release of doxorubicin and paclitaxel.[116] A nanogel based on coumarin-containing hyaluronic acid that responds to multiple stimuli (light and temperature) has also been developed for chemotherapy. This has been used to deliver poorly soluble drugs such as fluorescent di-strylbenzene derivatives and paclitaxel.[117] The drug doxorubicin has been modified using 2,6-diamino-pyridine to include an H-bond donor. This allows the drug to be conjugated via hydrogen bonds to the chemically cross-linked nonogel consisting of uracil-functionalized (H-bond acceptor) poly(p-phenylenevinylene), achieving a drug loading of 82%. In addition, a higher efficiency in killing cancer cells and a release time of several days were observed.[118] For high biocompatibility, chitosan was crosslinked both ionically and enzymatically. Encapsulation efficiencies of up to 67% were achieved with these nanogels, allowing for pH-controlled release.[119]

2.2.4 Micelle Release Systems

Micellar delivery systems based on various polymers are ideally suited for the transport of hydrophobic drugs. In doing so, these systems protect the drugs from elimination by the mononuclear phagocytic system and thus prolong blood circulation. In addition, polymeric micelle systems exhibit very good thermodynamic and kinetic stability, as well as stealth properties.[120-121] Biopolymers are also very popular for the preparation of micellar drug delivery systems.

Chitosan was used together with cholesterol to prepare an amphiphilic graft copolymer. This micelle system was loaded with curcumin and has shown enhanced cytotoxic activity against murine melanoma as well as human breast cancer cells.[122] To prepare sorafenide-loaded micelles, PEG 5000 and 6,7-Bis(3-hydroxyphenyl)pteridine-2,4-diamine (TG100-115) were conjugated to hydroxyethyl starch. Very rapid release was observed at low pH and high a-amylase-reducing conditions.[123] 3-Helix micelles based on peptide-PEG conjugates have a long

circulation half-life and efficient clearance. The loaded drug doxorubicin was released as soon as the peptide was enzymatically degraded.[124] Amphiphilic di- and triblock copolymers consisting of poly(2-oxazolines) were selected as micellar drug carriers for the hydrophobic drug paclitaxel. A very high loading capacity of 45 wt% as well as high water solubility, ease of preparation, stability and higher activity of the drug prove the excellent applicability of these delivery systems.[125]

ABA triblock copolymers with a hydrophobic block of poly(2-butyl-2-oxazoline) (PBuOx) and poly(2-methyl-2-oxazoline) (PMOx) as the hydrophilic block form micelles that can encapsulate taxanes for 1-2 weeks and still exhibit high toxicity against multiple cancer cell lines after release.[126] Combination therapy of paclitaxel and alkylated cisplatin, also transported in the amphiphilic block copolymer PMOx-*b*-PBuOx-*b*-PMOx, represents an improvement in ovarian and breast cancer therapy. This combination therapy leads to improved pharmacokinetics, slower release into serum, and improved distribution of the drug in the tumor.[127] The upper critical solution temperature (UCST) polymers consisting of acrylamide, acrylonitrile, or vinyl-4-pyridine can form triblock copolymers by addition of pH sensitive comonomers such as poly(dimethyl acrylamide), which aggregate to form stable micelles at the cloud point in solutions with pH between 4.75 and 7.0. Drug release from the micelles occurs at pH values below 4.7.[128] For the treatment of ocular inflammation, micelles constructed from PEG-*b*-poly(ε-caprolactone) and PEG-poly(lactic acid) were loaded with triamcinolone acetonide. A drug loading capacity of 12-25% was observed, as well as a 5-10-fold increase in water solubility of the drug triamcinolone acetonide. Suspension of the micelles in chitosan hydrogels resulted in both a release duration of one week and a greatly enhanced anti-inflammatory effect.[129]

In summary, there are countless ways to transport medications or to get them to the desired destination. Apart from the wide range of molecules that can be used as transporters, there are numerous transport systems. These transport systems can transport different drugs, such as cancer drugs or antibiotics. Targeted transport can also be made possible by attaching peptide molecules or other molecular structures to the surface of the transporters. In addition, there are many variations in the release of the transported drugs, ranging from chemical cleavage and enzymatic

cleavage to temperature- or light-induced release. However, despite the many advantages, such as reduced toxicity, targeted release or high loading capacity, the loading of the transporter with drugs is usually a complicated and sensitive process. In addition, the encapsulation of the drugs often follows a similar pattern, so that the drugs are always at the center of the transport systems. An interesting possibility here would be to explore a simpler way of encapsulating drugs and an alternative encapsulation pattern.

2.3 Polymer-Drug Conjugates

Polymer-drug conjugates have been explored since the 1950s (Figure 8). Despite initial skepticism, in 2013 the polymer therapeutics Copaxone and Neulasta were among the top ten best-selling drugs in the United States.[130]

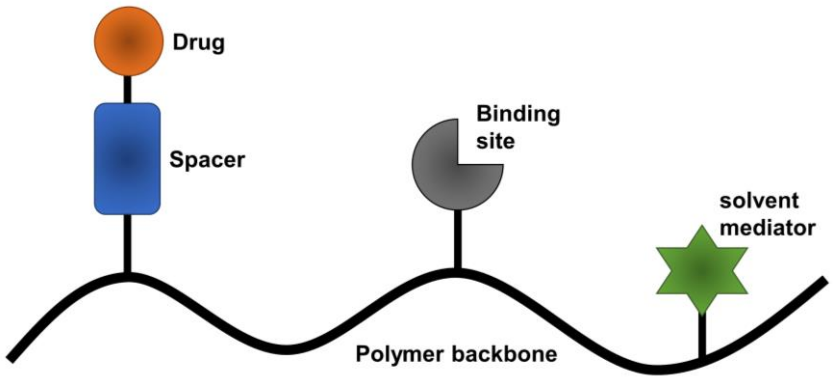

Figure 8: *Model of a polymer-drug conjugate according to Ringsdorf.*[131]

Various classes of drugs, such as proteins, peptides, and small molecule drugs, are conjugated with polymers to enhance their therapeutic effects.[132-135] In addition, targeted treatment can be carried out due to polymer conjugation, for more specific affinity to certain structures in cells and tissues is enabled.[136] Copaxone, mentioned above, is composed of a random copolymer consisting of the amino acids glutamine, tyrosine, alanine, and lysine and thus resembles the lipid-rich myelin layer of nerve cells. In multiple sclerosis, this is attacked by the immune cells, but the copolymer prevents this by binding the immune cells. This results in a reduction of the inflammatory reaction in the central nervous system.[137-139] Neulasta is the conjugation of PEG to filgrastim, a peptide hormone used to stimulate leukocyte formation. Due to the PEGylation of filgrastim, the half-life of the peptide hormone is significantly increased.[140] Apart from PEG, other polymers are also used, such as poly(2-hydroxypropyl)methacrylamide (PHPMA) and poly(lactide-co-glycolide) (PGLA).[134] During conjugation, other functional groups can be used in addition to the drug and polymer, for targeted mass transfer or to improve solubility.[131]

Kollidon® is a mixture of polyvinyl acetate and povidone, which can form a polymer matrix. This polymer mixture can find application as tablets, pellets, and granules with a sustained release.[141-143] Controlled-release ciprofloxacin (CIP) matrix tablets can be embedded in Kollidon® to increase their water solubility and stability.[144] Norfloxacin has also been mixed with Kollidon® to facilitate its mass transfer.[145] Reducing side effects while improving bioavailability has been the goal in chronic asthma therapy. For this purpose, nanoscale and biocompatible Kollidon® nanoparticles loaded with montelukast sodium were produced with up to 10-fold prolonged drug release.[146]

2.3.1 Polymer-Antibiotic Conjugates

Antimicrobial polymers also play a crucial role in combating microorganisms. This conjugation also has major advantages, such as better selectivity, lower toxicity, and most importantly, lower potential for the formation of resistant bacterial strains.[147-149] In fact, again, the most common form of conjugation is a temporary bond between polymer and antibiotic[150-157], although permanent bonding is of greater interest for this work. An example of temporary binding between polymer and antibiotic is the ester bond between poly(2-oxazolines) and various drugs. These poly(2-oxazoline)-drug conjugates have exhibited significantly slower hydrolytic release rates in plasma than the corresponding PEG and dextran-drug conjugates. This was due to the folding of the conjugate, as the hydrophobic drug was enveloped by the hydrophilic polymer, slowing the enzymatic attack on the ester bond between the drug and polymer.[158]

In contrast, an example of permanent conjugation is the antibiotic doxorubicin, which was conjugated with a polymer due to its antitumor properties.[159-161] In principle, permanent binding between a polymer and antibiotic is problematic, as antimicrobial activity is often significantly reduced. Nevertheless, some of these polymer-antibiotic conjugates have been investigated for their antimicrobial activity and resistance-forming potential. Cephradine and penicillin V were conjugated with PEG-lysine-polyurethane using different strategies. Cephradine was coupled to the polymer via a stable amide bond and penicillin V via a hydrolyzable bond. The penicillin-V conjugates showed good antimicrobial activity because the labile ester bond allows

the release of the antibiotic. In contrast, the stable amide bond between the polymer and cephradine prevents the release of cephradine, which means that the cephradine conjugate has no bactericidal activity.[162] Similarly, permanent binding of ciprofloxacin- and norfloxacin- to PEG showed a decrease in molar activity against gram-positive and -negative bacteria cells. Norfloxacin-PEG conjugates even completely lost their antimicrobial activity against the gram-positive *S. aureus*.[11]

Nevertheless, permanent binding between polymer and antibiotic has great potential as other therapeutic properties can be improved in this way. A polymer-antibiotic conjugate (PAC) was developed in early 1979 by Meada et al. Neocarzinostatin (NCS), an antibiotic and an antitumor agent, was conjugated with styrene maleic anhydride (SMA). The conjugation not only made the drug highly soluble in a variety of organic solvents and water, but also showed high antimicrobial activity against *Sarcina lutea*.[163] Gelatin (GL)-based polymers were conjugated with various fluoroquinolones, including ciprofloxacin (CIP), via a radical reaction. The prepared PACs were tested for their antimicrobial activity against *E. coli* and *K. pneumoniae*. In both cases, the antimicrobial activity is either at the same level as the free antibiotic or even lower, i.e., they are more active.[164] Conjugation of tobramycin to PEG resulted in a significant 3.2-fold improvement in antimicrobial activity against *P. aeruginosa* biofilms compared to tobramycin.[165] One way to combat the resistance mechanisms of *P. aeruginosa* is PEGylation of tobramycin, which was investigated by Bahamondez-Canas et al. It became evident that the PAC had a distinct advantage in antimicrobial activity against plankton, compared with unmodified tobramycin.[166] PEG-vancomycin conjugates could be applied to a surface via an acrylate end group at the other polymer end, showing a strong reduction in bacterial colony formation.[167] Eren et al. conjugated vancomycin with antimicrobial cationic polymers and PEG. Conjugation of an additional cationic polymer to the vancomycin PEG increased the antimicrobial activity against *S. aureus* to 0.5 $\mu g \cdot mL^{-1}$.[168] Another example of a permanently bound PAC is the polymer-antibiotic conjugate of PEG and moxifloxacin. This conjugation improves not only the lytic properties of the antibiotic but also the antimicrobial activity against *P. aeruginosa* and *S. aureus*.[169] The formation of antimicrobial nanoparticles was made possible by the covalent binding of *N*-thiolated β-lactam antibiotics to polyacrylate. These nanoparticles

exhibit not only better antimicrobial properties but also high activity against methicillin-resistant *S. aureus* (MRSA).[170]

To protect β-lactam antibiotics from the enzyme β-lactamase, penicillin V and amoxicillin were conjugated to various poly(vinylpyrrolidones).[171] Two different antibiotics, trimethoprim (TMP) and sulfamethoxazole (SMZ) were conjugated to poly(catechol). Both antibiotics inhibit different enzymes in the folic acid metabolic pathway.[172] He et al. investigated at the copolymerization of ciprofloxacin onto a copolymer consisting of glycidyl methacrylate (GMA), butyl acrylate (BA), and 2-(dimethylamino)ethyl acrylate methyl chloride (DMAEAMC). The antimicrobial activity of the conjugates was investigated using the bacterium *E. coli*. Basically, antimicrobial activity and solubility were found to be highly dependent on polymer composition.[173]

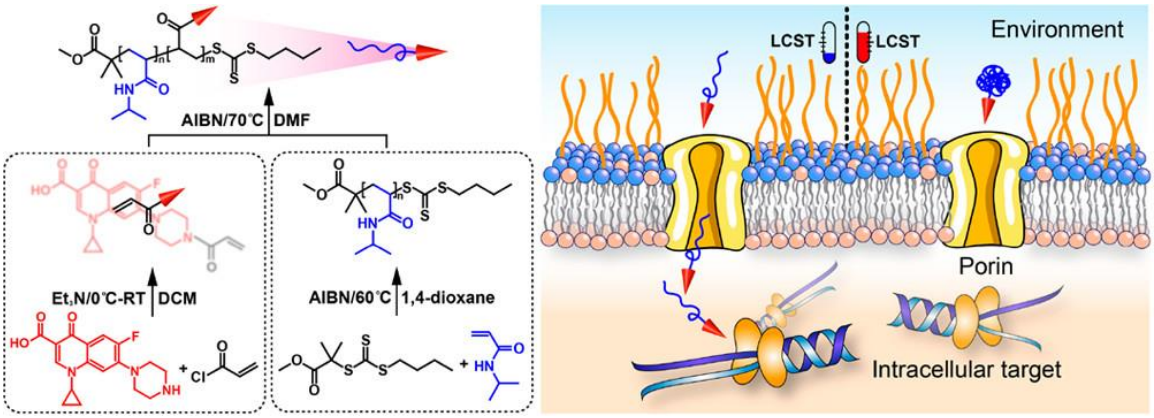

Figure 9: *Switchable control of antimicrobial activity is introduced here using an externally temperature-triggered stimulus to change the shape of a short, covalently attached "tail" on the polymer. This changes the size of the PAC so that access to intracellular targets through the porin channels can no longer be used.*[174]

Chang et al. conjugated ciprofloxacin to Poly(N-isopropylacrylamide) (PNIPAM) to allow thermoresponsive switching of antimicrobial activity. Once the PAC begins to agglomerate and precipitate at a certain temperature, it can no longer pass through the porin channels, thus switching off antimicrobial activity. This conjugation with PNIPAM resulted in an on-off ratio of 2-16 in the temperature range of 25-33 °C (Figure 9).[174] The Chair of Biomaterials and Polymer Sciences at the TU Dortmund University has also already dealt with the topic of polymer-antibiotic conjugates. The first steps were formed by the master's thesis of Harmuth, which deals with the

conjugation of the biocompatible PMOx with the broad-spectrum antibiotic CIP.[175] Unmodified ciprofloxacin was used as a terminating agent in the living, cationic polymerization of 2-methyl-2-oxazoline (MOx). For termination, the CIP was specifically attached to the polymer either through the piperazine group or carboxyl group. However, these PACs exhibited 1250-fold worse activity than ciprofloxacin. It became clear that not only direct termination with CIP, but also conjugation via the carboxyl group of the antibiotic lead to very poor antimicrobial activity. For this reason, the ciprofloxacin was modified with different spacers at the piperazine group to produce a possible antimicrobial activity. Furthermore, a variety of poly(2-oxazoline)s were used for conjugation. These PACs have shown antimicrobial activity of up to 0.31 µg · mL^{-1} against the bacterium *S. aureus*, i.e., a 1.4-fold increase in antimicrobial activity compared to CIP and 8.4 µg · mL^{-1} against the bacterium *E. coli*, i.e., a 280-fold deterioration in antimicrobial activity compared with CIP.[17] In addition, it was shown that the potential for resistance formation could also be significantly lowered by conjugating CIP with poly(2-oxazoline)s.[15] Subsequently, the antibiotic penicillin was also covalently bound to various poly(2-oxazoline)s by direct termination. Despite a lower antimicrobial activity due to the bonding, this PAC has a high antimicrobial activity in the presence of the enzyme penicillinase. Thus, resistance formation could also be inhibited here thanks to conjugation with a polymer.[16]

The numerous examples show that there are many different ways of modifying drugs. The combination of several drugs with each other promotes the actual effect of these and expands the spectrum of action, but still does not solve many problems. Release systems are very well suited for this purpose, because the targeted release of active ingredients reduces the toxicity and resistance formation of the drugs, for example, or improves their solubility. Depending on the site of application or the type of release of the active ingredients, different release systems can be selected to best meet the required conditions. Hydrogels are a special type of drug delivery because they can be used outside the human body and thus must withstand mechanical challenges. The modification of active ingredients with permanently bound polymers is a particular challenge. Here, it is important not to restrict the spectrum of action of the drugs and still be able to meet the challenges and solve existing problems.

These results show very great potential in the covalent binding of poly(2-oxazoline)s with various antibiotics, especially ciprofloxacin. Nevertheless, some open questions have remained and unsolved tasks regarding the antimicrobial activity and the exact mode of action of these PACs. For this reason, the present work is concerned with the elucidation, i.e., the mechanistic studies of the exact mode of action of the polymer-CIP conjugates.

3 Aims and Objectives

Based on the findings of MARTIN SCHMIDT's work[1], amphiphilic PACs have shown very good antimicrobial activity. In the present work, this finding was investigated in more detail with the aim of uncovering the mode of action of these PACs. The interaction between the amphiphilic PACs and the targets gyrase and topoisomerase IV is in the foreground of the investigations, as well as the presumed membrane activity caused by the amphiphilic polymer part of the conjugates. The exact mode of action and penetration of the PACs into the bacterial cell could be further investigated in this way.

In addition, the insights gained into the mode of action of amphiphilic PACs provide new ideas for improving their properties. Here, the idea was to maintain the amphiphilic properties, but at the same time increase the blood and cell toxicity, as well as the biocompatibility of the PACs. This could be made possible by replacing the hydrophobic polymer group with a biodegradable, less toxic group such as vitamin E. The hydrophilic portion would continue to be PMOx, due to its good solubility and stealth properties. Thus, all the advantages of the amphiphilic character would remain and the few difficulties would also be eliminated.

Furthermore, and also based on the preliminary work of MARTIN SCHMIDT[1], the interplay of non-covalent binding between the amphiphilic PACs and ABA triblock copolymers was investigated at the molecular level in this work. The focus was on investigating the deactivation and reactivation mechanism of this system at the molecular level. The detailed understanding of the interplay and dependencies of these two components could lead the way to transfer the system to other PACs or triblock copolymers.

4 Results

4.1 Amphiphilic Poly(2-oxazoline) Ciprofloxacin Conjugates

The PhD thesis of MARTIN SCHMIDT[1] contains first research approaches concerning amphiphilic polymer-antibiotic conjugates. However, only the synthesis of these amphiphilic PACs was investigated and no conclusions were drawn on the mechanistic mode of action of the PACs. The synthesis route and the composition of the amphiphilic polymers were taken from the work of MARTIN SCHMIDT[1] and further investigated in detail for their mechanistic effect. In addition, the results of this chapter were developed in collaboration with the students JOHANNA KEIL[176], JONAS TOPHOVEN[177] and MURAT FURKAN ORUC[178] as part of their final theses.

To improve membrane permeability, the antibiotic CIP, which exerts its effect at the target inside the bacteria, was conjugated with an amphiphilic block copolymer. Following a previously known coupling scheme, CIP was conjugated with a series of POx-based amphiphilic block copolymers (Scheme 1).[17]

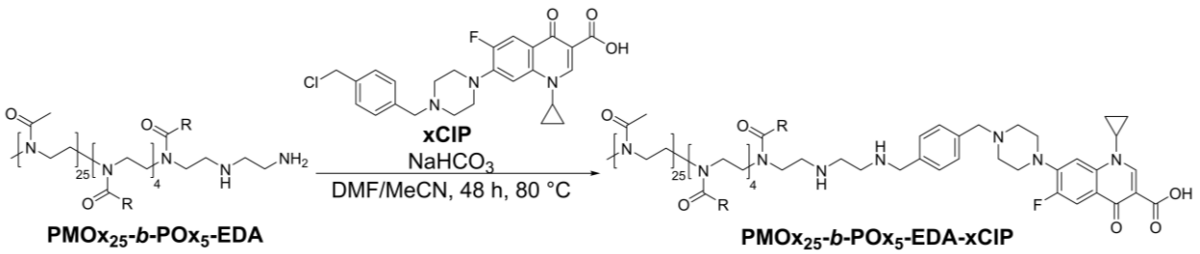

Scheme 1: *Synthesis strategy of the conjugation of xCIP with amphiphilic polymers based on a hydrophilic polymer (PMOx) and different hydrophobic polymers, R = -$(CH_2)_3$-CH_3 (PBuOx), -$(CH_2)_5$-CH_3 (PHexOx), -$(CH_2)_6$-CH_3 (PHeptOx), -$(CH_2)_7$-CH_3 (POctOx) and -$(CH_2)_8$-CH_3 (PNonOx).*[1, 179]

All amphiphilic PACs were synthesized by polymerization of the corresponding 2-alkyl-2-oxazolines, termination with ethylenediamine (EDA) and subsequent reaction with activated ciprofloxacin (xCIP). The analytical data, such as ^{1}H NMR and GPC, of the synthesized PACs are summarized in Table 1.

It is clear from the table that in most cases the target composition of the block copolymers and a degree of functionalization with xCIP of at least 90% were achieved. With the ratio between the hydrophilic and the hydrophobic repeating units

(HHR), the amphiphilic nature of the block copolymers can be calculated. The higher this value, the more the hydrophilic/hydrophobic balance (HHB) shifts toward a more hydrophilic character. However, the HHR value does not distinguish between POx with different hydrophobic units, because the hydrophobic contribution of these units depends on the length of the alkyl side chains.

Table 1: *Analytical data of amphiphilic PACs characterized by ^{1}H NMR spectroscopy.*[179]

PAC[a]	$M_{n,NMR}$ [g·mol^{-1}]	PDI	F^d_{NMR}[b]	HHR[c]	Term
PMOx$_{25}$-*b*-PBuOx$_5$-EDA-xCIP[e]	3300	1.27	87%	5	M$_{25}$-Bu$_5$
PMOx$_{15}$-*b*-PBuOx$_{15}$-EDA-xCIP[e]	3700	1.26	99%	1	M$_{15}$-Bu$_{15}$
PMOx$_6$-*b*-PBuOx$_{22}$-EDA-xCIP	3900	1.24	> 99%	0.3	M$_6$-Bu$_{22}$
PMOx$_{34}$-*b*-PHexOx$_7$-EDA-xCIP[f]	4500	1.17	> 99%	5	M$_{34}$-Hex$_7$
PMOx$_{23}$-*b*-PHexOx$_{20}$-EDA-xCIP[f]	5600	1.19	> 99%	1.2	M$_{23}$-Hex$_{20}$
PMOx$_7$-*b*-PHexOx$_{21}$-EDA-xCIP[f]	4400	1.18	> 99%	0.3	M$_7$-Hex$_{21}$
PMOx$_{19}$-*b*-PHeptOx$_4$-EDA-xCIP[d]	2800	1.15	> 99%	5	M$_{19}$-Hpt$_4$
PMOx$_{28}$-*b*-PHeptOx$_3$-EDA-xCIP[d]	3400	1.18	92%	9	M$_{28}$-Hpt$_3$
PMOx$_{34}$-*b*-PHeptOx$_5$-EDA-xCIP[d]	4300	1.26	77%	7	M$_{34}$-Hpt$_5$
PMOx$_{38}$-*b*-PHeptOx$_6$-EDA-xCIP[d]	4900	1.27	95 %	6	M$_{38}$-Hpt$_6$
PMOx$_{16}$-*b*-PHeptOx$_{15}$-EDA-xCIP[d]	4400	1.23	98%	1.1	M$_{16}$-Hpt$_{15}$
PMOx$_{14}$-*b*-PHeptOx$_{24}$-EDA-xCIP[d]	5800	1.23	> 99%	0.6	M$_{14}$-Hpt$_{24}$
PMOx$_{31}$-*b*-PoctOx$_6$-EDA-xCIP[f]	4300	1.29	> 99%	5	M$_{31}$-Oct$_6$
PMOx$_{21}$-*b*-POctOx$_{16}$-EDA-xCIP[f]	5300	1.20	> 99%	1.3	M$_{21}$-Oct$_{16}$
PMOx$_6$-*b*-POctOx$_{29}$-EDA-xCIP[f]	6300	1.17	> 99%	0.2	M$_6$-Oct$_{29}$
PMOx$_{26}$-*b*-PNonOx$_5$-EDA-xCIP[e]	3700	1.22	94%	5	M$_{26}$-Non$_5$
PMOx$_{18}$-*b*-PNonOx$_{18}$-EDA-xCIP[e]	5600	1.28	96%	1	M$_{18}$-Non$_{18}$
PMOx$_7$-*b*-PNonOx$_{26}$-EDA-xCIP	6300	1.29	90%	0.3	M$_7$-Non$_{26}$

[a]Degree of polymerization determined by ^{1}H NMR spectroscopy via comparison of the respective signals caused by the initiating group and the signals caused by the protons of the polymer backbone.
[b]Degree of functionalization determined by ^{1}H NMR spectroscopy via comparison of the respective signals caused by the initiating and the terminal CIP groups.
[c]The ratio of the hydrophilic and the hydrophobic repeating units of the polymer.
[d]The synthesis route and the composition of the amphiphilic polymers were taken from the work of MARTIN SCHMIDT[1].
[e]The composition of the amphiphilic polymers were taken from the work of JONAS TOPHOVEN.[177]
[f]The composition of the amphiphilic polymers were taken from the work of JOHANNA KEIL.[176]

The minimum inhibitory concentration (MIC$_{99}$) assay was used to investigate the antibacterial activity of amphiphilic PACs against a range of clinically relevant infectious and pathogenic bacterial strains. Here, the MIC value corresponds to the concentration at which 99% of bacteria are inhibited from growing. To better classify

the values, the obtained MIC values of amphiphilic PAC are compared with the MIC values of CIP and with the previously reported $PMOx_{30}$-EDA-xCIP.[15] Moreover, the respective EDA-terminated polymers show no antimicrobial activity against any bacterial strain (MIC > 500 µg · mL^{-1} in all cases).

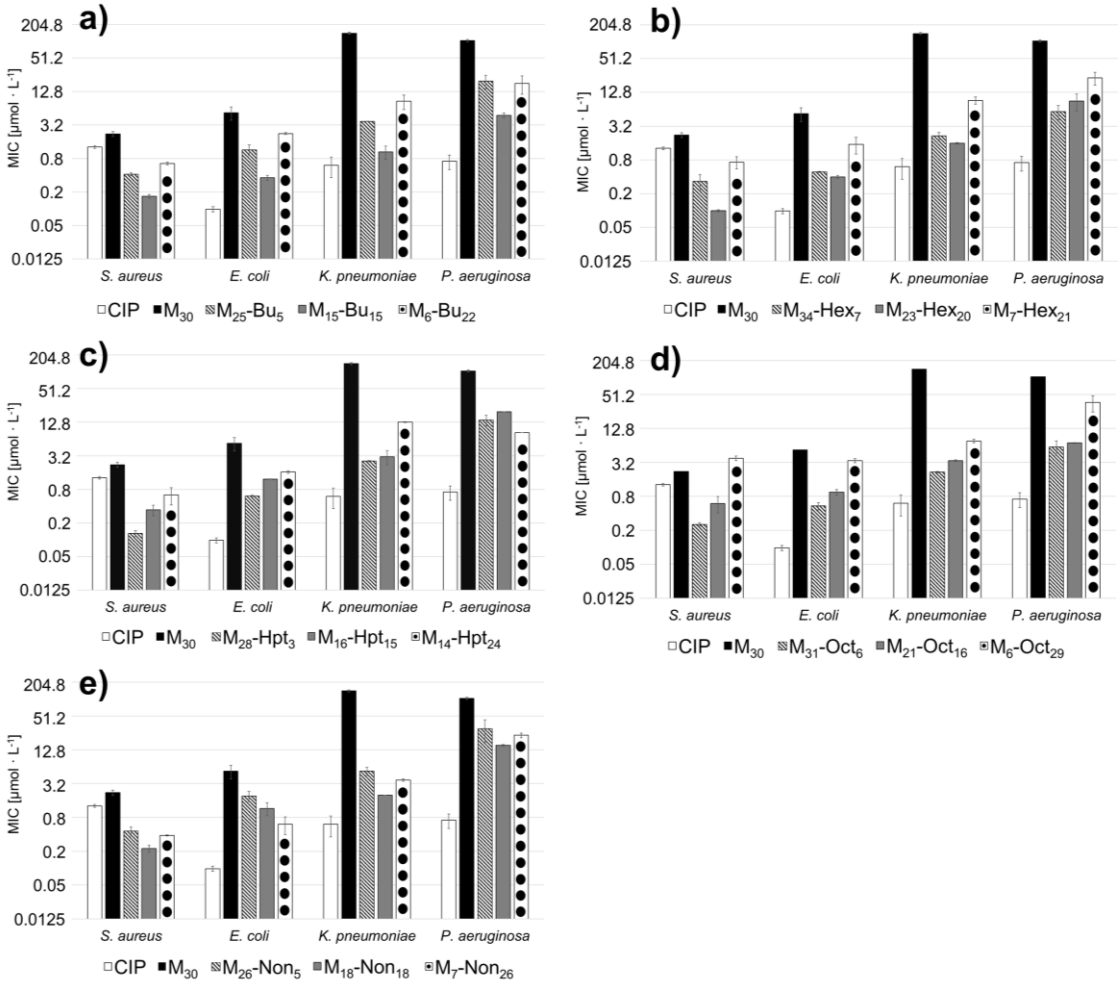

Figure 10: *MIC-values of $PMOx_{30}$-EDA-xCIP (black), different amphiphilic PACs: a)[177] striped: $PMOx_{25}$-b-$PBuOx_5$-EDA-xCIP (M_{25}-Bu_5), grey: $PMOx_{15}$-b-$PBuOx_{15}$-EDA-xCIP (M_{15}-Bu_{15}), dotted: $PMOx_6$-b-$PBuOx_{22}$-EDA-xCIP (M_6-Bu_{22}); b)[176] striped: $PMOx_{34}$-b-$PHexOx_7$-EDA-xCIP (M_{34}-Hex_7), grey: $PMOx_{23}$-b-$PHexOx_{20}$-EDA-xCIP (M_{23}-Hex_{20}), dotted: $PMOx_7$-b-$PHexOx_{21}$-EDA-xCIP (M_7-Hex_{21}); c)[178] striped: $PMOx_{28}$-b-$PHeptOx_3$-EDA-xCIP (M_{28}-Hpt_3), grey: $PMOx_{16}$-b-$PHeptOx_{15}$-EDA-xCIP (M_{16}-Hpt_{15}), dotted: $PMOx_{14}$-b-$PHeptOx_{24}$-EDA-xCIP (M_{14}-Hpt_{24}), The composition of the amphiphilic polymers were taken from the work of MARTIN SCHMIDT[1]; d)[176] striped: $PMOx_{31}$-b-$POctOx_6$-EDA-xCIP (M_{31}-Oct_6), grey: $PMOx_{21}$-b-$POctOx_{16}$-EDA-xCIP (M_{21}-Oct_{16}), dotted: $PMOx_6$-b-$POctOx_{29}$-EDA-xCIP (M_6-Oct_{29}); e)[177] striped: $PMOx_{26}$-b-$PNonOx_5$-EDA-xCIP (M_{26}-Non_5), grey: $PMOx_{18}$-b-$PNonOx_{18}$-EDA-xCIP (M_{18}-Non_{18}), dotted: $PMOx_7$-b-$PNonOx_{26}$-EDA-xCIP (M_7-Non_{26}) in comparison to CIP (white). All measurements were performed at least in triplicate, error bars represent standard deviations.[179] The biological examinations (CIP, M_{30}) and biological method of examination were taken from the work of MARTIN SCHMIDT[1].*

Against all tested bacterial strains, the amphiphilic PMOx-*b*-POx-EDA-xCIP conjugates exhibit high antimicrobial activities. They are even more active than the hydrophilic PAC $PMOx_{30}$-EDA-xCIP used for comparison. This reinforces the hypothesis that the amphiphilic nature of the polymer tail enhances the toxicity of the PACs to bacterial cells.

The amphiphilic PACs PMOx-*b*-PBuOx-EDA-xCIP exhibit the least hydrophobic nature. Nevertheless, as shown in Figure 10a, these PACs have up to eight times higher antimicrobial activity against *S. aureus* compared to the non-conjugated CIP (white) and up to 13 times higher activity compared to the hydrophilic $PMOx_{30}$-EDA-xCIP (black). The other two PACs, $PMOx_{25}$-*b*-$PBuOx_5$-EDA-xCIP (striped) and $PMOx_6$-*b*-$PBuOx_{22}$-EDA-xCIP (dotted), also have up to three times higher antimicrobial activity than the non-conjugated CIP against *S. aureus*. Against gram-negative bacteria, the amphiphilic PACs also exhibit higher antimicrobial activity than the hydrophilic PMOx-EDA-xCIP. The difference in activity against the bacterium *K. pneumoniae* is particularly clear, as the PAC shows an antimicrobial activity of 1.05 ± 0.28 µmol · L^{-1}, almost as active as the untreated CIP (0.60 ± 0.24 µmol · L^{-1}). In all cases, the most active derivative is the PAC with a HHR value of 1 ($PMOx_{15}$-*b*-$PBuOx_{15}$-EDA-xCIP). Nevertheless, higher or lower HHR values result in PACs that are more active than the hydrophilic $PMOx_{30}$-EDA-xCIP. Thus, an optimal HHR value exists, highlighting the importance of the hydrophilic/hydrophobic balance (HHB) for antimicrobial activity. Such effects have also been reported for membrane-active antimicrobial polymers in solution[180-181] and on surfaces.[106, 149, 182-183]

PACs with longer hydrophobic blocks show a similar trend to the PACs with the shortest hydrophobic block described above. The PHexOx-containing PACs also exhibit the highest antimicrobial activity at an HHR of 1. These are even more active against *S. aureus* than the corresponding PBuOx-containing PAC. Against the other bacterial strains, their activity is similar to that of the PBuOx-containing conjugate (Figure 10b). It is noticeable that the difference between the MIC values of the most hydrophilic PAC (HHR > 1) and the PAC with an HHR of 1 is less pronounced for gram-negative bacterial strains than for the corresponding PBuOx-containing PACs. Considering that the hexyl chain confers a more hydrophobic character to the respective repeating unit, a higher HHR in the PAC is sufficient to achieve the same

HHB as in the PBuOx-based PAC with a HHR of 1. Apparently, there is an optimal HHB for the highest PAC activity.

Therefore, the most active amphiphilic PACs with longer alkyl side chains in the hydrophobic blocks should be those with higher HHR values. The MIC values of the PHeptOx- and POctOx-containing PACs (Figure 10c and d) are also consistent with this hypothesis. The hydrophobic block NonOx has the longest alkyl side chain. Although these PACs are more antibacterially active than the corresponding hydrophilic PAC, they show independence of the ratio between hydrophilic and hydrophobic block. This unexpected result suggests that the maximum useful length of the alkyl side chain has been reached. In conclusion, it was successfully shown that conjugation of amphiphilic block copoly(2-oxazoline)s with xCIP leads to an increase in antibacterial activity. Compared to CIP, this activity is even an order of magnitude higher against *S. aureus*. Antimicrobial activity was also greatly improved against gram-negative bacterial strains compared with hydrophilic PAC, although the MIC values of CIP could not be achieved. One reason for this could be the membrane difference between the two bacterial species. This is because gram-negative bacteria have a double membrane, so penetration into the cell interior is more difficult than for *S. aureus*. In addition, the antibacterial activity depends on the HHB of the polymer tail, which can be optimized by varying the HHR value for each type of PAC.

A chain length dependence was observed for the hydrophilic PMOx-based PAC PMOx-EDA-xCIP. Thus, the antibacterial activity could be increased with shorter polymer chain length.[17] This could also be a way to further increase the activity of the amphiphilic PACs presented here.

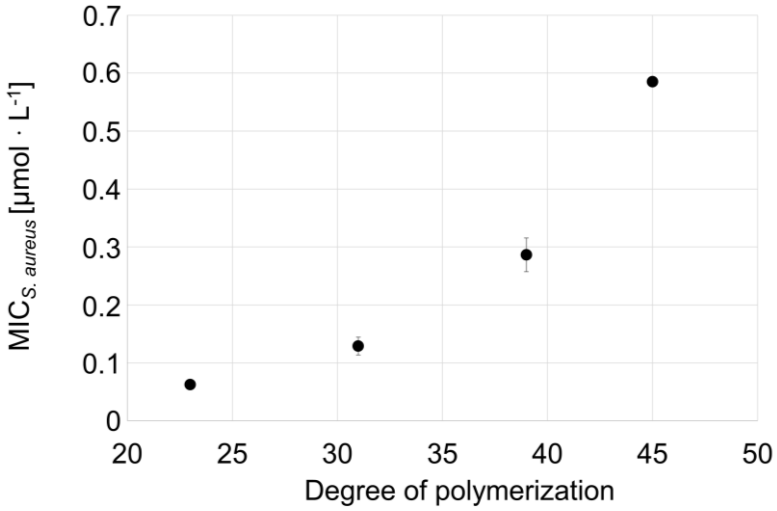

Figure 11: *Degree of polymerization (number of repeating units in the polymer chain) against $MIC_{S. aureus}$ value [µmol · L^{-1}] for $PMOx_{19}$-b-$PHeptOx_4$-EDA-xCIP (M_{19}-H_4), $PMOx_{28}$-b-$PHeptOx_3$-EDA-xCIP (M_{28}-H_3), $PMOx_{34}$-b-$PHeptOx_5$-EDA-xCIP (M_{34}-H_5) and $PMOx_{38}$-b-$PHeptOx_6$-EDA-xCIP (M_{38}-H_6). All measurements were performed at least in triplicate; error bars represent standard deviations.*[1, 176, 179]

For this reason, PACs with comparable HHR values and different degrees of polymerization were tested for their antimicrobial activity. For this purpose, $PMOx_{28}$-*b*-$PHeptOx_3$-EDA-xCIP was selected due to its very good antimicrobial activity and excellent solubility. As can be seen in Figure 11, the MIC values against *S. aureus* decrease significantly with increasing chain length. The shortest PAC $PMOx_{19}$-*b*-$PHeptOx_4$-EDA-xCIP shows up to 22-fold higher antimicrobial activity against *S. aureus* than CIP. In contrast, the PAC with the longest polymer length $PMOx_{38}$-*b*-$PHeptOx_6$-EDA-xCIP and a similar HHR value shows ten times lower activity than $PMOx_{19}$-*b*-$PHeptOx_4$-EDA-xCIP.

Several reasons could be possible for the significantly higher antimicrobial activity of amphiphilic PACs compared with pure CIP. The introduction of the amphiphilic structure of PACs should make them membrane-active, which may lead to perforation and disruption of phospholipid membranes. This is a typical behavior of amphiphilic antimicrobial polymers[168], which behave similarly to magainin, an antimicrobial membrane-active peptide.[184] Hemolysis activity testing for blood cells is a common method for determining the membrane-destroying properties of antimicrobial polymers.[147, 185] The hemocompatibility concentration of a compound at which 50% of porcine red blood cells lyse is referred to as HC_{50}. Without additives (PACs, DTAC), there was no hemolytic activity of the blood cells, i.e., the blood cells

were not destroyed and therefore do not show lysis. The release of hemoglobin after addition of 2 µL Triton X to red blood cells was considered as 100% lysis.

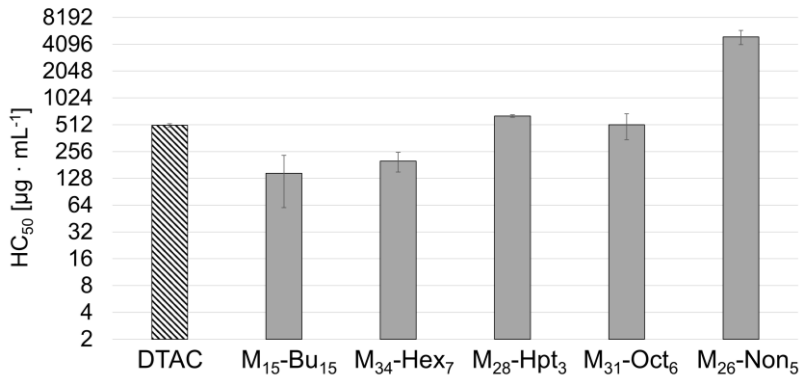

Figure 12: *HC_{50} values of DTAC, $PMOx_{15}$-b-$PBuOx_{15}$-EDA-xCIP (M_{15}-Bu_{15}), $PMOx_{34}$-b-$PHexOx_{7}$-EDA-xCIP (M_{34}-Hex_{7}), $PMOx_{28}$-b-$PHeptOx_{3}$-EDA-xCIP (M_{28}-Hpt_{3}), $PMOx_{31}$-b-$POctOx_{6}$-EDA-xCIP (M_{31}-Oct_{6}) and $PMOx_{26}$-b-$PNonOx_{5}$-EDA-xCIP (M_{26}-Non_{5}) tested against porcine red blood cells. All measurements were per-formed at least in triplicate; error bars represent standard deviations.*[176-177, 179]

Up to a concentration of 10 mg · mL^{-1}, all PACs were used and tested. PACs with an HHR value of about 1 or less, with the exception of $PMOx_{15}$-*b*-$PBuOx_{15}$-EDA-xCIP, are not soluble in blood cell buffer above 150 µg · mL^{-1} and did not cause lysis of blood cells at this concentration. The insoluble PACs were administered as a suspension at concentrations of 10 mg · mL^{-1} but did not lyse the blood cells either (less than 1% lysis). There are two possible explanations for these results: either the solubility of these PACs is not high enough to reach blood lysis-inducing concentrations or they do not destroy the cell membrane. Nevertheless, as can be seen in Figure 12, the membrane-active reference agent dodecyltrimethylammonium chloride (DTAC) and the soluble amphiphilic PACs exhibit a wide range of HC_{50} values.

The selectivity value is the ratio between the lytic activity against blood cells and the toxicity for bacterial cells. This value indicates how specific the membrane activity of the compounds is. The selectivity of the PACs was calculated by dividing the HC_{50} values by the $MIC_{S.\ aureus}$. The higher this value, the less likely membrane disruption is the underlying killing mechanism.

Table 2: *Overview of HC_{50} values, MIC_{99} values and the selectivity (S) against S. aureus.*[179]

PAC	HC_{50} [$\mu g \cdot mL^{-1}$]	$MIC_{S.aureus}$ [$\mu g \cdot mL^{-1}$]	HHR	$S_{S.aureus}$
DTAC	500 ± 20	5.30 ± 0.10		106
M_{15}-Bu_{15}	150 ± 90	0.62 ± 0.05	1	236
M_{34}-Hex_{7}	200 ± 50	1.48 ± 0.49	5	135
M_{28}-Hpt_{3}	640 ± 20	0.44 ± 0.05	9	1455
$M_{31}Oct_{6}$	500 ± 170	1.08 ± 0.07	5	474
M_{26}-Non_{5}	5000 ± 900	1.69 ± 0.30	5	2936

Some of the amphiphilic PACs have a low selectivity value suggesting that these compounds may act similarly to DTACs and thus exhibit membrane disrupting activity. However, most PACs have much higher selectivities. However, the significance of the data is too low to designate the membrane-destroying activity of the amphiphilic xCIP conjugates as the general underlying mechanism for the enhanced activity. They also show that PACs with an HHR of 1 or less, in particular, do not exhibit membrane-destroying activity.

A higher affinity for the CIP targets, the bacterial topoisomerases topoisomerase IV and DNA gyrase, would be another possible mechanism for the increased activity of xCIP conjugates compared to the original antibiotic.[186-187] Depending on the type of bacteria, both enzymes may be the primary or secondary target: DNA gyrase is usually the primary target in gram-negative bacteria and the secondary target in gram-positive bacteria.[187]

To test this theory, the polymer $PMOx_{19}$-*b*-$PHeptOx_{4}$-EDA and its xCIP conjugate were evaluated for their inhibitory activity against gyrase from the gram-negative bacterium *E. coli*.

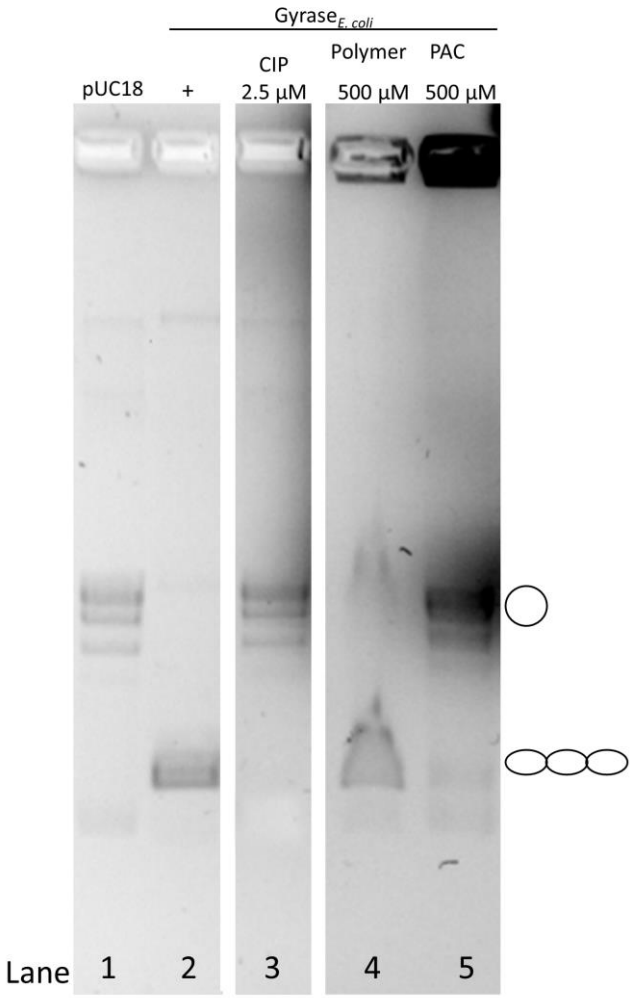

Figure 13: *Effect of different CIP (2.5 µM), PMOx$_{19}$-b-PHeptOx$_4$-EDA (500 µM) and PAC – PMOx$_{19}$-b-PHeptOx$_4$-EDA-xCIP (500 µM) concentrations on gyrase activity. Topoisomers were separated by electrophoresis on 1.3% agarose gels in TEP for 3.5 h at 55 V and 4 °C.*[179]

The enzyme was reconstituted by mixing the two subunits GyrA and GyrB[188-189] to study the inhibition of the gyrase. A mixture of the enzyme with CIP as a control and with the polymer PMOx$_{19}$-*b*-PHeptOx$_4$-EDA and with its xCIP conjugate was then prepared at a concentration of 500 µM. Incubation of the mixture was performed with relaxed pUC18 negatively supercoiled by gyrase in the presence of ATP. Relaxed and supercoiled species were separated according to their different electrophoretic mobilities by agarose gel electrophoresis (Figure 13). For complete inhibition of the gyrase, a CIP concentration of 2.5 µM was sufficient (Figure 13, lane 3).

Incomplete inhibition of gyrase activity by the POx-EDA-xCIP conjugate was observed at the highest possible concentration of 500 µM (Figure 13, lane 5). The

same polymer without CIP is not inhibitory at this high concentration. Thus, it is clear that conjugation of the polymer with CIP does not result in a higher affinity of the CIP function towards its bacterial targets. In fact, the inhibitory effect is reduced by two orders of magnitude. For several other POx-linked inhibitors, it had been previously shown that conjugation with POx does not significantly change the affinity for the respective target.[149, 190] It is therefore reasonable to assume that the xCIP structure is responsible for the altered interactions between the CIP unit and the cell target.

Nevertheless, the higher antimicrobial activity of amphiphilic PACs compared to CIP must find an explanation. A possible other alternative is a synergistically acting second pathway to kill bacterial cells. The membrane-destroying properties could be ruled out, thus another possibility that would lead to increased activity would be to increase the concentration of PACs in the bacterial cytoplasm. A higher concentration in the bacterial cytoplasm compared to CIP could be achieved if the PACs are not pumped out of the bacterial cells by the efflux pumps.

In previous work, the influence of efflux pumps on CIP and the conjugate activity of $PMOx_{30}$-EDA-xCIP was investigated by determining MIC values against *E. coli* wild-type cells and mutants with deactivated (JW0453) or overexpressed AcrAB-TolC efflux pumps (JW5503). Both compounds were shown to be affected by deactivation or overexpression of efflux pumps in the same manner. The MIC value decreases when the pumps are deactivated but increases when the pumps are overexpressed.

Thus, from the cells are transported by the AcrAB-TolC pumps, both CIP and its hydrophilic PMOx conjugates (see Figure 14a).[15] The same experiment was performed with selected amphiphilic PACs.

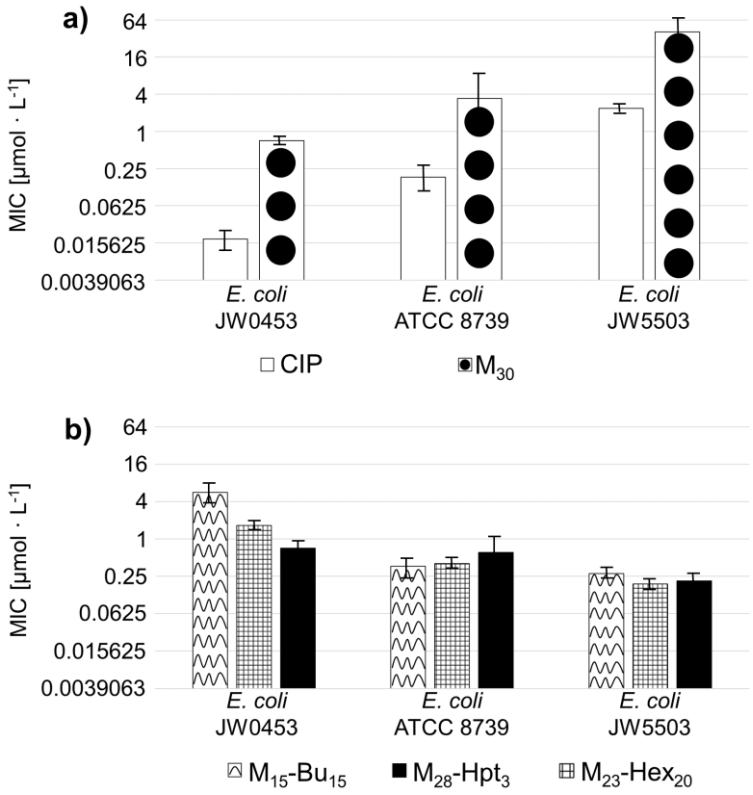

Figure 14: *Antimicrobial activity of CIP, xCIP and its POx-conjugates against E. coli ATCC 8739 and its mutants, JW0453 without AcrAB-TolC efflux pumps and JW5503 with overexpressed AcrAB-TolC efflux pumps. The MIC-values (reproduced) of CIP (empty) and PMOx$_{30}$-EDA-xCIP (dotted) are presented (The biological examinations and the method of examination were taken from the work of* MARTIN SCHMIDT[1]*) in a) and the MIC-values of PMOx$_{15}$-b-PBuOx$_{15}$-EDA-xCIP (waved, HHR =1, M$_{15}$-Bu$_{15}$), PMOx$_{23}$-b-PHexOx$_{20}$-EDA-xCIP (checkered, HHR = 1.15, M$_{23}$-Hex$_{20}$) and PMOx$_{28}$-b-PHeptOx$_{3}$-EDA-xCIP (full, HHR = 9.3, M$_{28}$-Hpt$_{3}$) are found in b). All measurements were performed at least in triplicate.*[176, 179] *The biological examinations (CIP, M$_{30}$) and biological method of examination were taken from the work of* MARTIN SCHMIDT[1]*.*

The amphiphilic PACs show little activity against the *E. coli* JW0453, but become more active with more efflux pumps expressed (Figure 14). This behavior is exactly the opposite of what was observed for CIP and PMOx$_{30}$-EDA-xCIP. So, it is clear that the effect is not due to the fact that CIP was modified and bound to a polymer, but to the amphiphilic nature of the POx tail.

Against the *E. coli* mutant JW0453 without efflux pumps, the PACs are over 10-fold less active than CIP. Thus, the higher HHR value, i.e., the increased hydrophilicity of the amphiphilic PACs leads to lower antimicrobial activity. The main reason for the high MIC values compared to CIP could be the results of the above activity assays.

However, the altered hydrophilicity could also affect membrane traversal. This suggests that the amphiphilic polymer adheres to the membrane rather than accumulating in the cytoplasm.

Surprisingly, the activity of amphiphilic PACs against *E. coli* wild type is almost as high as that of CIP against *E. coli* and up to ten times higher than that of hydrophilic PACs. This could be the first indication that the PACs cannot be pumped out of the cells so easily. As a consequence, the local concentration of amphiphilic PACs in the cytoplasm would be higher than with CIP, which would compensate for the lower target affinity of the PACs. However, the PACs are more active against the *E. coli* wild type than against the *E. coli* mutant without efflux pumps. Since both have the same target for the PACs, this allows only one conclusion: more PAC molecules are taken up into the wild type than into the JW0453 mutant. So, the membranes of *E. coli* cells become more permeable to amphiphilic PACs due to the presence of efflux pumps. It is possible that the amphiphilic conjugates enter the cells through the efflux pumps. An argument for this is provided by the last experiment. Here, the three amphiphilic PACs are tested against the *E. coli* mutant JW5503 with overexpressed efflux pumps. The results show that the amphiphilic PACs are more than 10-fold more active than CIP and 100-fold more active than the hydrophilic PMOx -EDA-xCIP. This clearly indicates that the amphiphilic character of the polymers is responsible for the excellent activity against bacterial cells with overexpressed efflux pumps.

One of the most important mechanisms of resistance to CIP is the overexpression of efflux pumps. Since overexpression of these pumps does not negatively affect amphiphilic PACs, it is possible that they have a lower potential to induce bacterial resistance. A modified MIC assay was used to investigate the development of bacterial resistance to the amphiphilic PACs $PMOx_{23}$-*b*-$PHexOx_{20}$-EDA-xCIP, $PMOx_{28}$-*b*-$PHeptOx_{3}$-EDA-xCIP, and $PMOx_{31}$-*b*-$POctOx_{6}$-EDA-xCIP. For this purpose, the bacterial cells grown at the highest possible antibiotic concentration (half the MIC) were collected after 24 hours and used for the next MIC assay. This procedure was repeated for at least 15 days or until MIC levels exceeded 200 µmol · L^{-1}. *S. aureus* and *E. coli* were selected as representative gram-positive and gram-negative test bacteria, respectively. The results are shown in comparison

with those of CIP and the hydrophilic PMOx$_{30}$-EDA-xCIP reported previously (Figure 15a).

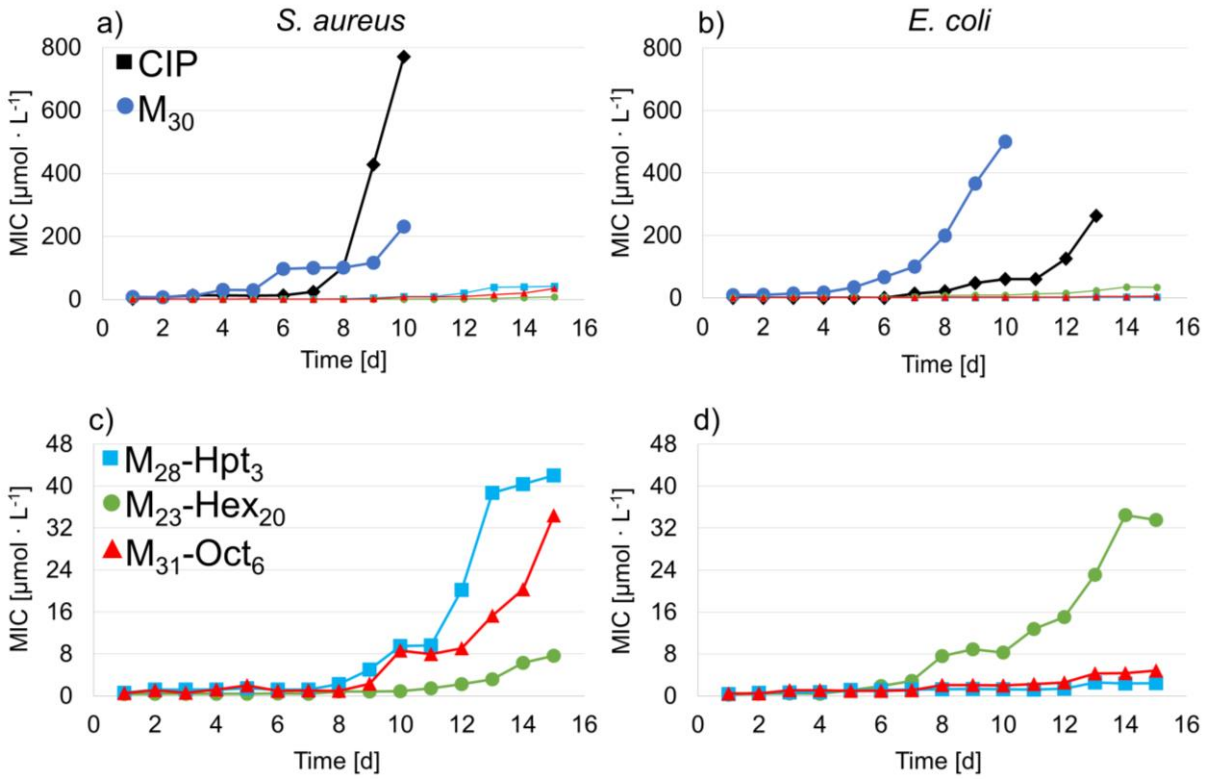

Figure 15: *Resistance test for the compounds CIP (black, reproduced), PMOx$_{30}$-EDA-xCIP (dark blue, reproduced), PMOx$_{23}$-b-PHexOx$_{20}$-EDA-xCIP (green, HHR = 1.15, M$_{23}$-Hex$_{20}$), PMOx$_{28}$-b-PHeptOx$_3$-EDA-xCIP (light blue, HHR = 9.3, M$_{28}$-Hpt$_3$), PMOx$_{31}$-b-POctOx$_6$-EDA-xCIP (red, HHR = 5.2, M$_{31}$-Oct$_6$) for a), c) S. aureus and b), d) E. coli, respectively. c) and d) are showing the data for the last three PACs in higher magnification.[176, 179] The biological examinations (CIP, M$_{30}$) and biological method of examination were taken from the work of MARTIN SCHMIDT[1].*

Figure 15a clearly shows that *S. aureus* cells become resistant to CIP and PMOx$_{30}$-EDA-xCIP after 10 days under the given conditions. After 10 days, the MIC$_{S.\ aureus}$ level is up to 620 times higher than the baseline level for CIP and 56 times higher for PMOx$_{30}$-EDA-xCIP. In contrast, *S. aureus* shows a very slow evolution of resistance to the amphiphilic PACs (Figure 15c). The MIC value of PMOx$_{28}$-*b*-PHeptOx$_3$-EDA-xCIP increases only by a factor of 210 to 42 µmol · L^{-1} after 15 days. The PAC PMOx$_{31}$-*b*-POctOx$_6$-EDA-xCIP, with a similar HHR but longer side chains exhibits similar behavior. In contrast, the MIC value for the hydrophobic PMOx$_{23}$-*b*-PHexOx$_{20}$-EDA-xCIP increases only 85-fold with a lower HHR value. It is important to note that the MIC$_{S.\ aureus}$ value of the latter amphiphilic PAC on the first day is ten times lower

than the $MIC_{S.\ aureus}$ value of CIP. Thus, the $MIC_{S.\ aureus}$ value of $PMOx_{28}$-*b*-$PHeptOx_3$-EDA-xCIP increases only by a factor of 3 after 15 days, during which the highest possible evolutionary pressure is exerted on the bacterium, in direct comparison with the activity of CIP against the non-resistant bacterium. Thus, to slow down the development of resistance in *S. aureus*, amphiphilic modification of CIP is a very efficient way. In this context, the PAC with the most hydrophobic character (lowest HHR value) shows the greatest potential.

A different response to resistance testing was observed for *E. coli* (see Figure 15b and d). From CIP, the $MIC_{E.\ coli}$ level increases from 0.10 to 262 µmol · L^{-1} within 13 days. This 2620-fold decrease in activity is significantly higher than for *S. aureus*. After as little as 10 days, the $MIC_{E.\ coli}$ of $PMOx_{30}$-EDA-xCIP increased from 5.33 to 400 µmol · L^{-1} (75-fold decrease in activity), indicating similar behavior to *S. aureus* as well as less pronounced resistance formation than CIP. The $MIC_{E.\ coli}$ value of $PMOx_{28}$-*b*-$PHeptOx_3$-EDA-xCIP increases from 0.61 to 2.48 µmol · L^{-1} after 15 days. Compared to the homopolymer $PMOx_{30}$-EDA-xCIP and CIP, the formation of resistance to this amphiphilic conjugate is much slower. While $MIC_{E.\ coli}$ levels of CIP increased by three orders of magnitude within 13 days, $MIC_{E.\ coli}$ of $PMOx_{28}$-*b*-$PHeptOx_3$-EDA-xCIP increased only by a factor of 4 after 15 days. The resistance-forming behavior of $PMOx_{31}$-*b*-$POctOx_6$-EDA-xCIP is also very similar, as the MIC value increases only by a factor of nine after 15 d. However, the most hydrophobic PAC $PMOx_{23}$-*b*-$PHexOx_{20}$-EDA-xCIP is an exception, as its MIC value increases 86-fold compared to the initial value. Again, the amphiphilic nature of the PAC is the key factor that greatly delays the formation of resistance in *E. coli* cells.

Depending on the respective structure of the amphiphilic conjugates, the formation of bacterial resistance is influenced (Fig. 15c and d). Thus, the mutations leading to this resistance are likely to be different and specific for the respective PAC.

Previous studies have shown that both CIP- and $PMOx_{30}$-EDA-xCIP-induced resistance are due to the same mutation in *S. aureus* topoisomerase IV. This leads to a structural change in the enzyme. However, $PMOx_{30}$-EDA-xCIP-resistant cells were found to be fully susceptible to CIP.[15] Presumably, CIP induces a secondary mutation that is not triggered by the PMOx conjugate. To investigate the effects of

the different mutations induced by the different conjugates, the resistant bacterial cells were tested for their susceptibility to CIP and to the conjugates. The results from Figure 16 clearly show that xCIP conjugation not only alters the rate of resistance formation, but most likely also the type of mutation.

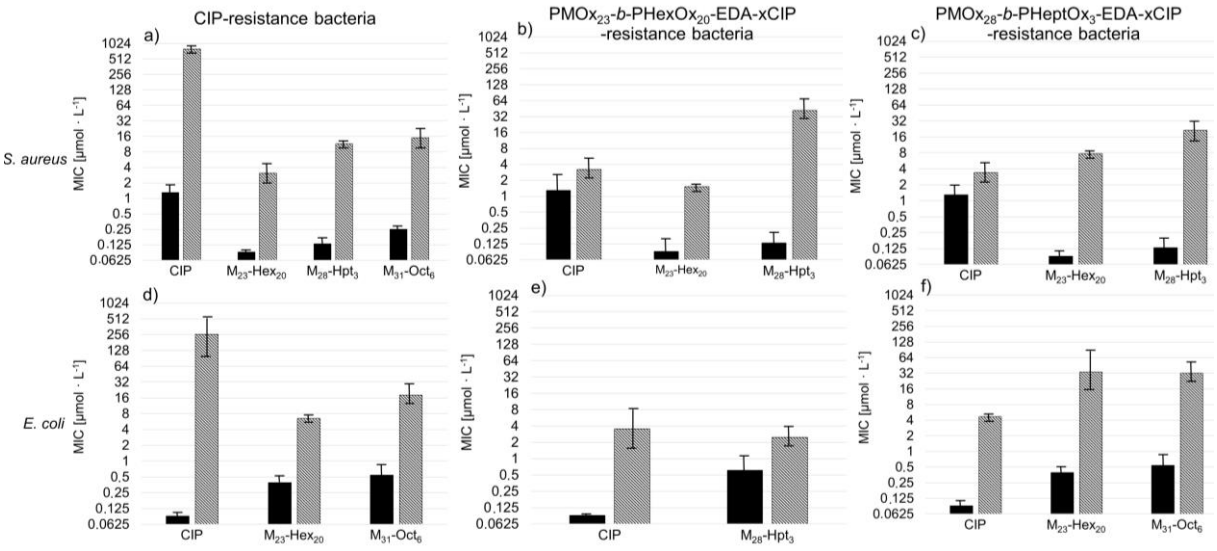

Figure 16: *Cross-Testing Matrix. MIC values of CIP and the conjugates PMOx$_{23}$-b-PHexOx$_{20}$-EDA-xCIP (M$_{23}$-Hex$_{20}$), PMOx$_{28}$-b-PHeptOx$_{3}$-EDA-xCIP (M$_{28}$-Hpt$_{3}$) and PMOx$_{31}$-b-POctOx$_{6}$-EDA-xCIP (M$_{31}$-Oct$_{6}$) for the different non-resistant bacteria cells (black) and resistant bacteria cells (striped). All measurements were performed at least in duplicate.[179] The biological method of examination was taken from the work of MARTIN SCHMIDT[1].*

The mutations of *S. aureus* and *E. coli* leading to CIP resistance show that the activity of the PACs against these CIP-resistant cells was also reduced compared to that against the non-resistant cells (Figure 16a and d). Nevertheless, the PACs show very good activities against the CIP-resistant bacterial cells. Among them, the amphiphilic PAC PMOx$_{23}$-*b*-PHexOx$_{20}$-EDA-xCIP can be highlighted as it is more than 100 times more active against the CIP-resistant *S. aureus* cells and still 30 times more active against CIP-resistant *E. coli* than the antibiotic itself. For the reason that the PACs still has such high activity against the CIP-resistant cells, they are an attractive alternative to CIP. This observation is likely due to the secondary resistance mechanism of CIP, the induction of efflux pump overexpression. As noted in previous studies, this resistance mechanism does not affect amphiphilic PACs in the same way as CIP. On the contrary, the PACs appear to utilize the efflux pumps to possibly penetrate bacterial cells better than CIP.

Conversely, resistance of *S. aureus* to amphiphilic PACs only slightly affects susceptibility to CIP (Figures 16b and c, factor 3 higher MIC value). So, mutations induced by PACs are different from those leading to CIP resistance. It is possible that these mutations are specific to the polymer rather than the CIP motif. In contrast, the *E. coli* mutants that have become resistant to the PACs are also resistant to CIP (Figure 16e and f). Thus, these induced mutations are more specific for the CIP motif. In summary, it is clear that conjugation of CIP with differentially structured POx is a powerful tool for influencing the activity of the antibiotic and slowing the development of resistance.

In the last step, the cell viability of mammalian cells after incubation with the amphiphilic PACs was investigated. This was tested on adherent human mesenchymal stem cells (hMSC) using the AlamarBlue assay. Mesenchymal stem cells are neither transformed cell lines nor immortalized cells, but represent primary progenitor cells that can be cultured over multiple passages. This cell type is instrumental in tissue regeneration and repair and can be found in various tissues such as fat, bone marrow, or muscle.[191] In addition, hMSC cells are highly diverse as they have a high differentiation capacity.[192-193]

The cell viability of hMSC after treatment with amphiphilic PACs at concentrations of 50, 100 and 200 µg · mL^{-1} for 24 hours is shown in Figure 17. In the tested concentration range, all PACs show a cell viability of at least 85%, thus the amphiphilic PACs do not exhibit cell toxic effects on hMSC cells. Only for the more hydrophilic PACs were tested at concentrations of 200 µg · mL^{-1} due to their solubility. Even the highest concentration does not lead to cytotoxicity in hMSC after 24 hours of incubation. These results are consistent with previous studies in which CIP-related toxicity to stem cells was found only at much higher concentrations.[194-195]

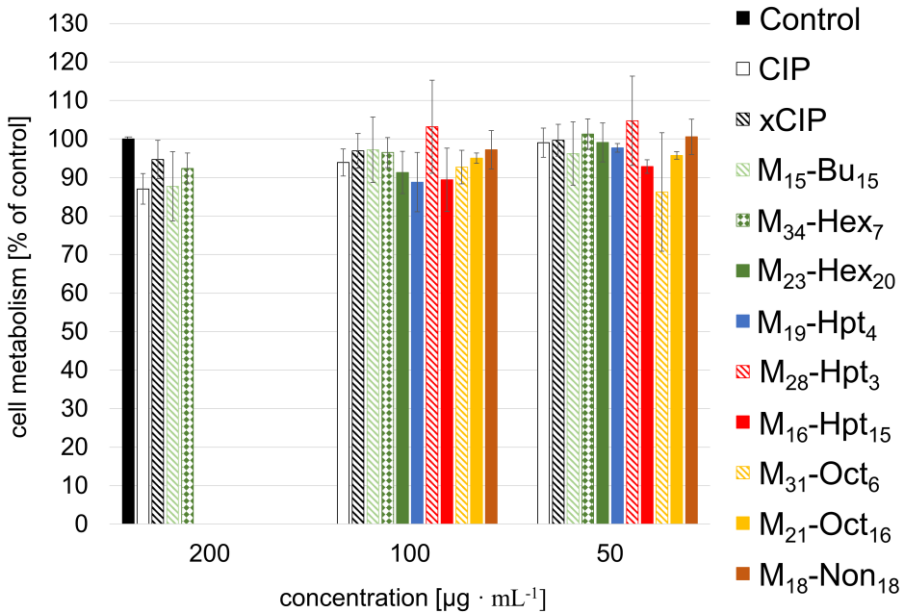

Figure 17: *AlamarBlue Assay with 1.5 x 10^4 adherent hMSC per mL treated with white: CIP, black striped: xCIP, blue: $PMOx_{15}$-b-$PBuOx_{15}$-EDA-xCIP (M_{15}-Bu_{15}), red striped: $PMOx_{34}$-b-$PHexOx_7$-EDA-xCIP (M_{34}-Hex_7), red: $PMOx_{23}$-b-$PHexOx_{20}$-EDA-xCIP (M_{23}-Hex_{20}), green striped: $PMOx_{19}$-b-$PHeptOx_4$-EDA-xCIP (M_{19}-Hpt_4), green checked: $PMOx_{28}$-b-$PHeptOx_3$-EDA-xCIP (M_{28}-Hpt_3), green: $PMOx_{16}$-b-$PHeptOx_{15}$-EDA-xCIP (M_{16}-Hpt_{15}), yellow striped: $PMOx_{31}$-b-$POctOx_6$-EDA-xCIP (M_{31}-Oct_6), yellow: $PMOx_{21}$-b-$POctOx_{16}$-EDA-xCIP (M_{21}-Oct_6) and brown: $PMOx_{18}$-b-$PNonOx_{18}$-EDA-xCIP (M_{18}-Non_{18}) in RMPI/FCS for 24 h.*[179]

In summary, it is clear that due to the ease of synthesis and variability of amphiphilic POx, a variety of new opportunities have opened up. Conjugation of CIP with amphiphilic POx block copolymers has shown not only to be an effective strategy to enhance the antimicrobial activity of the antibiotic, but also to slow down the development of resistance in bacterial strains *S. aureus* and *E. coli*. The amphiphilic character of the PACs plays a crucial role. Although this is responsible for a lower affinity towards the CIP target, the concentration of PACs in the cytoplasm is greatly increased by their entry into the cells through or with the help of efflux pumps. Even against CIP-resistant bacterial strains, the PACs show good antimicrobial activities, due to the overexpression of efflux pumps as a secondary resistance mechanism. The induced resistance mechanisms of the PACs prove to be specific for the HHB of the respective POx tail. Thus, conjugation of approved antibiotics with amphiphilic polymers is a feasible alternative to control the activity of these drugs and minimize resistance formation.

4.2 Amphiphilic Vitamin E-Polymer-Ciprofloxacin Conjugates

Further, amphiphilic block copolymers should be prepared consisting of two non-toxic blocks. As concluded in the previous section, PMOx is still suitable as a hydrophilic block due to its stealth properties, but a replacement must be found for the hydrophobic block. Vitamin E (VitE) is an excellent choice for this purpose, due to its hydrophobic properties and biocompatibility. But this cannot be polymerized as before because it is not a typical monomer for living cationic ring-opening polymerization. This molecule must be incorporated into the polymer in a different way, namely as an initiator. However, before vitamin E (VitE) can be used as an initiator for polymers, it must be modified at the hydroxyl group. For this purpose, 4-(bromomethyl)benzoyl bromide (BMB) was used for modification.[196] ^{1}H NMR analysis and ESI-MS are used to verify the success of this reaction.

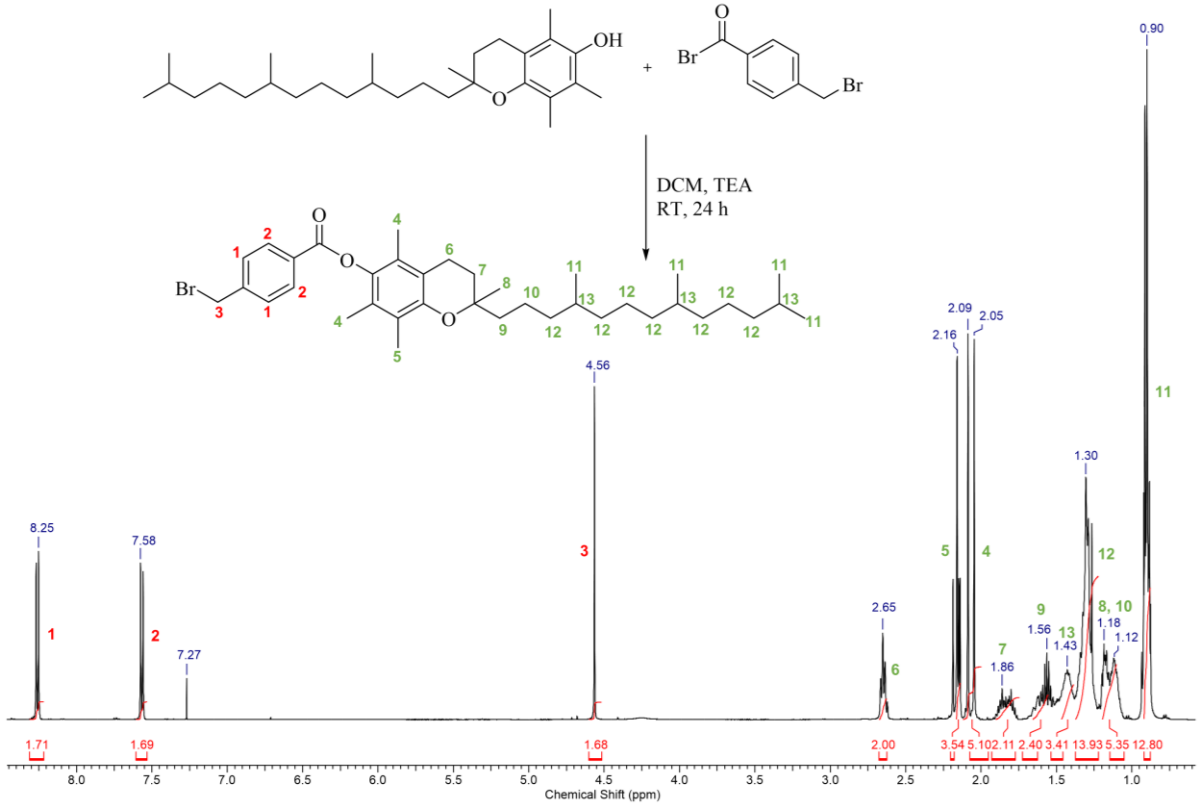

Figure 18: *Reaction of vitamin E with 4-(bromomethyl)benzoyl bromide in dichloromethane (DCM) at room temperature with addition of triethylamine (TEA) and ^{1}H NMR of vitamine E 4-(bromomethyl)benzoate (VitE-BMB) in $CDCl_3$ at 400 MHz.*[196]

Figure 18 shows also the results of the ^{1}H NMR analysis method. The signals of both vitamin E and 4-(bromomethyl)benzoate are clearly detected in the ^{1}H NMR spectrum without impurities. Nevertheless, the success of the nucleophilic substitution cannot be proven with certainty using this method, which is why an ESI-MS spectrum of this compound were also measured (Fig.19).

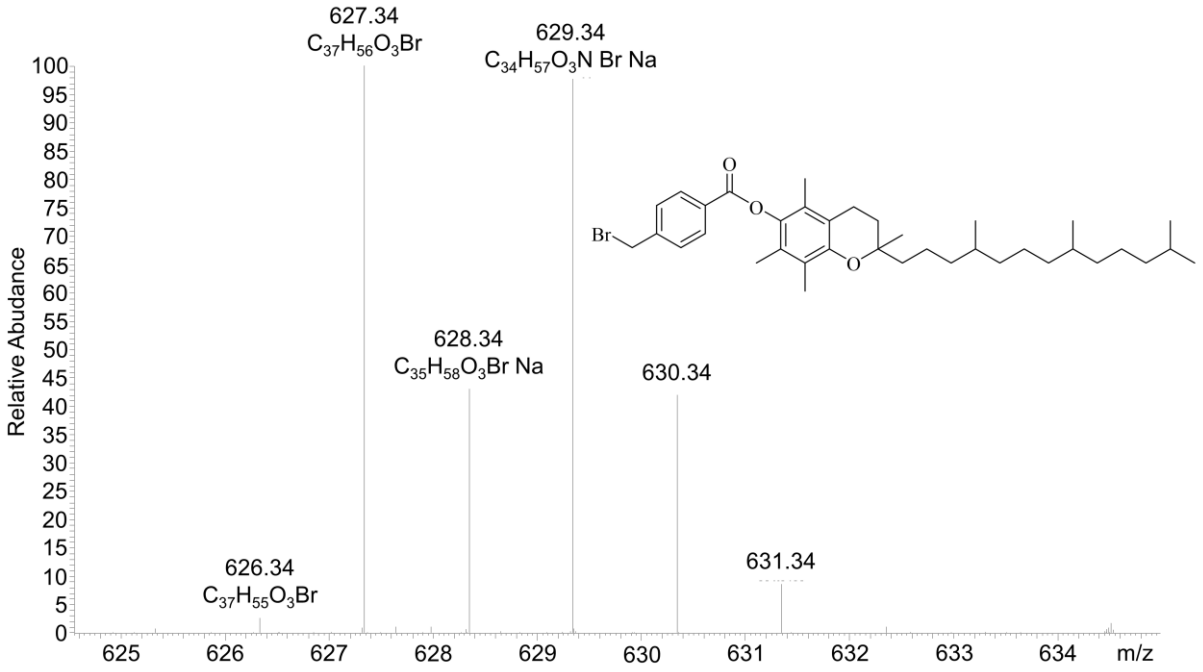

Figure 19: *ESI-MS of vitamine E 4-(bromomethyl)benzoate (VitE-BMB).*

This analytical method also confirms the bond between the two molecules, so that a molar mass of 626.34 g/mol and the ionised form ($[M+H]^{+}$) of 627.34 g/mol can be detected. Thus, it can be assumed that the synthesis of vitamine E 4-(bromomethyl)benzoate (VitE-BMB) could be carried out successfully and a clean product in the form of a yellow honey-like liquid could be produced.

Furthermore, this product was used as a polymer starter for a living cationic ring-opening polymerisation. In order to produce a polymer that is as amphiphilic as possible, the polymerisation was carried out with 2-methyl-2oxazoline (MOx) as can be seen below (Fig. 20). Using ^{1}H NMR spectroscopy, it was found that a PMOx started with VitE-BMB could be synthesised with a high purity. All signals in the ^{1}H NMR spectrum can be assigned to the expected polymer structure, indicating that polymer chains were successfully started with VitE-BMB and functionalized with EDA. The red numbers indicate the signals of VitE-BMB and show that both the alkyl

chain (signals 12-16) and the aromatic (signals 5 and 6) are intact and still very visible in the ^{1}H NMR. In addition, signal 4 shows a shift from 4.56 ppm to 4.76 ppm, indicating that the bromine is no longer present and has been replaced by another molecule. This signal thus confirms the successful binding to the PMOx polymer and exhibits an integral of 1.97, which also fits the two protons present. The analysis of the obtained ^{1}H NMR spectrum results in a degree of polymerization of 30 suggesting quantitative conversion (green signals). The integral of EDA shows a value of 5.89 and corresponds to a termination of 98%. GPC measurements were carried out to check the polydispersion index. A polydispersion index of Đ = 1.17 was determined for the polymer shown, which corresponds to a living polymerisation.

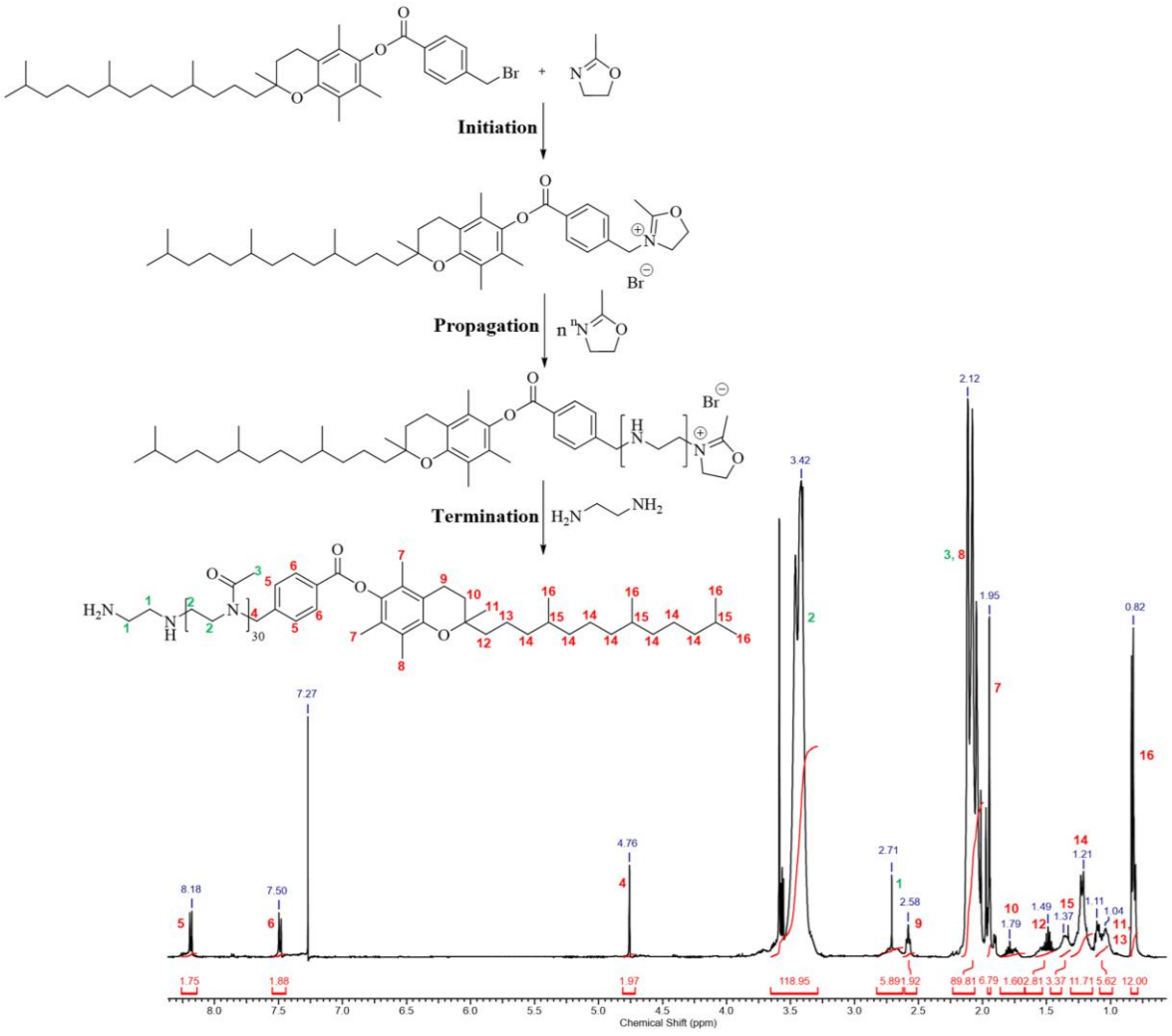

Figure 20: *Schematic overview of the living cationic ring-opening polymerisation of 2-methyl-2-oxazoline started with VitE-BMB and ^{1}H NMR spectrum of VitE-BMB-PMOx$_{30}$-EDA recorded in $CDCl_3$ at 400 MHz.*

In addition to ^{1}H NMR spectroscopy, MALDI-TOF measurements were also performed to further characterise the polymer (Fig. 21). The found m/z values correlate with the expected masses of the polymer VitE-BMB-PMOx$_{30}$-EDA with potassium as the counterion (blue). The spectrum clearly shows a second generation (40%) of signals, which also exhibits a polymer started with vitamin E. However, here the counterion is a proton, which also occurs as a possibility due to the addition of acid (orange). Based on the spectrum, transfer or termination reactions during polymerization can be excluded, since both generations to be detected show the desired product. Thus, the MALDI underscores the results from Figure 20 and confirms the successful synthesis of the polymers started with vitamin E.

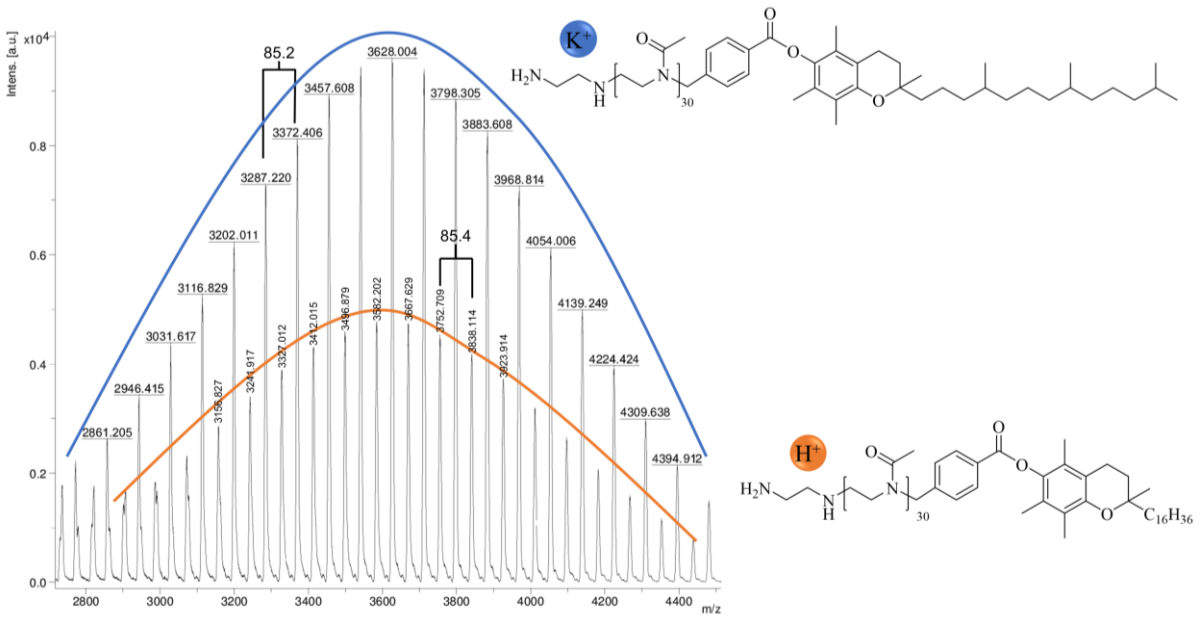

Figure 21: *MALDI-TOF of the polymer VitE-BMB-PMOx$_{30}$-EDA.*

As the GPC measurement has already shown, the polymerisation corresponds to a living character. The new initiator must therefore fulfil the conditions of a living cationic ring-opening polymerisation. For this purpose, the propagation rate constant of 2-methyl-2-oxazoline must be determined. This is important for the living, ring-opening polymerisation of 2-R-oxazolines because individual polymer blocks should be synthesised that are as defined as possible. It must be ensured that a high conversion of monomer takes place during polymerisation and thus the set ratio of monomer to initiator in the form of the degree of polymerisation (DP) is achieved. For this purpose, the initiator vitamine E 4-(bromomethyl)benzoate (VitE-BMB) was used. Starting from a polymerisation batch, samples were taken at regular intervals and

immediately analysed by ^{1}H NMR spectroscopy. The reaction follows second-order reaction kinetics during propagation. A monomer always reacts with a living chain end. Provided that no termination and transfer reactions occur during polymerisation, the concentration of active chain ends is constant over the course of the reaction.[197] With these assumptions, the reaction order can be formally reduced to a pseudo-first order reaction, which only depends on the concentration of residual monomer and the reaction time. Table 3 shows the polymerization time and temperature used and the calculated conversion. Here, the conversion was calculated using the samples taken from the ^{1}H NMR, more precisely from the ratio of monomer to polymer.

Table 3: *Polymerisation times and temperatures during the polymerisation of MOx and the determined turnovers of the respective monomer.*

Polymer	Time [min]	Temperature [°C]	Turnover [%]
VitE-BMB-PMOx	0	RT	0
VitE-BMB-PMOx	30	110	23
VitE-BMB-PMOx	60	110	81
VitE-BMB-PMOx	120	110	95
VitE-BMB-PMOx	180	110	99

By plotting $\ln(c_{M,0}/c_M)$ against time, the propagation rate constant k_p is determined from the slope of the compensation line. Figure 22 thus shows that there is a linear relationship between $\ln(c_{M,0}/c_M)$ and the reaction time, i.e. the conditions of living cationic ring-opening polymerisation are fulfilled. The calculated propagation rate constant of the polymerisation shown is $3.19 \cdot 10^{-3} \pm 1.32 \cdot 10^{-4}$.

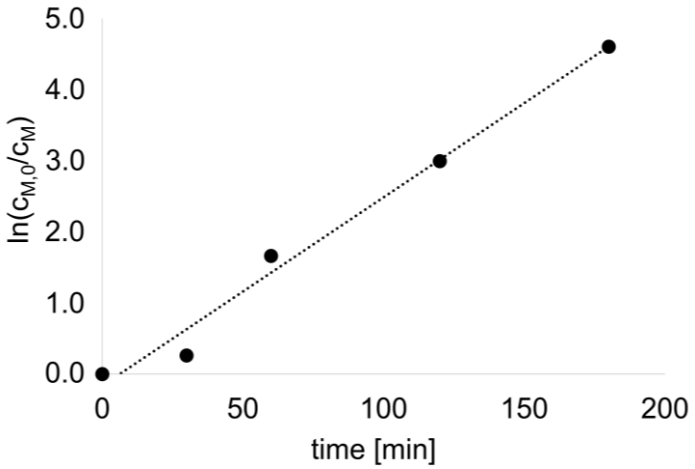

Figure 22: *Plot of the determined $\ln(c_{M,0}/c_M)$ values against the reaction time t to determine the reaction rate constants of the polymerisation of MOx initiated with VitE-BMB in deuterated acetonitrile.*

In addition, MOx-based polymers of different lengths were prepared with the VitE initiator and subsequently conjugated with ciprofloxacin to generate antimicrobially active PACs. Table 4 summarizes the analytical data of all polymer-antibiotic conjugates produced.

Table 4: *Analytical data of amphiphilic PACs characterized by ^{1}H NMR spectroscopy.*

PAC[a]	$M_{n,NMR}$ [g·mol^{-1}]	Đ	F^d_{NMR}[b]	Term
VitE-BMB-PMOx$_{10}$-EDA	1500	1.12	98%	VP$_{10}$
VitE-BMB-PMOx$_{22}$-EDA	2300	1.14	97%	VP$_{25}$
VitE-BMB-PMOx$_{30}$-EDA	3200	1.17	97%	VP$_{30}$
VitE-BMB-PMOx$_{56}$-EDA	5200	1.19	99%	VP$_{56}$
VitE-BMB-PMOx$_{90}$-EDA	8300	1.19	98%	VP$_{90}$
VitE-BMB-PMOx$_{11}$-EDA-xCIP	2100	1.16	83%	VitE-PMOx$_{11}$
VitE-BMB-PMOx$_{23}$-EDA-xCIP	3100	1.17	90%	VitE-PMOx$_{23}$
VitE-BMB-PMOx$_{31}$-EDA-xCIP	3800	1.19	94%	VitE-PMOx$_{31}$
VitE-BMB-PMOx$_{56}$-EDA-xCIP	5900	1.21	97%	VitE-PMOx$_{56}$
VitE-BMB-PMOx$_{90}$-EDA-xCIP	8700	1.24	90%	VitE-PMOx$_{90}$

[a]Degree of polymerization determined by ^{1}H NMR spectroscopy via comparison of the respective signals caused by the initiating group and the signals caused by the protons of the polymer backbone.
[b]Degree of functionalization determined by ^{1}H NMR spectroscopy via comparison of the respective signals caused by the initiating and the terminal CIP groups.

The antibacterial activity of the amphiphilic PACs against a number of clinically relevant infectious and pathogenic bacterial strains (*S. aureus*, *E. coli*, *K. pneumonia, P. aeruginosa*) was determined using the minimal inhibitory concentration (MIC$_{99}$) test. The MIC value in our setup corresponds to the concentration at which 99% of the bacteria are inhibited in growth. This value is compared with the MIC value of CIP. In addition, the respective EDA-terminated polymers show no antimicrobial activity against any microbial strain (MIC > 500 µg · mL^{-1} in all cases).

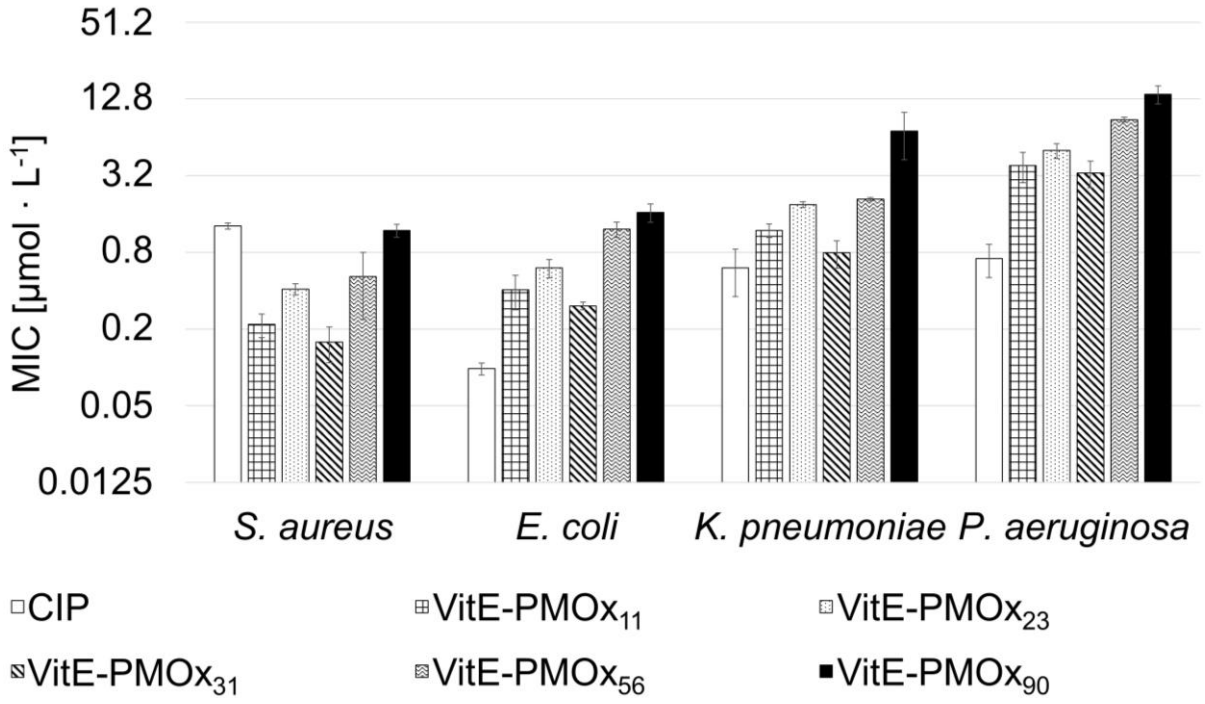

Figure 23: *MIC values of ciprofloxacin (white), checkered: VitE-BMB-PMOx$_{11}$-EDA-xCIP (VitE-PMOx$_{11}$), dotted: VitE-BMB-PMOx$_{23}$-EDA-xCIP (VitE-PMOx$_{23}$), striped: VitE-BMB-PMOx$_{31}$-EDA-xCIP(VitE-PMOx$_{31}$), waved: VitE-BMB-PMOx$_{56}$-EDA-xCIP (VitE-PMOx$_{56}$), black: VitE-BMB-PMOx$_{90}$-EDA-xCIP (VitE-PMOx$_{90}$). Values are expressed as mean ± SD (n = 3). The biological examinations (CIP) and biological method of examination were taken from the work of* MARTIN SCHMIDT[1].

The amphiphilic VitE-BMB-PMOx-EDA-xCIP conjugates exhibit high antimicrobial activities against all bacterial strains tested (Figure 23). In addition, all tested PACs have much higher antimicrobial activity than the homopolymer Me-PMOx$_{31}$-EDA-xCIP.[15] Compared to the gram-positive bacterial strain *S. aureus*, the PAC VitE-BMB-PMOx$_{31}$-EDA-xCIP (0.16 ± 0.04 μmol·L^{-1}) has up to 8 times better antimicrobial activity than CIP. Even the longest conjugate with 90 repeat units of PMOx has as good an antimicrobial effect (1.19 ± 0.14 μmol·L^{-1}) as ciprofloxacin. Against the gram-negative bacterial strains, none of the PACs produced exhibited much higher antimicrobial activity than CIP. Nevertheless, a clear trend can be seen, because the conjugate VitE-BMB-PMOx$_{31}$-EDA-xCIP shows a better antimicrobial effect than the other compositions in all cases. This conjugate has the same antimicrobial activity (0.79 ± 0.19 μmol·L^{-1}) against *K. pneumoniae* as the unreacted CIP. This excellent antimicrobial effect can be explained by the micellation[198] of the conjugates. As already mentioned, vitamin E promotes micelle formation, which is why the

conjugates can form stable micelles (Fig.24) and can thus enter the bacterial cell more easily.

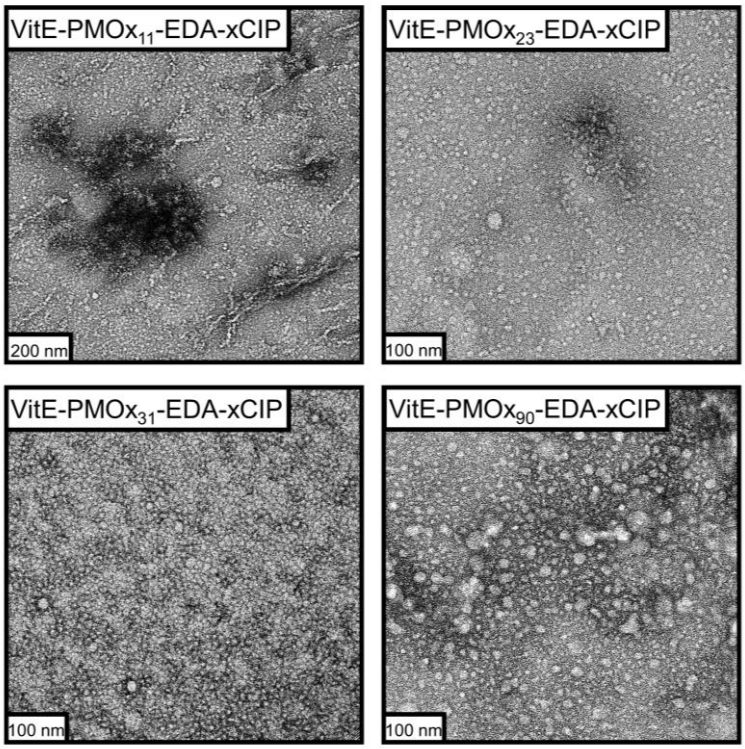

Figure 24: *Transmission electron microscopy (TEM) images of the block copolymers VitE-PMOx$_{11}$-EDA-xCIP, VitE-PMOx$_{23}$-EDA-xCIP, VitE-PMOx$_{31}$-EDA-xCIP and VitE-PMOx$_{90}$-EDA-xCIP.*

The study of the critical micelle formation concentration (CMC) of the PACs also revealed that the micelles formed very differently, at concentrations ranging from $2.2 \cdot 10^{-2}$ mol·L^{-1} to $3.1 \cdot 10^{-5}$ mol·L^{-1} (Fig.25). This result was also expected, because the amphiphilic conjugates with a smaller molar mass, VitE-PMOx$_{11}$-EDA-xCIP and VitE-PMOx$_{31}$-EDA-xCIP formed stable micelles quite rapidly. The VitE-PMOx$_{56}$-EDA-xCIP conjugate, on the other hand, has a very long polymer tail, so that it tends to wrap around the hydrophobic components of the conjugate. This results in micelle-like aggregates with a hydrophobic core and a hydrophilic tangle around it, which also form quite late.

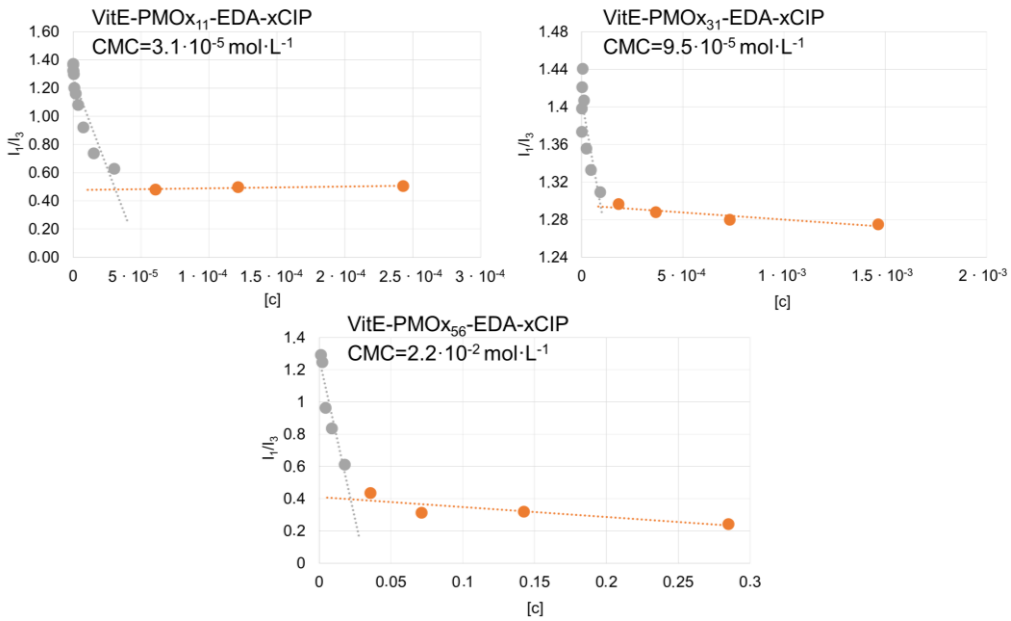

Figure 25: *Measurement of the critical micelle formation concentration of VitE-PMOx$_{11}$-EDA-xCIP, VitE-PMOx$_{31}$-EDA-xCIP and VitE-PMOx$_{56}$-EDA-xCIP using a fluorescence spectrometer.*

Apparently, an optimal balance between the hydrophobic VitE and hydrophilic PMOx must exist in order to form stable micelles. However, an increase in the molar mass also shows a deterioration in the antimicrobial effect, as can be seen in Figure 26.

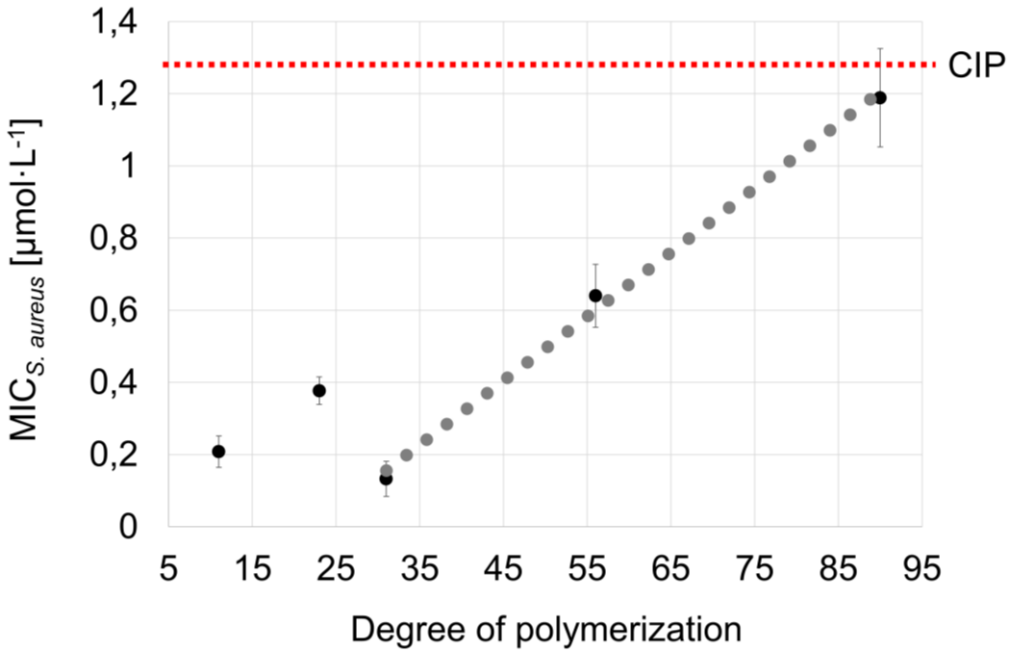

Figure 26: *Degree of polymerization against the MIC$_{S.\ aureus}$ value [µg·mL^{-1}] for VitE-BMB-PMOx$_{11}$-EDA-xCIP (VitE-PMOx$_{11}$), VitE-BMB-PMOx$_{23}$-EDA-xCIP (VitE-PMOx$_{23}$), VitE-BMB-PMOx$_{31}$-EDA-xCIP(VitE-PMOx$_{31}$), VitE-BMB-PMOx$_{56}$-EDA-xCIP (VitE-PMOx$_{56}$), VitE-BMB-PMOx$_{90}$-EDA-xCIP (VitE-PMOx$_{90}$). Values are expressed as mean ± SD (n = 3).*

However, this trend was also expected and is consistent with the relationship between molar mass and antimicrobial activity studied in previous work.[17, 179] In addition, it is clear that a plateau forms in the range of small molar masses and that the antimicrobial effect of the PACs remains approximately the same. This can also be justified by the similar micelle size of these PACs. Previously conducted studies have shown that VitE-PMOx$_{23}$ and VitE-PMOx$_{31}$ have somewhat the same micelle size, allowing them to enter the bacterial cell equally well and thus leading to the similar antimicrobial activity. Thus, a deterioration of the antimicrobial activity only occurs from a polymer repeat unit of more than 30.

As shown, amphiphilic VitE-PACs are more active than CIP, for this reason there must be a second synergistic pathway to kill bacterial cells. As shown in previous work, the increase in concentration of PACs in bacterial cytoplasm compared to CIP can be achieved when PACs are not pumped out of bacterial cells by efflux pumps. Previously, the effect of these efflux pumps on CIP and PMOx$_{30}$-EDA-xCIP was investigated by determining MIC levels against *E. coli* wild-type cells and mutants with deactivated (JW0453) or overexpressed AcrAB-TolC efflux pumps (JW5503). Both compounds are affected by deactivation or overexpression of efflux pumps in the same way, so that both CIP and its hydrophilic PMOx conjugates are transported out of the cell by AcrAB-TolC pumps.[179] In addition, the fully synthetic amphiphilic PACs based on hydrophobic poly(2-oxazoline)s were shown to exhibit exactly the opposite effect. Against the *E. coli* JW0453, these PACs were 30 times less active than CIP and 10 times more active against the *E. coli* JW5503.[179] The same experiment was performed with an amphiphilic VitE PAC.

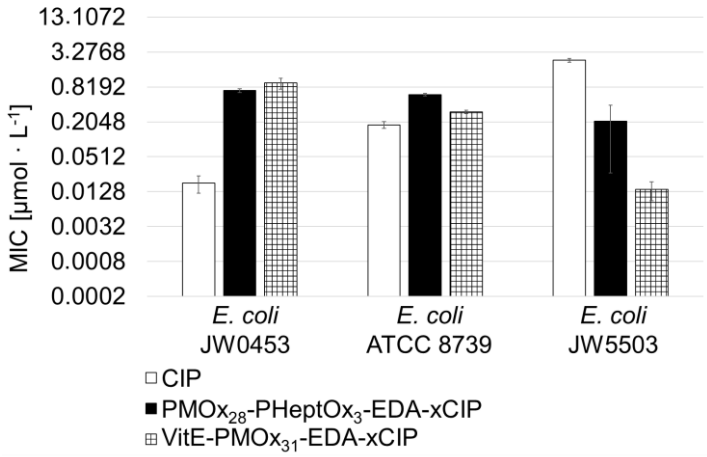

Figure 27: *Antimicrobial activity of CIP, $PMOx_{28}$-$PHeptOx_3$-EDA-xCIP and VitE-$PMOx_{31}$-EDA-xCIP (VitE-$PMOx_{31}$) against E. coli ATCC 8739 and its mutants, JW0453 without AcrAB-TolC efflux pumps and JW5503 with overexpressed AcrAB-TolC efflux pumps. The MIC-values (reproduced) of CIP (white), xCIP (striped) and VitE-$PMOx_{31}$-EDA-xCIP (checkered). All measurements were performed at least in triplicate. Values are expressed as mean ± SD (n = 3).*

As can be seen in Figure 27, VitE-$PMOx_{31}$ shows good activity against JW0453, but becomes more active as more efflux pumps are expressed. This behavior is exactly the opposite of that observed for CIP and the hydrophilic PAC $PMOx_{30}$-EDA-xCIP, but is consistent with the behavior from the fully synthetic PACs.[179] Thus, the effect is not due to the fact that CIP is modified and bound to a polymer, but to the amphiphilic nature of the POx tail. The VitE-$PMOx_{31}$ shows up to 50 times less active against the *E. coli* JW0453 bacteria than the CIP. In contrast, it is up to 170 times higher active than CIP against the bacteria with overexpressed efflux pumps and up to 14 times better compared to M_{28}-Hpt_3.[179] The trend is clearly the same as for the previously studied amphiphilic PACs based on hydrophobic and hydrophilic poly(2-oxazoline)s.[179] The antimicrobial effect is weakest against the mutant *E. coli* with deactivated AcrAB-TolC efflux pumps and increases simultaneously with the increase in efflux pumps. Thus, this implies that more PAC molecules are taken up into the wild type than into the mutant JW0453. Thus, the presence of efflux pumps in *E. coli* cells makes their membranes more permeable to the amphiphilic PACs, allowing them to enter the cells through the efflux pumps. The morphology of VitE-$PMOx_{31}$ also contributes very much to the very high antimicrobial activity, as these PACs can form stable micelles, as already shown. These micelles can efficiently enter the bacterial cell and even use the efflux pumps as an entry gate.

Although efflux pump overexpression is one of the major resistance mechanisms of bacterial cells to CIP, there is a possibility that the VitE-PMOx$_{31}$ has a lower potential to induce bacterial resistance. The development of bacterial resistance to the amphiphilic PAC VitE-PMOx$_{31}$ was determined using a modified MIC assay. In addition, the mixture of non-covalently bound VitE-PMOx$_{31}$ and CIP was investigated with regard to the potential for resistance formation and to examine a synergistic effect in this regard. For this purpose, bacterial cells grown at the highest possible antibiotic concentration (half of the MIC) were collected after 24 hours and used for the next MIC test. This procedure was repeated for at least 18 days or until MIC levels were above 200 μmol·L^{-1}. *S. aureus* and *E. coli* were selected as representative gram-positive and gram-negative test bacteria. Results are shown in comparison with those of CIP and the hydrophilic PMOx$_{30}$-EDA-xCIP reported previously (Figure 28a-b).

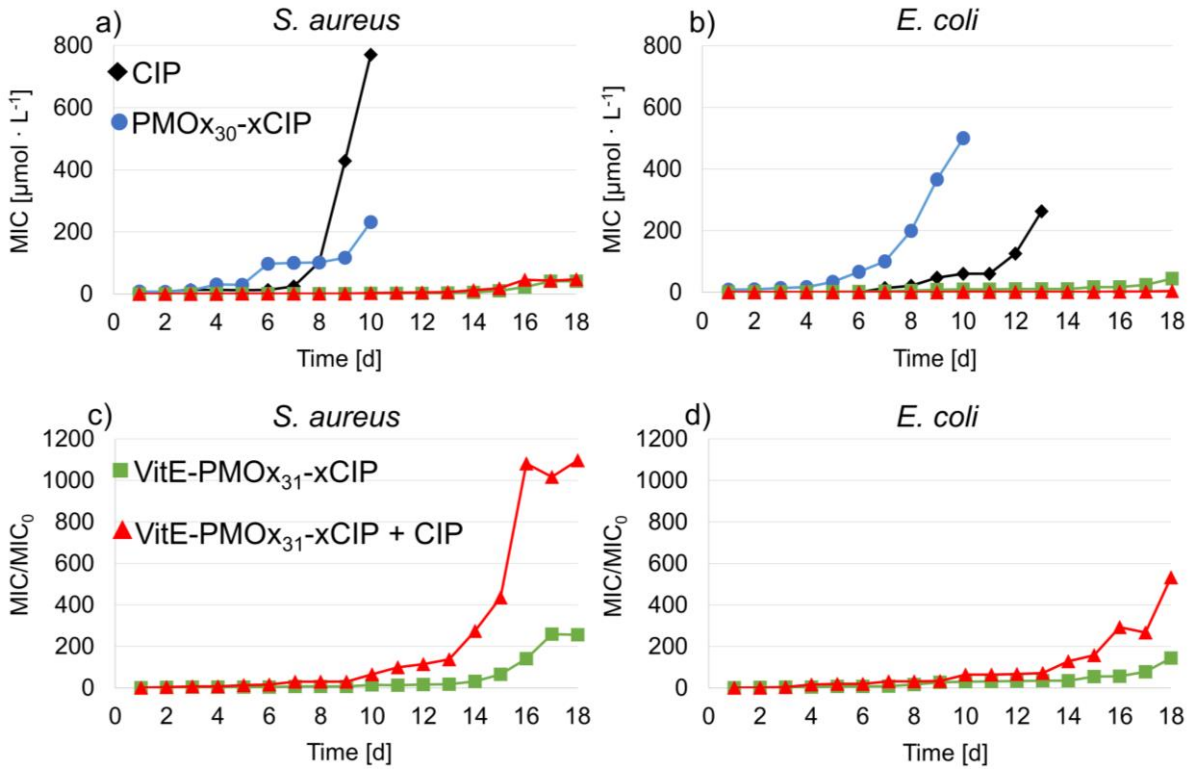

Figure 28: *Resistance test for the compounds VitE-PMOx$_{31}$-EDA-xCIP (green, VitE-PMOx$_{31}$) and VitE-PMOx$_{31}$-EDA-xCIP with unbound CIP (red, VitE-PMOx$_{31}$) (in a ratio of molar 1:1, MIC was based on the molar mass of VitE-PMOx$_{31}$) for a) S. aureus and b) E. coli, respectively. a) and b) are showing the data for the last three PACs in higher magnification. Values are expressed as mean ± SD (n = 3). The biological examinations (CIP, PMOx$_{30}$-xCIP) and biological method of examination were taken from the work of MARTIN SCHMIDT[1].*

Figure 28 shows that after 13 days at the latest, *S. aureus* and *E. coli* have built up resistance to CIP and after 10 days to $PMOx_{30}$-EDA-xCIP. After 10 days, the $MIC_{S.\ aureus}$ value is up to 620 times higher against CIP and up to 56 times higher against $PMOx_{30}$-EDA-xCIP than at the beginning of this test series (Fig. 28a). A different response to resistance formation was observed in *E. coli* (Fig. 28b). The $MIC_{E.\ coli}$ value of CIP increases 2620-fold, this extreme drop in activity is extremely higher than in *S. aureus*. The $MIC_{E.\ coli}$ value of $PMOx_{30}$-EDA-xCIP increases from 5.33 to 400 $\mu mol \cdot L^{-1}$ (75-fold decrease in activity) after 10 d, indicating less pronounced resistance formation than CIP and similar behavior to *S. aureus*.

The development of resistance to VitE-PMOx31 after 18 days of *S. aureus* shows that a MIC/MIC_0 value of 265 is achieved, as can be seen in Figure 28c. In contrast, VitE-$PMOx_{31}$ with unbound CIP (molar ratio of 1:1) clearly shows that the MIC/MIC_0 value increases to 1096 after 18 days. Thus, the addition of CIP to VitE-$PMOx_{31}$ has no influence on the development of resistance in contrast to pure VitE-$PMOx_{31}$. A look at Figure 28d shows the same effect. This shows the development of resistance to VitE-$PMOx_{31}$ after 18 days of *E. coli*, which reaches a MIC/MIC_0 value of 144. VitE-$PMOx_{31}$ with unbound CIP (molar ratio of 1:1) has a MIC/MIC_0 value of 533 after 18 days. Therefore, the addition of CIP to VitE-$PMOx_{31}$ has no influence on the development of resistance in contrast to pure VitE-$PMOx_{31}$. Furthermore, it is even clear that the addition of free CIP to VitE-$PMOx_{31}$ actually accelerates the development of resistance in both bacteria.

Nevertheless, a synergistic effect between CIP and VitE-$PMOx_{31}$ can be recognized. Against *S. aureus*, CIP has an MIC value of 1.3 $\mu mol \cdot L^{-1}$ and VitE-$PMOx_{31}$ has an MIC value of 0.2 $\mu mol \cdot L^{-1}$. The mixture of VitE-$PMOx_{31}$ with unbound CIP shows an MIC value of 0.04 $\mu mol \cdot L^{-1}$. The MIC value of the mixture was related to the molar mass of VitE-$PMOx_{31}$ to obtain the molar MIC. This synergistic effect can also be seen with *E. coli*. Here, CIP has an MIC value of 0.09 $\mu mol \cdot L^{-1}$ and VitE-$PMOx_{31}$ has an MIC value of 0.3 $\mu mol \cdot L^{-1}$. The mixture of VitE-$PMOx_{31}$ with unbound CIP shows an MIC value of 0.008 $\mu mol \cdot L^{-1}$. This shows a significant increase in the antimicrobial effect of VitE-$PMOx_{31}$ through the addition of unbound CIP.[32, 199-200] It should be noted that CIP is much more active against *E. coli* and therefore the MIC values of the mixtures should be related to the total CIP concentration, i.e. the current value

multiplied by two. For example, the mixture of VitE-PMOx$_{31}$ with unbound CIP would result in a corrected MIC value of 0.008 μmol·L^{-1} · 2 = 0.016 μmol·L^{-1}. Here, the correction was not incorporated into all MIC values, but only shown for one value as an example.

As already known, both CIP- and PMOx$_{30}$-EDA-xCIP-induced resistance lead to a mutation in *S. aureus* topoisomerase IV, i.e., a structural change in the enzyme. In addition, amphiphilic PACs consisting of hydrophilic and hydrophobic poly(2-oxazolines) were shown to still exhibit high antimicrobial activity against CIP-resistant bacteria. This also confirms the theory that the increased formation of efflux pumps by the bacteria facilitates the penetration of the PACs into the bacterial cell.[15] Here, the resistant bacterial cells were also tested for their susceptibility to CIP and the VitE conjugate. The matrix shown in Figure 29 clearly demonstrates that the VitE-PMOx$_{31}$-EDA-xCIP not only alters the rate of resistance formation, but most likely also the nature of the mutation.

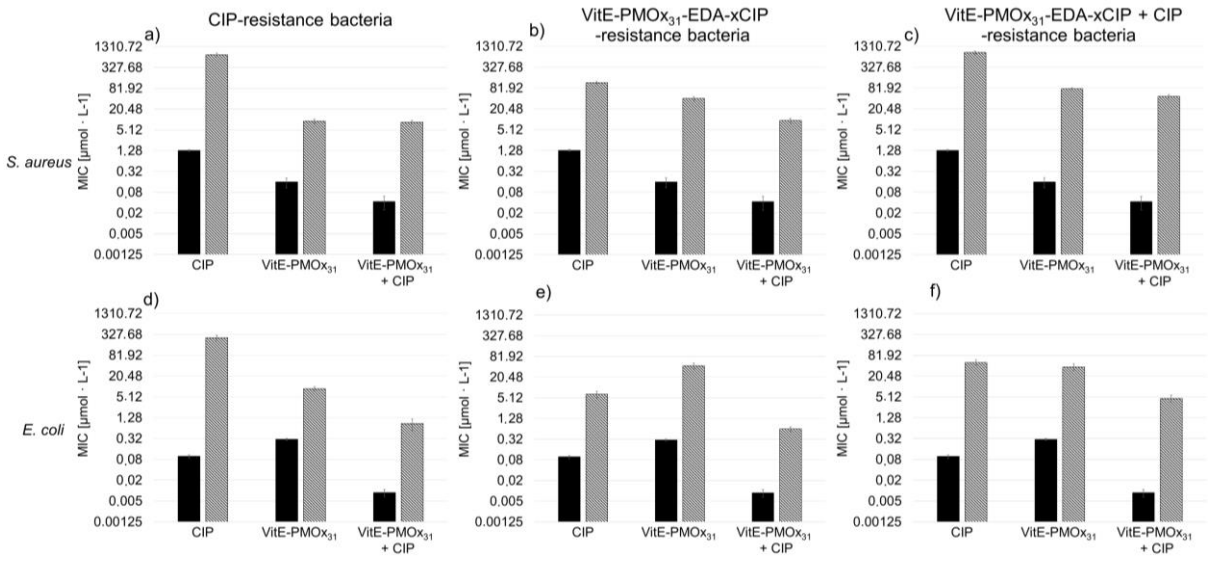

Figure 29: *Cross-testing matrix with MIC values of CIP and the conjugate VitE-PMOx$_{31}$-EDA-xCIP and the mixture VitE-PMOx$_{31}$-EDA-xCIP with CIP (molar ratio of 1:1, MIC was based on the molar mass of VitE-PMOx$_{31}$) for the different non-resistant bacteria cells (black) and resistant bacteria cells (striped). Values are expressed as mean ± SD (n = 3). The biological method of examination was taken from the work of MARTIN SCHMIDT[1].*

Although Figure 29a and d shows that the mutations leading to CIP resistance also reduce the activity of the PAC and the mixture of PAC and CIP, both are still very

active against the CIP-resistant bacteria. The antimicrobial activity is more than 90 times more active against the CIP-resistant *S. aureus* cells and still 30 times more active against CIP-resistant *E. coli* than the antibiotic itself. Thus, this effect is most likely also due to the fact that CIP induces the overexpression of efflux pumps as a secondary resistance mechanism and the amphiphilic PAC increasingly uses these efflux pumps as a gate of entry into the bacterial cells. Thus, as shown above, VitE-PMOx$_{31}$-EDA-xCIP is not affected by the CIP-induced resistance mechanism in the same way.

A closer look at Figure 29b and e reveals that the *S. aureus* and *E. coli* mutants that have become resistant to the PAC are also resistant to CIP by a factor of 80. Apparently, the mutations induced by the PAC in the two bacterial strains are also specific for the CIP motif. In addition, CIP also exhibits poor MIC values against the bacteria that have become resistant to the mixture of VitE-PMOx$_{31}$-EDA-xCIP and CIP (Figure 29c and f). However, this was also to be expected, since the CIP in the mixture induces the same resistances against which CIP tries to act. Nevertheless, these examples show that conjugation of CIP with VitE and POx is a powerful tool for influencing the activity of the antibiotic and slowing the development of resistance.

Thus, these amphiphilic VitE-PACs show similar trends to fully synthesized amphiphilic conjugates presented in the previous chapter.[179] The crucial difference is in the hydrophobic group, vitamin E. Vitamin E is a naturally occurring molecule in the environment[201-203] and replaces here the synthetically produced hydrophobic groups poly(2-butyl-2-oxazoline), poly(2-hexyl-2-oxazoline), poly(2-heptyl-2-oxazoline), poly(2-octyl-2-oxazoline) and poly(2-nonyl-2-oxazoline). In addition, the PMOx exhibits stealth properties[204-205], so that the prepared polymer and subsequently the conjugate would not need to exhibit cell lytic properties towards red blood cells and cell toxic properties. For examination the cell lytic properties of red blood cells, the hemocompatibility concentration of a compound at which 50% of porcine red blood cells lyse (HC$_{50}$) was determined. The hemolytic activity of the blood cells was not present without additives (PACs, DTAC), i.e. the blood cells were not destroyed and therefore do not show lysis. The release of hemoglobin after addition of 2 μL Triton X to the red blood cells was considered as 100% lysis. All PACs tested showed no hemolytic properties and a minimum HC$_{50}$ value of

20000 μg·mL^{-1}. This means that by using vitamin E instead of other hydrophobic poly(2-oxazoline)s, red blood cell lysis can be reduced to less than 1%.

Furthermore, it was investigated whether these conjugates affect the cell viability of mammalian cells. This was tested on rat alveolar macrophages (AM, NR8383) using the AlamarBlue assay. Macrophages are effector cells of the innate immune system and play an important role in the clearance of pathogens.[206] A look at the cell viability of NR8383 cells (Fig. 30) after treatment with the VitE-based amphiphilic PACs at different concentrations (50, 100, 200 μg·mL^{-1}) for 24 h clearly shows the same trend as before.

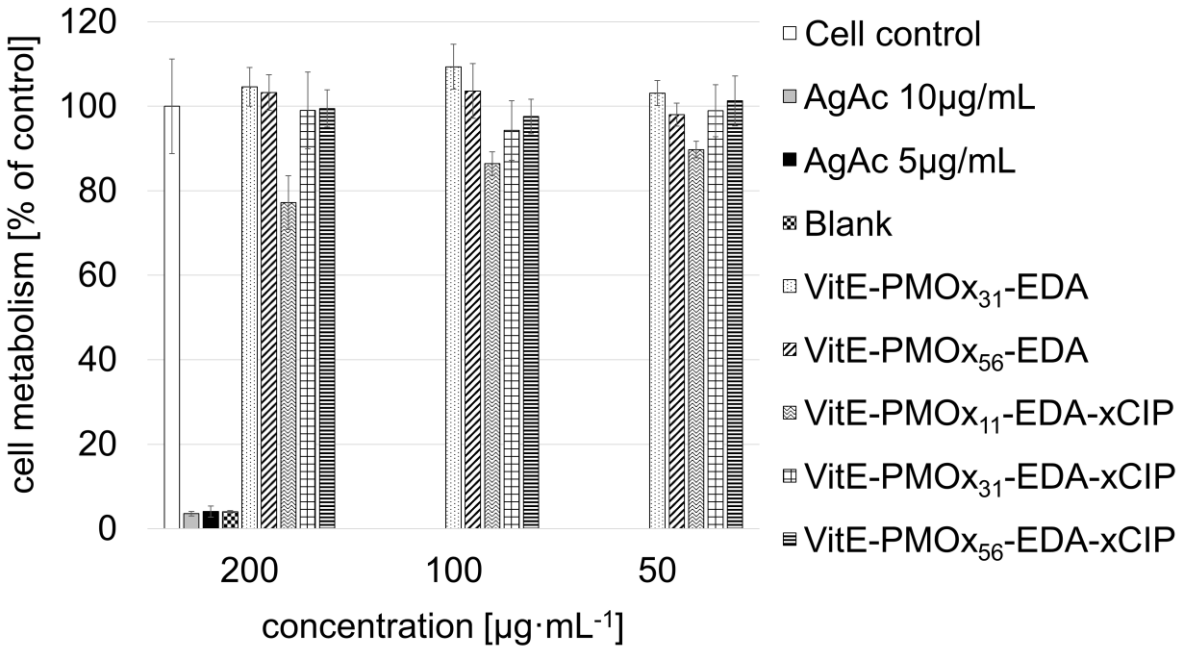

Figure 30: *AlamarBlue Assay with NR8383 cells treated with white: Cells, grey: AgAc 10 µg·mL^{-1}, black: AgAc 5 µg·mL^{-1}, black checkered: blank, dotted: VitE-BMB-PMOx$_{31}$-EDA, striped: VitE-BMB-PMOx$_{56}$-EDA, waved: VitE-BMB-PMOx$_{11}$-EDA-xCIP, checkered: VitE-BMB-PMOx$_{31}$-EDA-xCIP, cross-strip: VitE-BMB-PMOx$_{56}$-EDA-xCIP in RMPI/FCS for 24 h. Values are expressed as mean ± SD (n = 3-4).*

In all cases, the cell viability exceeds 80%, showing that these PACs show no cell toxic effects towards NR8383 in the concentration range tested. Even such a high concentration as 200 μg·mL^{-1} does not induce cytotoxicity in NR8383 after 24h of incubation. These results are consistent with previous studies, which reported CIP-related toxicity on stem cells only at much higher concentrations.[194-195]

In summary, it can be said that the modification of vitamin E worked very well and could be detected with ^{1}H NMR, FT-IR as well as with ESI-MS. Subsequently, this initiator was used to initiate a living cationic ring-opening polymerisation with the monomer 2-methyl-2-oxazoline. The propagation rate of the initiator was investigated and the finished polymer was characterised using ^{1}H NMR spectroscopy and MALDI-TOF. The synthesised initiator clearly exhibits the properties of a living polymerisation. The polymers started with it could also be clearly detected and characterized. In addition, conjugation with ciprofloxacin resulted in up to 9-fold higher antimicrobial activity against *S. aureus* than CIP. The resistance potential to the two bacterial strains *S. aureus* and *E. coli* was greatly reduced by derivatization. In addition, these PACs also appear to tend to concentrate in the bacterial cytoplasm by entering bacterial cells through the efflux pumps. This enables the amphiphilic PACs to exhibit good antimicrobial activity against CIP-resistant bacteria. Another important aspect is the lack of both blood and cell toxic properties. Thus, amphiphilic PACs based on VitE and PMOx exhibit not only excellent antimicrobial properties, but also low resistance formation and the absence of cell-toxic properties.

Taking this further, an interesting aspect would be the targeted control of antimicrobial activity and the associated possible reduction in the development of resistance.

4.3 Control of PACs by reversible non-covalent cross-linking

The doctoral thesis of MARTIN SCHMIDT[1] contains first research approaches concerning amphiphilic polymer-antibiotic conjugates and ABA triblock copolymers. However, no conclusions were drawn on the mechanistic mode of action of the polymers with each other. The synthesis route and the composition of the polymers were taken from the work of MARTIN SCHMIDT[1] and further investigated in detail for their mechanistic effect. In addition, the results of this chapter were developed in collaboration with student JONAS TOPHOVEN[207] as part of his master's thesis.

Reversible crosslinking of amphiphilic PACs allows the formation of novel structural motifs and control of antimicrobial activity. These PACs exhibit higher antimicrobial activity[170], greater efficacy against biofilms[208], and more stability[171], as previously shown. In addition, the amphiphilic PACs have been found to form spherical or wormlike micelles to penetrate bacterial cells via efflux pumps. The cross-linking of these micelles, may involve control of antimicrobial activity. As a result, the larger aggregates are no longer able to penetrate the bacterial cells via the efflux pump inlets (see Figure 31).

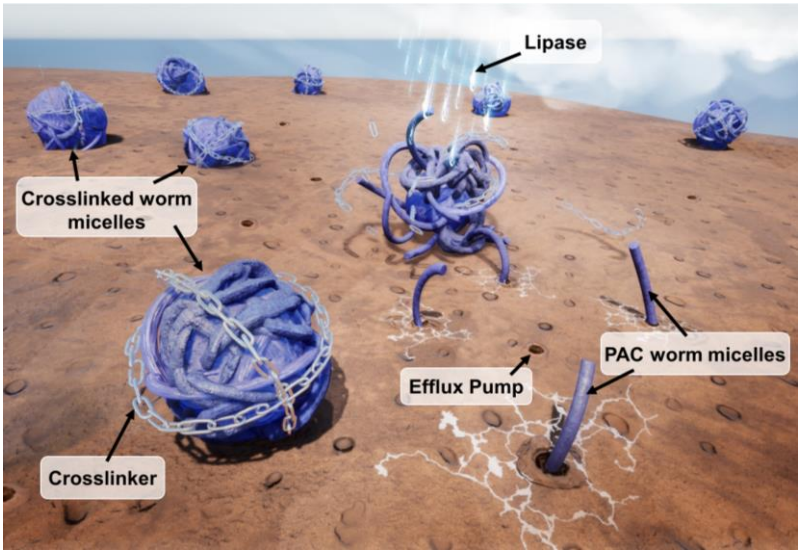

Figure 31: *Illustration of the general concept of controlling the activity of cross-linked, antibacterial worm micelles based on CIP-based antibiotic polymer conjugates (PAC) on a bacterial surface. The worm micelles are inactive in its cross-linked state and can be released and activated by the cross-linker cleaving enzyme lipase. The activated worm micelles enter the bacterial cell via their efflux pumps and kill the cell from within.*

To ensure that the superstructure of the amphiphilic PACs is not compromised, the crosslinking of these must be reversible. For this purpose, amphiphilic multiblock copolymers with hydrophobic outer blocks were chosen as cross-linkers because they often form hydrogels and microgels. The assumption was that the PAC worm micelles would be incorporated into these gels without their nanostructure being destroyed during nanoprecipitation.[209-212] The hydrophobic outer blocks of the multiblock copolymers were introduced as lipase-cleavable units to ensure reversible crosslinking. After hydrolytic cleavage by lipase, the cross-linked micelles should dissolve and release the active CIP worm micelles (Figure 31).

A series of multiblock copolymer POx with two cleavable ester end groups was synthesized to find the most suitable non-covalent cross-linker for the POx-CIP micelles. The hydrophobicity of these end groups was varied by using octanoic acid or oleic acid. The polymer backbone varied from hydrophilic poly-2-methyl-oxazoline (PMOx) to amphiphilic triblock copolymers with hydrophobic blocks in the middle, such as (PHeptOx) or poly-2-phenyl-oxazoline (PPhOx) (Table 5).

Table 5: *Analytical data of triblock copolymers by ^{1}H NMR spectroscopy, nanoprecipitation method and MIC-Tests. The MIC values in Table 1 are expressed as mean ± SD (n = 3–4).*

Polymer	Isolated Yield	Content conjugate[a]	$MIC_{S.a.}$[b] [µg·mL^{-1}]	On-Off-Faktor$_{S.a.}$	F^d_{NMR}[c]	Đ[f]
C_8-$PMOx_{36}$-C_8	-				98%	1.06
C_{18}-$PMOx_{36}$-C_{18}	-				96%	1.07
C_8-$PMOx_{13}$-*b*-$PHeptOx_{26}$-*b*-$PMOx_{13}$-C_8	30%	n.d.	7 ± 2	1-2	99%	1.17
C_8-$PMOx_5$-*b*-$PPhOx_9$-*b*-$PMOx_5$-C_8	10%	1:0.64	6 ± 2	1-2	96%	1.15
C_8-$PMOx_{10}$-*b*-$PPhOx_{10}$-*b*-$PMOx_{10}$-C_8[e]	15%	1:0.58	16 ± 3	5	99%	1.22
C_8-$PMOx_{17}$-*b*-$PPhOx_{20}$-*b*-$PMOx_{17}$-C_8	43%	1:0.35	102 ± 19	14	98%	1.20
C_8-$PMOx_{10}$-*b*-$PPhOx_{20}$-*b*-$PMOx_{10}$-C_8[d]	63%	1:0.6	527 ± 25	135	99%	1.21
C_8-$PMOx_{10}$-*b*-$PPhOx_{40}$-*b*-$PMOx_{10}$-C_8[e]	62%	1:0.64	88 ± 13	24	96%	1.19

[a] mol% of Me-$PMOx_{15}$-*b*-$PHeptOx_{16}$-EDA-xCIP in the isolated aggregate.
[b] Statistical error from at least 3 measurements.
[c] Degree of functionalization determined by ^{1}H NMR spectroscopy via comparison of the respective signals caused by the initiating group *trans*-1,4-dibrom-2-buten and the terminal acid group.
[d] The synthesis route and the composition of the amphiphilic polymer were taken from the work of MARTIN SCHMIDT.[1]
[e] The synthesis route and the composition of the amphiphilic polymer were taken from the work of JONAS TOPHOVEN.[207]
[f] The dispersity was calculated from the GPC: Đ = M_w/M_n.

Nanoprecipitation was performed by dissolving the prepared multiblock copolymers with the highly active CIP conjugate Me-PMOx$_{15}$-*b*-PHeptOx$_{16}$-EDA-xCIP in ethanol at a molar ratio of 1:1 (mol/mol) and then adding it to strongly stirring water. Successful binding of aggregates was determined by visible turbidity of the solution. This turbidity was absent only for the telechelic homopolymers when precipitated with the worm micelles. All other end-group esterified triblock copolymers clouded the mixture after precipitation, as can be seen in Table 5.

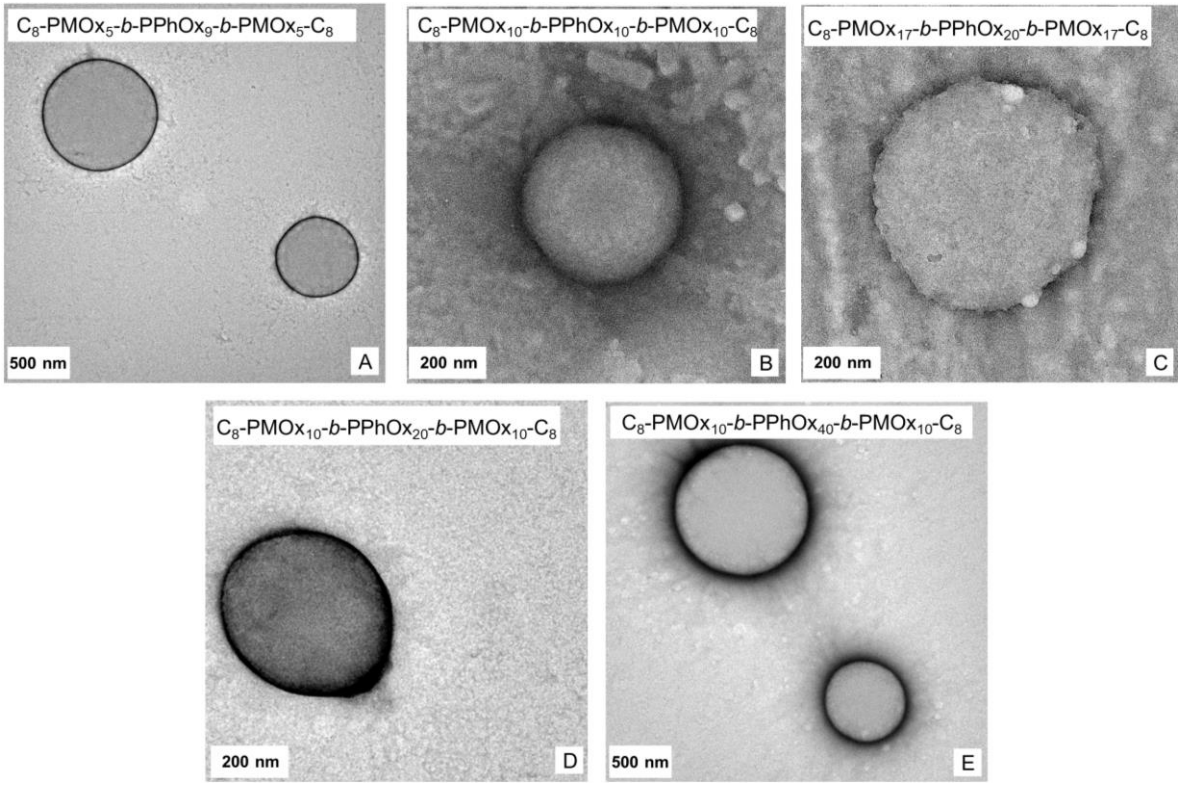

Figure 32: *Transmission electron microscopy (TEM) images of the block copolymers resulting from nanoprecipitation of the respective amphiphilic ABA triblock copolymers A: C_8-PMOx$_5$-b-PPhOx$_9$-b-PMOx$_5$-C_8, B: C_8-PMOx$_{10}$-b-PPhOx$_{10}$-b-PMOx$_{10}$-C_8, C:[207] C_8-PMOx$_{17}$-b-PPhOx$_{20}$-b-PMOx$_{17}$-C_8, D: C_8-PMOx$_{10}$-b-PPhOx$_{20}$-b-PMOx$_{10}$-C_8, E: C_8-PMOx$_{10}$-b-PPhOx$_{40}$-b-PMOx$_{10}$-C_8.*

These turbid mixtures, or more precisely the isolated water-insoluble solids, were analyzed by TEM. However, in the previous step, the amphiphilic triblock copolymers alone were also dissolved in ethanol and precipitated in water in order to study its morphology by TEM. From Figure 32, it is clear that all the polymers precipitate as a sphere with no particular structural motifs.

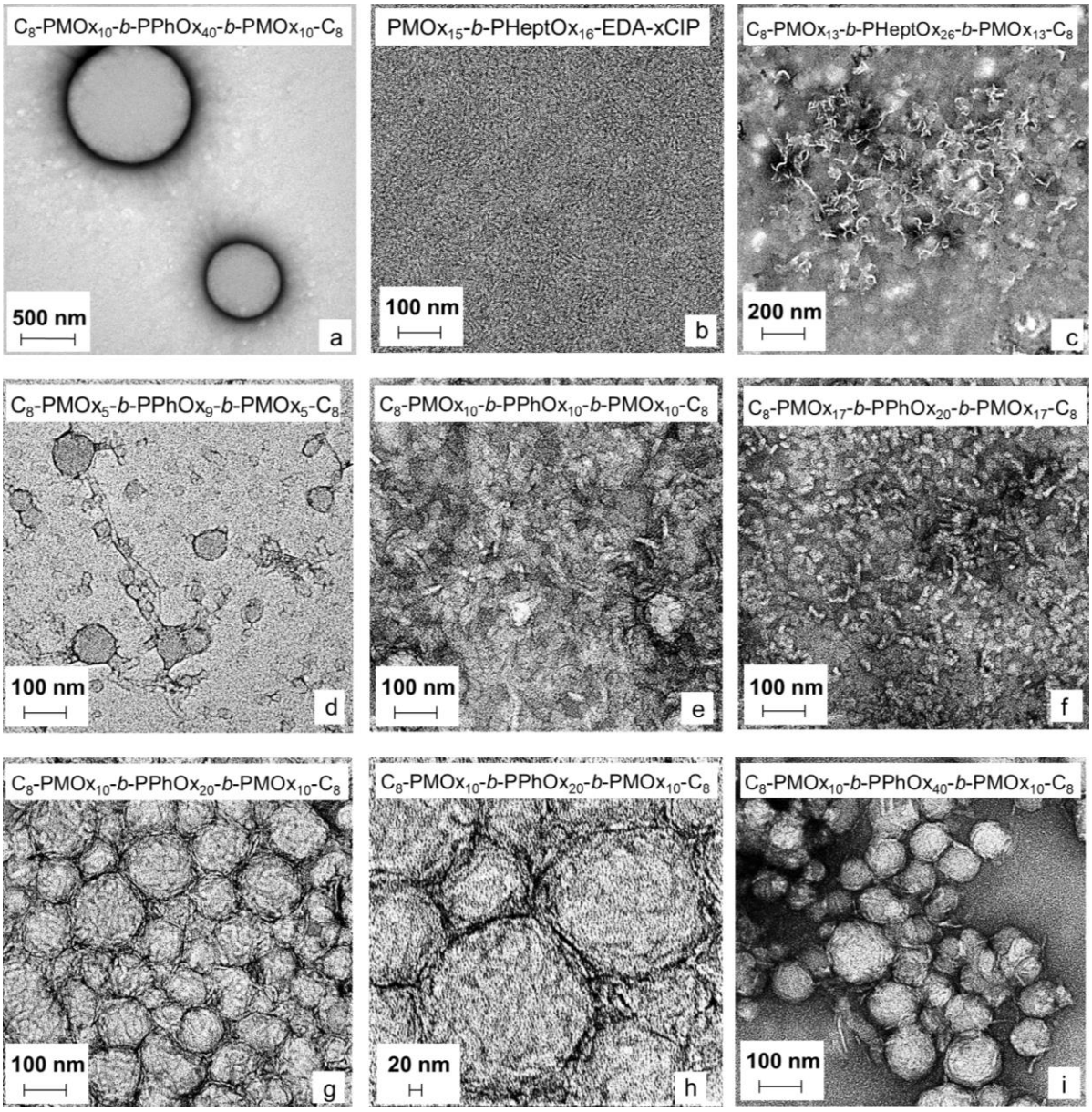

Figure 33: *TEM measurements of structures formed by nanoprecipitation from ethanol to water. a: C_8-$PMOx_{10}$-b-$PPhOx_{40}$-b-$PMOx_{10}$-C_8, b: Me-$PMOx_{15}$-b-$PHeptOx_{16}$-EDA-xCIP. Precipitates with Me-$PMOx_{15}$-b-$PHeptOx_{16}$-EDA-xCIP: c: C_8-$PMOx_{13}$-b-$HeptOx_{26}$-b-$PMOx_{13}$-C_8, d: C_8-$PMOx_5$-b-$PPhOx_9$-b-$PMOx_5$-C_8, e:[207] C_8-$PMOx_{10}$-b-$PPhOx_{10}$-b-$PMOx_{10}$-C_8, f:[207] C_8-$PMOx_{17}$-b-$PPhOx_{20}$-b-$PMOx_{17}$-C_8, g: C_8-$PMOx_{10}$-b-$PPhOx_{20}$-b-$PMOx_{10}$-C_8, h: C_8-$PMOx_{10}$-b-$PPhOx_{40}$-b-$PMOx_{10}$-C_8, i:[207] C_8-$PMOx_{10}$-b-$PPhOx_{20}$-b-$PMOx_{10}$-C_8. Precipitation was performed from an ethanolic solution of the polymers and polymer mixtures in an excess of water. Samples were stained with Ruthenium chloride. The TEM investigations and the crosslinking method were taken from the work of* MARTIN SCHMIDT[1].

Nanoprecipitation of the CIP conjugate leads to rod or worm micelles (Figure 33b). Figure 33c shows particles without an ordered structure surrounded by somehow bent, elongated worm micelles. This is the result of mixing a triblock copolymer with a

PHeptOx as a midblock with the CIP conjugate. This structural change indicates the mixing of the two components, i.e., the triblock copolymer and the diblock copolymer CIP conjugate, as well as the formation of a new structure. This behavior is known from numerous other studies reporting mixed block copolymers and the structures formed.[213-214] The triblock copolymers that have PPhOx as a midblock appear to form aggregates in combination with the PAC, which in all cases contain the unmodified worm micelles. It can be concluded that the different polymers do not mix and therefore the triblock copolymer can only act as a cross-linker (Fig. 33d-i). Thus, the type of crosslinking depends on the structure of the coprecipitated triblock copolymer.

Rather loose, fiber-like structures are formed with the short polymers C_8-PMOx$_5$-*b*-PPhOx$_9$-*b*-PMOx$_5$-C_8 and C_8-PMOx$_{10}$-*b*-PPhOx$_{10}$-*b*-PMOx$_{10}$-C_8 (see Fig. 33d and e). The number of crosslinks increases as the length of the triblock copolymers increases, leading to denser structures. Nevertheless, the triblock copolymer C_8-PMOx$_{17}$-*b*-PPhOx$_{20}$-*b*-PMOx$_{17}$-C_8 forms loose, filamentous networks with the CIP conjugate. Thus, not only the length of the triblock copolymers but also their hydrophilic/hydrophobic balance seems to play a crucial role in the crosslinking of the worm micelles. The triblock copolymers with a longer hydrophobic midblock C_8-PMOx$_{10}$-*b*-PPhOx$_{20}$-*b*-PMOx$_{10}$-C_8 and C_8-PMOx$_{10}$-*b*-PPhOx$_{40}$-*b*-PMOx$_{10}$-C_8 yield nanostructured particles resembling densely cross-linked worm micelles. SAXS measurements of the dried and swollen aggregates confirmed the structural motif of the wool-cluster-like aggregates with C_8-PMOx$_{10}$-*b*-PPhOx$_{20}$-*b*-PMOx$_{10}$-C_8 and Me-PMOx$_{15}$-*b*-PHeptOx$_{16}$-EDA-xCIP visible in the TEM image (Fig.34).

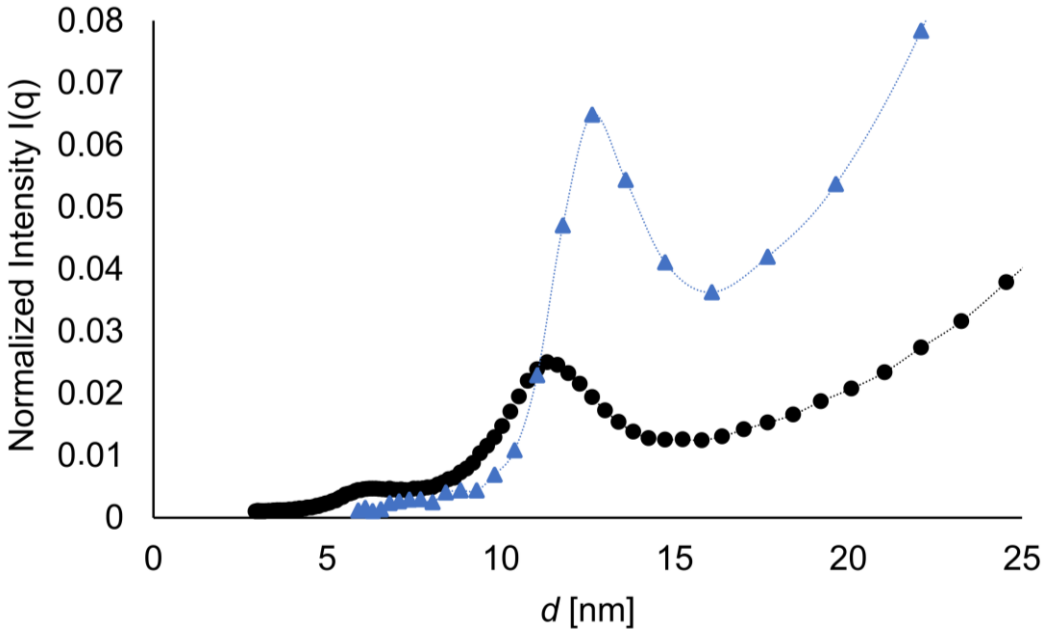

Figure 34: *Small-angle X-ray scattering (SAXS) traces of dry (black) and swollen (blue) C_8-PMOx$_{10}$-b-PPhOx$_{20}$-b-PMOx$_{10}$-C_8 with Me-PMOx$_{15}$-b-PHeptOx$_{16}$-EDA-xCIP, so wool-cluster-like particles. The measurements were carried out for 1 h and 25 °C. Intensities were normalized to the total number of counts of the respective measurement, q was calculated by $q = 4\pi\sin(\theta)/\lambda$ (2θ = diffraction angle) and d was calculated using $d = 2\pi/q$.*

The so-called d-value, which can be translated as the distance between the micelles, shows a strong correlation peak of 11.3 nm for the dried aggregates. After swelling in water, the correlation peak is shifted to 12.7 nm. This study proves that the aggregates in both dried and swollen forms most likely have the same ordered structure, which also indicates the high stability of this supramolecular structure. Thus, a water uptake of 42% can be calculated for the cross-linked worm micelles based on the SAXS measurement. Possible crosslinking mechanisms for the structures shown in the TEM images are shown in Figure 35. It is important to note that only the end groups of the triblock copolymers act as crosslinking groups for the worm micelles, while the PPhOx midblock does not interact with them. For this reason, the micelles retain their shape even in the cross-linked state.

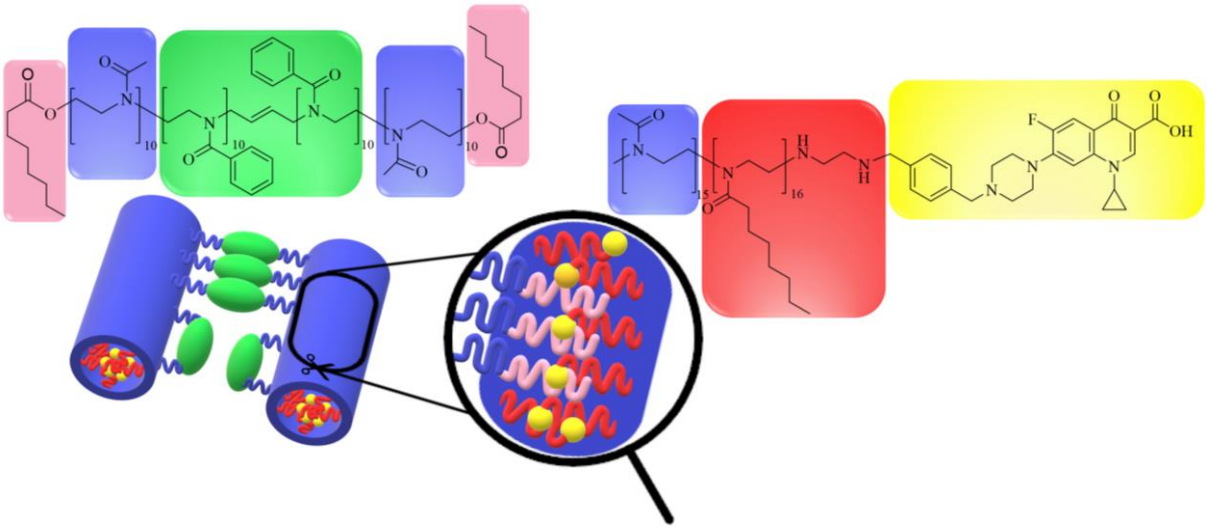

Figure 35: *Schematic representation of the macromolecular crosslinking between triblock copolymers and a worm micelle forming PAC. Interaction between the triblock copolymer C_8-$PMOx_{10}$-b-$PPhOx_{20}$-b-$PMOx_{10}$-C_8 and Me-$PMOx_{15}$-b-$PHeptOx_{16}$-EDA-xCIP.*

Based on ^{1}H NMR spectra, it was found that the triblock copolymers and the CIP conjugate did not precipitate in the same ratio (1:1 mol/mol) as present in the stock solution, but the precipitate contained only 27 to 39 mol% of the CIP conjugate (see Table 5). These figures are in line with expectations, since centrifugation was used to purify the cross-linked worm micelles. The large spheres formed by the triblock copolymers can be easily centrifuged, whereas the worm micelles originating from the CIP conjugate cannot be isolated in this way, and therefore not fully cross-linked worm micelles are lost during purification (Fig. 36).

The polymers C_8-$PMOx_{10}$-*b*-$PPhOx_{20}$-*b*-$PMOx_{10}$-C_8 and Me-$PMOx_{15}$-*b*-$PHeptOx_{16}$-EDA-xCIP were varied in a molar ratio of 2:1 and 1:2 in the ethanolic stock solution to investigate whether the composition and yield of the cross-linked worm micelles could be affected. Nanoprecipitation with the 2:1 molar ratio resulted in a precipitate containing only 29 mol% of the CIP conjugate. The reason for the 39 mol% decrease for the precipitate from the solution with the 1:1 mol triblock copolymer/mol CIP conjugate ratio is the high excess of the triblock copolymer. In contrast, the precipitate from the solution with a ratio of 1:2 mol triblock copolymer/mol CIP conjugate contained 39 mol% of the CIP conjugate. This suggests that this composition is the most stable structure in the nanoprecipitation experiment and cannot be altered by increasing the amount of CIP conjugate.

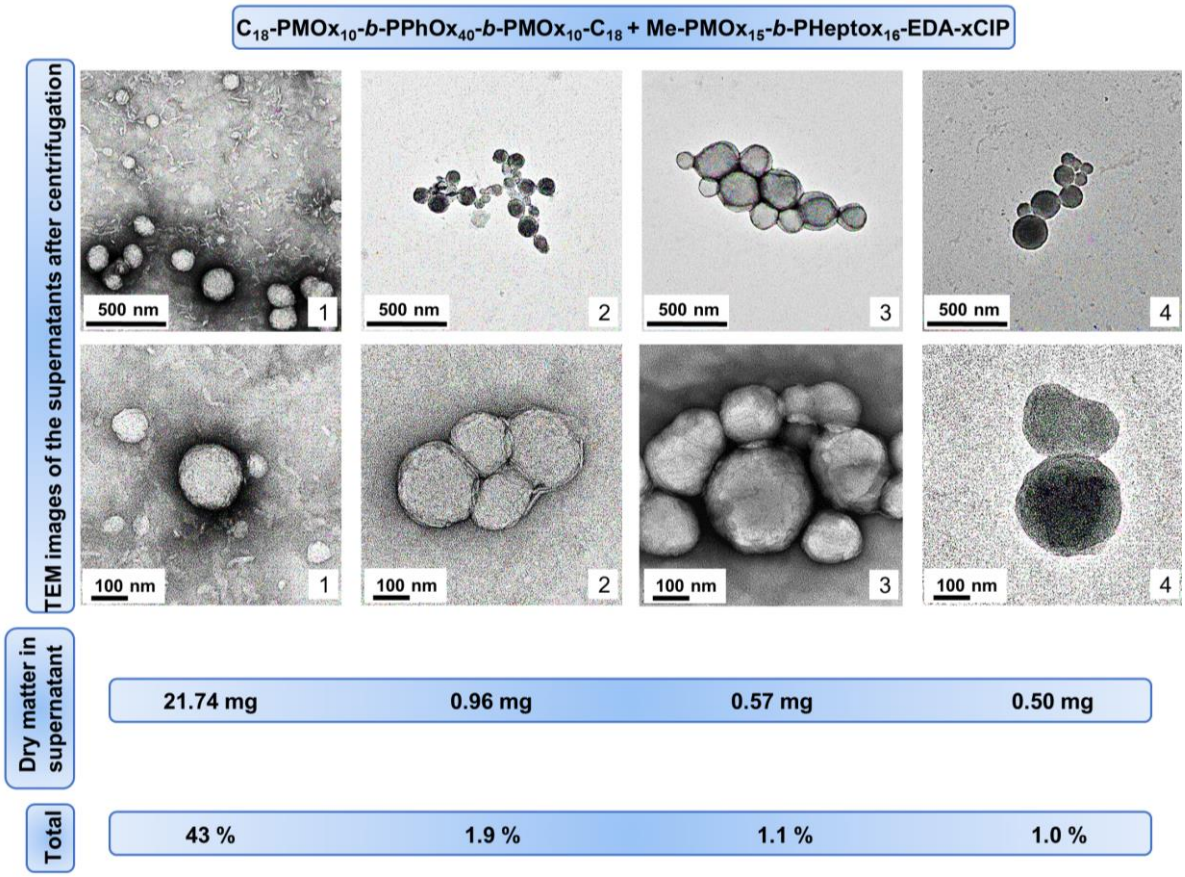

Figure 36: *Overview of the centrifugation steps for the Me-PMOx$_{15}$-b-PHeptOx$_{16}$-EDA-xCIP cross-linked with the polymer C$_{18}$-PMOx$_{10}$-b-PPhOx$_{40}$-b-PMOx$_{10}$-C$_{18}$. According to the nanoprecipitation method, the first time was centrifuged several times for 10 minutes at 6000 rpm. The dry mass indicates the mass after drying in the lyophilisation unit. The total mass balance indicates the percentage share of the dry mass of the respective supernatant in the total initial weight. For clarity, the TEM images are shown both at a lower magnification level, where the white bar corresponds to 500 nm, and at a higher magnification, where the white bar corresponds to 100 nm.*[207]

The deactivation of the antimicrobial effect of the cross-linked worm micelles was determined using a minimum inhibitory concentration (MIC) test against the bacterium *S. aureus*. In this test, the cross-linked micelles were dispersed in a bacterial growth medium, incubated overnight with the bacterial cells, and the lowest concentration that inhibited at least 99% of bacterial cell growth was determined photometrically (Fig. 37). The highest deactivation of 135 compared to the free conjugate is shown by the aggregate of Me-PMOx$_{15}$-*b*-PHeptOx$_{16}$-EDA-xCIP with C$_8$-PMOx$_{10}$-*b*-PPhOx$_{20}$-*b*-PMOx$_{10}$-C$_8$. In contrast, the deactivation of PAC by the triblock copolymers with lower PPhOx content or shorter chain length is much lower. The reason for this, as already discussed, is the lower stability of the aggregates formed. The triblock copolymer C$_8$-PMOx$_{13}$-*b*-PHeptOx$_{26}$-*b*-PMOx$_{13}$-C$_8$ also shows very low

deactivation, due to the mixing of the two components. These mixed micelles both no stable aggregates and are thus available on the surface of the bacterial cells.

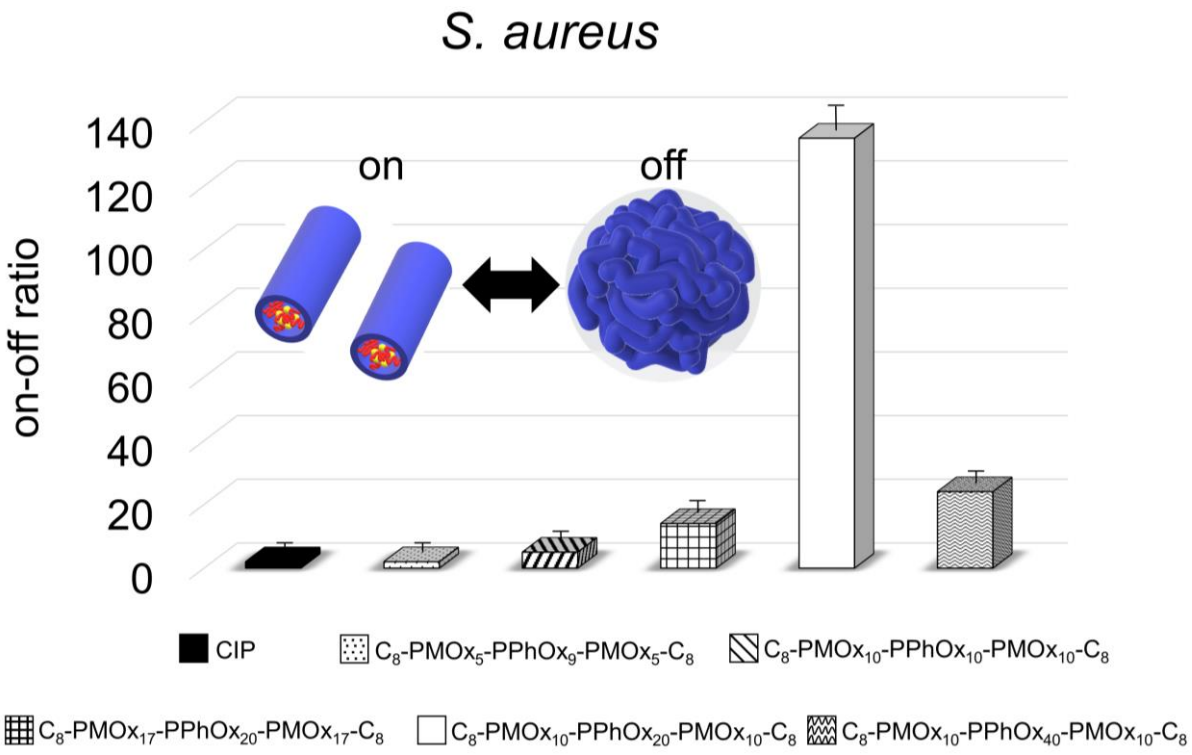

Figure 37: *On-off ratio of the cross-linked conjugate Me-PMOx$_{15}$-b-PHeptOx$_{16}$-EDA-xCIP with different triblock copolymers. C$_8$-PMOx$_5$-b-PPhOx$_{10}$-b-PMOx$_5$-C$_8$ (dotted), C$_8$-PMOx$_{10}$-b-PPhOx$_{10}$-b-PMOx$_{10}$-C$_8$ (striped), C$_8$-PMOx$_{17}$-b-PPhOx$_{20}$-b-PMOx$_{17}$-C$_8$ (checkered), C$_8$-PMOx$_{10}$-b-PPhOx$_{20}$-b-PMOx$_{10}$-C$_8$ (white) and C$_8$-PMOx$_{10}$-b-PPhOx$_{40}$-b-PMOx$_{10}$-C$_8$ (waved) and the MIC-values of CIP (black).[207] Values in Figure 37 are expressed as mean ± SD (n = 3–4). The on-off ratio is defined as MIC value of the CIP conjugate in the aggregate divided by MIC of the free CIP conjugate. The biological examinations (CIP) and biological method of examination were taken from the work of MARTIN SCHMIDT[1].*

The next step is to transfer this concept to other types of micelles, such as round micelles. One such PAC that forms round or sperical micelles due to the molar ratio of PHeptOx/PMOx is Me-PMOx$_{22}$-*b*-PHeptOx$_8$-EDA-xCIP. This conjugate was nanoprecipitated with C$_8$-PMOx$_{10}$-*b*-PPhOx$_{20}$-*b*-PMOx$_{10}$-C$_8$ from an ethanolic solution containing a 1:1 ratio (mol/mol) of the two polymers. Figure 38 clearly shows that the triblock copolymer also crosslinks the spherical micelles and thus does not affect the structure of the CIP conjugates. The aggregate also shows a greatly reduced activity of the CIP conjugate by a factor of 42.

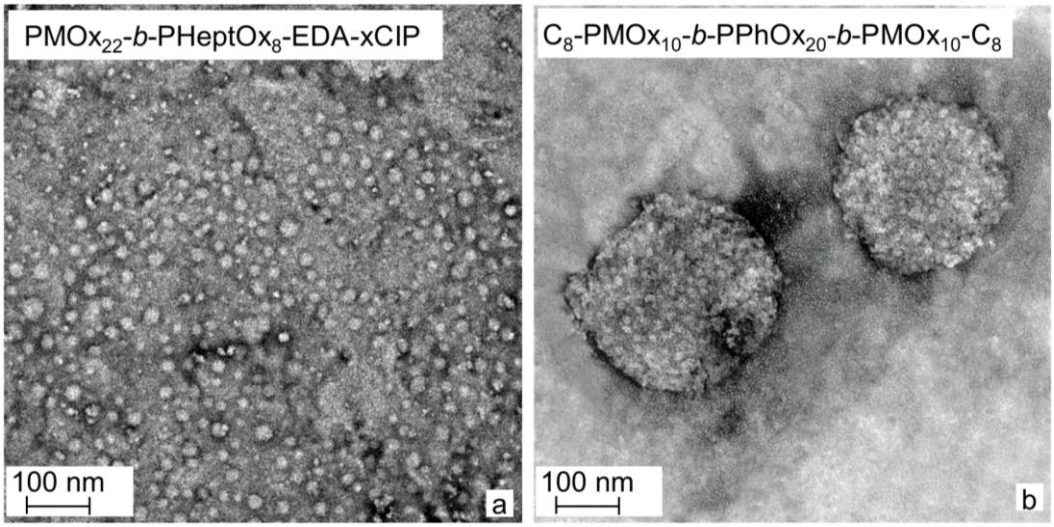

Figure 38: *TEM images of spherical micelles and the crosslinking of these with a triblock copolymer. a: spherical micelles consisting of Me-PMOx$_{22}$-b-PHeptOx$_8$-EDA-xCIP formed by nanoprecipitation and b: the aggregates consisting of triblock copolymer C$_8$-PMOx$_{10}$-b-PPhOx$_{20}$-b-PMOx$_{10}$-C$_8$ and CIP conjugate Me-PMOx$_{22}$-b-PHeptOx$_8$-EDA-xCIP. The TEM investigations and the crosslinking method were taken from the work of* MARTIN SCHMIDT[1].

The structure of these aggregates shown is mainly stabilized by the hydrophobic end groups. For this reason, cleavage of these end groups would abolish the crosslinking of the micelles. For this purpose, the esterified triblock copolymers were nanoprecipitated in water, isolated by centrifugation, and suspended in aqueous NaOH (0.03 M). After stirring for two hours at room temperature, the turbid suspension cleared in all cases except for the suspension of C$_8$-PMOx$_{10}$-*b*-PPhOx$_{40}$-*b*-PMOx$_{10}$-C$_8$, which did not clear even after 7 days. The same protocol was also applied to the cross-linked micelles. After incubation with NaOH for 2-12 hours, the clearing point was reached, the solution was neutralized with hydrochloric acid, dried under air flow, and subjected to MIC assay against *S. aureus*. It was shown that hydrolytic cleavage of the ester end groups of the triblocopolymer resulted in the breaking of the crosslinking points, leading to complete activation of the CIP conjugate. Hydrolysis of the coprecipitates leads to coexisting spherical micelles formed by the triblock copolymer without ester end groups and the free worm micelles formed by the CIP conjugate (Fig. 39B). Examination of the solution by dynamic light scattering also confirmed the complete disintegration of the aggregates after reaching the clearing point (Fig. 39).

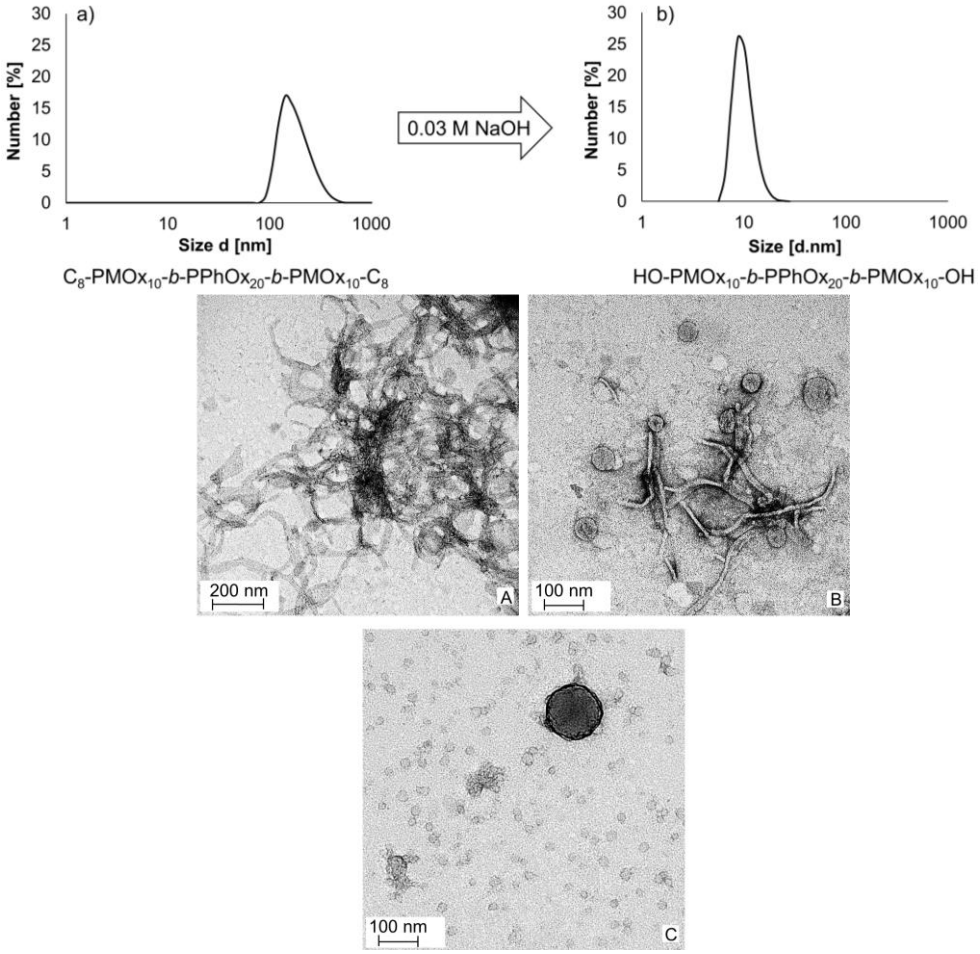

Figure 39: *DLS measurements of the ABA triblock copolymer C_8-$PMOx_{10}$-b-$PPhOx_{20}$-b-$PMOx_{10}$-C_8 bevor (a) and after (b) hydrolysis with 0.03 M NaOH. TEM measurements of the hydrolysed triblock copolymer C_8-$PMOx_{10}$-b-$PPhOx_{20}$-b-$PMOx_{10}$-C_8 loaded with Me-$PMOx_{15}$-b-$PHeptOx_{16}$-EDA-xCIP (A, B) and hydrolysed triblock copolymer C_8-$PMOx_{10}$-b-$PPhOx_{20}$-b-$PMOx_{10}$-C_8 (C).[207] The TEM investigations and the crosslinking method were taken from the work of MARTIN SCHMIDT[1].*

Of particular interest is the question of whether this result can also be achieved in the catalysis of ester cleavage by the enzyme lipase. For this purpose, lipase was added to the cross-linked micelle suspensions at a neutral pH and stirred at 37 °C for at least 18 hours or until the clarification point was reached. Full antibacterial activity of the respective CIP conjugate was also achieved against *S. aureus* in the clarified solutions. Kinetic studies were then performed with the CIP conjugate cross-linked by C_8-$PMOx_{10}$-*b*-$PPhOx_{20}$-*b*-$PMOx_{10}$-C_8. To ensure comparability, the same amount of lipase was treated for different time periods and the mixture was then subjected to the MIC assay against *S. aureus*. The ester cleavage reaction was drastically slowed down due to the dilution in the MIC assay, so that no significant ester cleavage occurs when the MIC values are determined. At the beginning of the reaction, CIP

conjugate activation occurs very rapidly. After two hours, the $MIC_{S.aureus}$ value is 12 µg · mL^{-1}, which means that 33% of the CIP conjugate has already been released. As soon as 18 hours have passed, the $MIC_{S.aureus}$ value drops to 4 µg · mL^{-1}. This value corresponds to that of the free CIP conjugate in such a mixture, which means that practically the entire conjugate has been released after this time. In conclusion, a lipase concentration typical for the human body could be suitable to completely reactivate the worm micelles from their cross-linked aggregates.

In summary, this study demonstrated that non-covalent crosslinking with suitable amphiphilic multiblock copolymers can control the bioactivity of a bioactive, self-assembled supramolecular structure by nanoprecipitation. This method neither destroys the supramolecular structure and is both efficient and reversible. But to enable crosslinking, the crosslinking multiblock copolymers must be perfectly matched in composition and structure.

4.4 Summary

In summary, the mode of action of the amphiphilic PACs could be investigated in more detail. It was found that the amphiphilic polymer and, consequently, the HHB play a crucial role in the antimicrobial activity of the PACs. More specifically, even the antimicrobial activity against the bacterium *S. aureus* is significantly improved compared to the non-conjugated CIP. Thus, this membrane-active moiety not only helps to penetrate the bacterial cells, but also facilitates the PACs to concentrate in the cell. It was found that the amphiphilic PACs enter the bacterial cells through the efflux pumps. This gives them a distinct advantage over the unmodified CIP. This is because the formation of the efflux pumps is a crucial and important resistance mechanism of the bacterial cells. Thus, the bacteria achieve exactly the opposite of what they actually want by overexpressing the efflux pumps. This principle benefits the amphiphilic PACs, so that they not only enter the bacterial cells through the efflux pumps and can concentrate there, but they also reduce the potential for resistance formation.

Furthermore, the amphiphilic PACs were further optimized as their solubility potential and biocompatibility still showed potential for improvement. For this reason, a replacement for the hydrophobic blocks of the previously synthesized amphiphilic PACs was sought. For this purpose, vitamin E seems to be the optimal solution, because due to its alkyl tail, this molecule is highly hydrophobic but shows very good biocompatibility. Thus, vitamin E was first converted into an initiator for living cationic ring-opening polymerization. Subsequently, polymers based on PMOx with different lengths were prepared to investigate the influence of molar mass on antimicrobial activity. Initially, VitE-PACs showed very similar trends and results as previously prepared amphiphilic PACs. The key difference and also advantage of VitE-PACs was achieved with better solubility and lack of hemolytic properties.

Lastly, the antimicrobial effect of the PAC was brought under control, so that a targeted control of this could be made possible. For this purpose, amphiphilic triblock copolymers were used, which form particles by self-assembly after nanoprecipitation. These triblock copolymers were mixed with an amphiphilic PAC Me-PMOx$_{15}$-*b*-

PHeptOx$_{16}$-EDA-xCIP and precipitated together from ethanol into rapidly stirring water. The resulting aggregates form quite unique morphologies, depending on the structure and length of the triblock copolymers. Crucially, the middle block of the triblock copolymers differs in structure from the hydrophobic block of the PAC to avoid mixing of these blocks. For this reason, poly(2-phenyl-2-oxazoline) is ideally suited as a midblock for the triblock copolymers. This results in reversible crosslinking of the PAC, which forms worm-like micelles. The reversible properties are critical for controlling antimicrobial activity, because crosslinking of the worm micelles turns off the antimicrobial activity. By enzymatic hydrolysis of the ester end groups of the triblock copolymers with lipase, the crosslinking is dissolved, the PAC worm micelles are released and are again fully antimicrobially active.

5 Experimental Part

5.1 Materials

All reactions, distillations and polymerizations were carried out under inert gas (argon). The water content of dry solvents can be checked by Karl Fischer titration (< 0.5 ppm). Chloroform was distilled over alumina and under reduced pressure and stored on molecular sieve (4 Å) under inert gas. *N,N*-dimethylformamide as well as acetonitrile were each distilled over phosphorus pentaoxide and then over potassium carbonate and also stored under inert gas on molecular sieve (3 Å). The monomers 2-methyl-2-oxazoline, 2-ethyl-2-oxazoline, 2-butyl-2-oxazoline, 2-hexyl-2-oxazoline, 2-heptyl-2-oxazoline, 2-octyl-2-oxazoline, 2-nonyl-2-oxazoline and 2-phenyl-2-oxazoline were distilled once without calcium hydride and once over calcium hydride. Once under reduced pressure, *N,N*-diethylethanamine, p-toluenesulfonic acid methyl ester and ethane-1,2-diamine were distilled. For purification, *α,α'*-dibromo-*p*-xylene and 1,4-dibromobutene were recrystallized from chloroform and n-heptane. Ciprofloxacin, *α*-tocopherol, 4-bis(bromomethyl)benzene, sodium thiosulfate, magnesium sulfate, 2-ethylhexanoyl chloride, 2-chloroethylammonium chloride, polyethylene glycol monomethyl ether (200, 2000 g-mol-1), triton X-100 (ACROS), mesyl chloride, tosyl chloride, valeronitrile, heptanenitrile, octanenitrile, nonannitrile, decannitrile, ethanolamine, triethylamine, *N*-[3-(dimethylamino)-propyl]-methacrylamide, *N,N*-dimethylacrylamide, chloroacetic acid chloride, sodium azide, sodium hydrogen carbonate, sodium chloride, sodium dihydrogen phosphate dihydrate, sodium hydroxide, sodium citrate, citric acid monohydrate, glucose monohydrate, hydrochloric acid, acetic acid, formic acid, dithranol, nutrient medium (standard 1) were used without further purification steps. Germs *Escherichia coli* (gram-negative, ATCC 25922), *Klebsiella pneumoniae* (gram-negative, ATCC 13883), *Pseudomonas aeruginosa* (gram-negative, ATCC 17423), *Staphylococcus aureus* (gram-positive, ATCC 25323), were obtained from the German Collection of Microorganisms and Cell Cultures (DSMZ). Fresh pig blood was provided by local butcher shops. *E. coli* ATCC 8739, *E. coli* JW0453 and *E. coli* JW5503 were obtained from the Keio collection.

5.2 Devices and methods

Nuclear Magnetic Resonance Spectroscopy (NMR)

^{1}H NMR spectra in deuterated solvents ($CDCl_3$, DMSO-d_6, D_2O) were recorded on the FT spectrometers of Burker, type DPX-300 (300 MHz), DRX-400 (400 MHz), DRX-500 (500 MHz) or Varian, type Inova 500 (500 MHz). The protons of the not fully deuterated solvent serve as the internal standard. In Hz, the coupling constant J was given and the signal rates of the chemical shifts δ were given in parts per million (ppm). The ACD/SpecManager 12.0 program was used to evaluate the ^{1}H NMR spectra obtained. The following abbreviations were used for the multiplicities arising from spin-spin coupling: s (singlet), d (doublet), t (triplet), q (quartet), quin (quintet), brs (broad signal), and m (multiplet).

Matrix-assisted laser desorption/ionization (MALDI)

The *dried droplet method* was used for sample preparation. Here, 30 mg of the universal matrix dithranol and 10 mg of the sample were each dissolved in 1 mL of chloroform. A mixture of 30 µL of universal matrix and 30 µL of sample was then prepared and mixed well. Before 1 µL of the mixture was dropped onto the 8280784 MTP 384 target plate ground steel BC sample disc, the sample disc was covered with scotch tape. The matrix-sample mixture was dropped onto the sample disc and waited until the solvent evaporated. Then, 1 µL was again dropped onto the sample disk. This curtain was repeated a few times until there was enough sample on the sample plate. Finally, it was waited until the solvent evaporated completely. MALDI-TOF measurements were performed on the Bruker Autoflex II using a nitrogen laser (λ = 337.1 nm) and controlled with FlexControl software. After obtaining the spectra, they were analyzed with the FlexAnalysis program. The calculation of the theoretical molecular masses was performed by using the following isotopes: ^{12}C = 12.000 g·mol^{-1}, ^{16}O = 15.995 g·mol^{-1}, ^{14}N = 14.003 g·mol^{-1}, ^{1}H = 1.008 g·mol^{-1}, ^{79}Br = 78.918 g·mol^{-1}, $^{1}H^{+}$ = 1.0072766 g·mol^{-1} and K = 38.9637 g·mol^{-1}.

Electrospray ionization (ESI)

The ESI-MS measurements were performed on a LTQ Orbitrap XL (Thermo) mass spectrometer. The polymer samples were dissolved in Ethanol at a concentration of 100 µmol·mL^{-1}. Nominal nitrogen back pressure and ESI voltage were adapted to the respective analyte, varying between 0.4 and 1.4 psi and 1.8 kV, respectively. The profile mass spectra were obtained as full scan data in positive mode by accumulation of 2 µ scans in the mass range m/z 50-2000 with a resolution of 100.000. The measurement accuracy was <5ppm (<1ppm internal log).

Gel permeation chromatography (GPC)

The GPCMax system from Viscotek was used to perform the GPC measurements. This instrument includes a refractive index (RI) detector, which was tempered to 55 °C. The pre-column TSKgel® and two TSKgel® GMHHR-M 7.8 x 300 mm (5 µm pore size) columns from Tosch separated the samples during the run. They were kept at a constant 60 °C using a column oven. The flow rate was 0.7 mL-min-1 with the running medium N,N-dimethylformamide including 20 mmol·L^{-1} LiBr. Polystyrene standards from Viskotek were used. The injection volume of the samples was 200 µL with a concentration of 3 mg·mL^{-1}. Before each measurement, the samples were equilibrated for 12 h and then filtered with a 0.2 µm PTFE filter. The determination of number average molecular weight (Mn), weight average molecular weight (Mw) and polydispersity index (PDI) was possible by the elugram obtained.

Infrared spectroscopy (FT – IR)

The FT-IR measurements were performed on a Burker alpha spectrometer equipped with an ATR pressure module. The spectra were recorded at a single refractive diamond window in attenuated total reflection (ATR). A resolution of 4 cm^{-1} was chosen with 70 scans per measurement in a wavenumber range of 400 - 4000 cm^{-1}. Liquid samples were dropped from the diamond window and solid samples were fixed using pressure modulus. The data was analyzed with the Opus software (Bruker).

Freeze-drying

Samples, which are in a round bottom flask with a large ground joint, were frozen in liquid nitrogen. After connecting the frozen flasks to the Alpha 1-4 LDplus freeze-drying system from Christ, the water was sublimed at 1-10^{-3} mbar and -56 °C.

Dynamic light scattering (DLS)

Amphiphilic polymers were analyzed on the Zetasizer Nano S (Zen 1600) from Malvern Industries to determine the hydrodynamic diameter. For this purpose, the nanoprecipitation method was carried out in advance so that an aqueous solution was available for the subsequent DLS measurement.

Ultraviolet–visible spectroscopy

Spectroscopic measurements were performed on two different spectrometers from Analytik Jena. The first was a Specord 210 double-beam photometer at 25 °C and the second was a Specord S600 single-beam photometer. The temperature of the Specord S600 was controlled by a Peltier element (0 - 95 °C).

Fluorescence spectroscopy for the determination of the critical micelle formation concentration (CMC)

Fluorescence spectroscopic measurements were performed on a Hitachi F-2700 fluorescence spectroscope at 25 °C. First, a stock solution of 0.1 mM pyrene in methanol was prepared. Then, a dilution series of the desired polymer (20-40 mg) was prepared and 10 µL of pyrene from the stock solution was added to each sample. The polymer samples were analyzed at an absorbance of 334 nm and an emission of 344 nm with absorption bands I_1 = 373nm and I_3 = 383 nm. Spectra were evaluated using Hitachi's FT Solutions software. A sudden increase in emission intensity indicates the formation of micelles.

Dialyses

Dialysis membranes with different molecular weight cut offs (MWCO) of 1000 or 2000 $g \cdot mol^{-1}$ in deionized water or abrotated methanol were used to perform the dialyses. Conditioning of the dialysis membrane is required prior to dialysis in methanol. For this purpose, the dialysis tubing was placed in a beaker containing 50 mL of deionized water and 50 mL of abrotated methanol was slowly added. 50 mL of the resulting methanol/DF water solution was removed, and then 50 mL of methanol was added again. This procedure was repeated four times. After the last step (approximately 95% methanol by volume), the dialysis tubing could be used for dialysis in methanol or stored in the refrigerator in methanol. Dialyses in deionized water did not require prior conditioning of the dialysis tubing. To perform dialysis, the dialysis membrane was previously sealed at both ends with freezer bag clamps. Samples were then dissolved in the appropriate solvent (deionized water or methanol) and filled into the dialysis membrane. Dialysis against deionized water was performed for 24 h in 800 mL deionized water and dialysis against methanol was performed within 4 h in also 800 mL methanol. Finally, the solvent was removed and the purified sample could be obtained.

Nanoprecipitation method

9.5 mg of the polymer-antibiotic conjugate (PAC) and the equimolar amount of cross-linker polymer were dissolved in 0.4 mL ethanol. The method was also performed with the only the cross-linker polymers and the PAC, respectively. The whole ethanolic solution was added to 2.4 mL of very fast stirring deionized water contained in a snap cap within 10 seconds using a syringe and the mixture was stirred for 2 h. The precipitate was isolated upon centrifugation (HERMLE Z300) at 6000 rpm for 10 min and the solid was washed with distilled water three times.

End group hydrolysis of ABA triblock copolymers

10 mg of the cross-linked PAC obtained be nanoprecipitation was suspended in 2 mL of aqueous 0.03 M NaOH and stirred at 37 °C. The hydrolysis success is evaluated optically or by means of the DLS measurement. After reaching the clearing

point, the solution was neutralized with 0.1 M hydrochloric acid and subjected to the MIC-test. The same experiment was performed with and aqueous lipase solution (2 $mg \cdot mL^{-1}$). Here, the solution was subjected to the MIC-test without neutralizing.

Scanning electron microscopy (SEM)

Scanning electron micrographs (SEM) were performed on the Hitachi S4500 instrument with an excitation voltage of 1 kV. For this purpose, ABA triblock copolymer samples were dropped from an aqueous solution with a concentration of 0.5-10 wt.% onto a sample holder. After evaporation of the solvent at 60 °C, the sample was measured.

Transmission electron microscopy (TEM)

Transmission electron micrographs were acquired on an Talos F200X microscope operating at an accelerating voltage of 200 kV. The polymer samples were dissolved with 1 wt% in distilled water and dropped on carbon-coated copper grids allowing the solvent to evaporate. A staining solution was prepared as follows. 0.2 g of ruthenium chloride hydrate and 10 mL (5 wt%) sodium hypochlorite were dissolved in 100 mL distilled deionized water. The grids with the polymeric sample were incubated with three droplets of staining solution. After 20 min, the samples were analyzed by transmission electron microscopy (TEM).

Small-angle X-ray scattering (SAXS)

SAXS measurements were performed on the Bruker NANOSTAR instrument using a VANTEC-2000 detector and an IμS microfocus source (Incoatec GmbH) with a Cu anode (wavelength λ = 0.154 nm) and integrated Montel optics. Calibration was performed with a silver behenate standard and the distance between the samples and the detector was 107 cm. All measurements were performed at room temperature and under vacuum. Samples were filled both dry and swollen into fused silica capillaries, which were sealed at both ends. The SAXS measurements were each recorded over one hour, followed by azimuthal integration to obtain the

scattered intensities as a function of the magnitude of the scattering vector $q = 4\pi\sin(\theta)/\lambda$ (2θ = diffraction angle).

5.3 Syntheses

Destillation of 2-Oxazolines

A Vigreux still including flask, stirring fish and spider was stored overnight in the drying cabinet at 150 °C. After the distillery was set up, it was baked under vacuum and cooled under argon. The respective monomer was placed in a 100 mL heated round bottom flask containing calcium hydride. Now the mixture was stirred at the still under 400 mbar at 40 °C for one hour. Finally, distillation was carried out at the required pressure and temperature.

Table 6: Overview of distillation conditions of various monomers.

Monomer	Pressure [mbar]	Temperature [°C]
2-Methyl-2-oxazolin	40	40
2-Ethyl-2-oxazolin	45	72
2-Phenyl-2-oxazolin	1.9	117

2-Methyl-2-oxazolin

^{1}H-NMR (400 MHz, CHLOROFORM-*d*): δ (ppm) = 1,93 (m, 3 H); 3,78 (t, J = 9,29 MHz, 9,78 MHz, 2 H); 4,19 (t, J = 9,29 MHz, 9,78 MHz 2 H).

Synthesis of 2-heptyl-2-oxazoline

In a 250 mL round bottom flask with a large ground glass, 28.49 mL (28.49 g, 228 mmol, 0.93 eq.) of octanenitrile, 16.67 mL (16.67 g, 273 mmol, 1.2 eq.) of ethanolamine, and 1 g (4.6 mmol, 0.02 eq.) of zinc acetate were added and heated to reflux at 130 °C for 24 h. The reaction mixture was then refluxed. After the reaction mixture was cooled to room temperature, 100-200 mL of cyclohexane was added. A separatory funnel was then used to wash the organic phase 5 times with 400 mL of water until it turned yellow. After the last wash with saturated NaCl solution, the organic phase was dried over magnesium sulfate. For better separation of the magnesium sulfate, the mixture was centrifuged, filtered and finally dried on a

rotary evaporator. Using a Vigreux still, the product was dry distilled over calcium hydride at 8 mbar and 120 °C.

^{1}H-NMR (400 MHz, CHLOROFORM-*d*): δ (ppm) = 0,83 (m, 3 H); 1,27 (m, 9 H); 1,62 (m, 2 H); 2,26 (t, *J* = 9,29 MHz, 9,78 MHz, 2 H); 3,76 (m, *J* = 9,29 MHz, 9,78 MHz, 2 H); 4,15 (m, *J* = 7,34 MHz, 7,83 MHz, 2 H).

Synthesis of hydrophobic 2-Oxazolines

In a 250 mL round bottom flask, (228 mmol, 1 eq.) nitrile, 16.35 mL (16.67 g, 273 mmol, 1.2 eq.) ethanolamine, and 1 g (4.6 mmol, 0.02 eq.) zinc acetate were placed and heated to reflux for 72 h (2-butyl-2-oxazoline) or 24 h at 140 °C. For purification, the product was distilled twice, both times using a Vigreux still. The first distillation was carried out at suitable conditions. The second distillation was a dry distillation over calcium hydride.

Table 7: Overview of reaction and distillation conditions of various monomers.

Monomer	Nitrile	Pressure [mbar]	Temp [°C]
2-Butyl-2-oxazolin	Valeronitrile: 23.69 mL	65	140
2-Hexyl-2-oxazolin	Heptanenitrile: 31.3 mL	0	140
2-Oktyl-2-oxazolin	Nonanenitrile: 39.7 mL	0	140
2-Nonyl-2-oxazolin	Decanenitrile: 42.60 mL	0	140

2-Butyl-2-oxazolin

^{1}H-NMR (400 MHz, CHLOROFORM-*d*): δ (ppm) = 0,89 (m, 3 H); 1,35 (sx, *J* = 7,34 MHz, 7,83 MHz, 15,16 MHz, 2 H); 1,59 (qi, *J* = 7,83 MHz, 15,16 MHz 2 H); 2,24 (t, *J* = 7,34 MHz, 7,83 MHz, 2 H); 3,79 (t, *J* = 9,29 MHz, 9,78 MHz, 2 H); 4,18 (t, *J* = 9,29 MHz, 9,78 MHz, 2 H).

Distillations with a microdistillery

Using a heated microdistill, the following reactants were dry distilled over calcium hydride. The product obtained was stored as a clear liquid under argon in the freezer.

Table 8: Overview of distillation conditions of various low molecular weight reactants.

Educt	Pressure [mbar]	Temperature [°C]
p-Toluolsulfonsäuremethylester	0	125
Ethylendiamin	45	60
Triethylamin	30	40
N,N-Diisopropylethylamin	25	40

Recrystallization of α,α'-dichloro-p-xylene and 2,4-Dibromobutene

In a 250 mL round-bottom flask, 100 mL of chloroform was placed and *α,α'*-dichloro-*p*-xylene or 100 mL of n-heptane was placed and 2,4-dibromobutene was added until a saturated solution was obtained. On the rotary evaporator, the remaining solid was dissolved at 44 °C and then the clear reaction solution was concentrated to two-thirds of its volume. After storing the flask overnight in the refrigerator, white crystals were obtained. These were filtered off and dried under air flow. The remaining solution was again concentrated on the rotary evaporator and placed in the refrigerator. This procedure was repeated until no more crystals precipitated.

Synthesis of the α,α'-dichloro-p-xylene linker

A 250 mL Schlenk flask with stirring fish was stored overnight in a drying oven at 150 °C. After cooling the Schlenk flask, 332 mg (1.00 mmol, 1 eq.) ciprofloxacin, 877 mg (5.00 mmol, 5 eq.) recrystallized α,α'-dichloro-p-xylene, and 168 mg (2.00 mmol, 2 eq.) sodium bicarbonate were added and inerted three times. Subsequently, 10 mL of a mixture of dry solvents DMF and acetonitrile (1:1) was added and stirred at 80 °C for three days. The first purification step was precipitation in ice-cold diethyl ether, followed by centrifugation and drying of the solid under air flow. Next, the contaminated product was purified by column chromatography. For this purpose, a running mixture of 300 mL of DCM:MeOH (20:1) was prepared with a splash of acetic acid. The eluate from the column was collected and rotated in on the rotary evaporator until only a drop of yellowish liquid remained. This solution was again precipitated in ice-cold diethyl ether and placed in the freezer overnight. The next

day, the reaction mixture was centrifuged at 5000 rpm for 15 minutes. The ether was decanted off and the product obtained was dried on the air stream.
^{1}H-NMR (400 MHz, CHLOROFORM-*d*): δ (ppm) = 1,22 (m, 2 H); 1.37 (m, 2 H); 2,69 (m, 4 H); 3,35 (m, 4 H); 3,52 (m, 1 H); 3,61 (m, 2 H); 4,59 (m, 2 H); 7,38 (m, 5 H); 8,03 (m, 1 H); 8,79 (s, 1 H).

Synthesis of amphiphilic AB diblock copolymers

To a 50 mL heated Schott flask, 15 mL of the dry solvent acetonitrile was placed under argon and 0.142 mL (0.94 mmol, 1 eq.) of the initiator methyl tosylate was added. Now the first monomer 2-methyl-2-oxazoline was added, depending on the desired repeat unit. For example, here 1.99 mL (23.50 mmol, 25 eq.) of 2-methyl-2-oxazoline was added to the given solution. The reaction mixture was polymerized in a microwave oven at 100 °C for 1.5 h. The reaction mixture was then heated. In the next step, a second hydrophobic monomer was added under argon, in this example 697 µL (4.70 mmol, 5 eq.) 2-heptyl-2-oxazoline. The polymerization was also carried out in a microwave at 130 °C for 2 h. The polymerization was then carried out under argon. Subsequently, the polymerization was terminated under argon using 0.627 mL (9.40 mmol, 10 eq.) ethylenediamine and the reaction mixture was stirred in an oil bath at 45 °C for three days. Dialysis in abrotated methanol for 4 h was performed for purification. The clean product was rotated in and dried at fine vacuum.

Me-PMOx$_{28}$-*b*-PHeptOx$_3$-EDA

^{1}H-NMR (400 MHz, CHLOROFORM-*d*): δ (ppm) = 0,85 (m, 6 H); 1,27 (m, 17 H); 1,56 (m, 4 H); 2,12 (br. s., 84 H); 2,33 (br. s., 8 H); 2,74 (m, 13 H), 3,02 (s, 3 H); 3,42 (m, 128 H).

Synthesis of polymer xCIP conjugates

In a 250 mL Schlenk flask, 94 mg (0.02 mmol, 2 eq.) ciprofloxacin, 17 mg (0.02 mmol, 2 eq.) sodium bicarbonate, and, for example, 131 mg (0.1 mmol, 1 eq.) Me-PMOx$_{28}$-*b*-PHeptOx$_3$-EDA were placed and inerted three times. Then, a mixture of 10 mL dry DMF and acetonitrile (1:1) was added and stirred for 24 h at 80 °C in an oil bath. On the rotary evaporator, the product was concentrated and dialyzed for 4 h

in abrotated methanol. Finally, the solvent of the product was rotated in and the product was dried at fine vacuum.

Me-PMOx$_{27}$-*b*-PHeptOx$_3$-EDA-xClP

^{1}H-NMR (400 MHz, CHLOROFORM-*d*): *δ* (ppm) = 0,87 (m, 8 H); 1,19 (m, 2 H); 1,28 (m, 16 H); 1,36 (m, 2 H); 1,28 (m, 2H); 1,59 (m, 4 H); 2,14 (br. s., 82 H); 2,34 (br. s., 9 H); 2,66 (m, 10 H), 3,04 (m, 3 H); 3,45 (br. s., 132 H); 7,35 (m, 7 H); 8,02 (m, 1 H); 8,76 (m, 1 H).

Synthesis of ABA triblock copolymers

The polymerization was carried out in a dry 50 mL Schott flask. For this, 15 mL of dry acetonitrile was placed under argon and 316.50 mg (1.477 mmol, 1 eq.) of 2,4-dibromobutene was added and completely dissolved. First, the hydrophobic block was polymerized, here as an example, 2-heptyl-2-oxazoline. For this purpose, 2.2 mL (14.78 mmol, 10 eq.) of 2-heptyl-2-oxazoline was added to the mixture and polymerized for 2 h at 130 °C in a microwave. Subsequently, the second monomer, 2-methyl-2-oxazoline 2.4 mL (28.77 mmol, 20 eq.), was added under argon and polymerized for 3 h at 100 °C in the microwave. The termination of the polymerization can be with a carboxylic acid, such as octanoic acid, oleic acid, or lauric acid, or with an OH group. For termination with a carboxylic acid, 210 µL (1.2 mmol, 2.4 eq.) of Hünig base and 1.2 mmol (2.5 eq.) of the corresponding carboxylic acid were added to the polymer mixture and stirred for three days at 50 °C in an oil bath. The product was purified by dialysis in methanol for 4 h. For termination with an OH group, 16.48 mL (6.6 eq.) of 0.2 M KOH solution was added to the polymer mixture, also under argon, and stirred at 50 °C for three days in an oil bath.

Okt-PMeOx$_{12,5}$-*b*-PHeptOx$_{11}$-*b*-PMeOx$_{12,5}$-Okt

^{1}H NMR (400 MHz, Chloroform-*d*) *δ*(ppm): 5.56 – 5.46 (m, 2H, -CH2-CH-CH-CH2-), 4.18 (q, J = 5.7, 4.8 Hz, 4H, -CH2-CH2-O-CO-), 3.44 (dq, J = 13.1, 7.0, 6.5 Hz, 113H,-NR-CH2-CH2-NR-), 2.45 – 2.17 (m, 13H,-CO-CH2-CH2), 2.16 – 1.97 (m, 67H, -NCO-CH3), 1.66 – 1.47 (m, 21H, -CO-CH2-CH2), 1.27 (dt, J = 10.6, 6.0 Hz, 87H, -COCH2-CH2- CH2-CH2- CH2-CH2-CH3), 0.95 – 0.77 (m, 31H, Alkyl-CH3).

HO-PMeOx$_{12,5}$-*b*-PHeptOx$_{11}$-*b*-PMeOx$_{12,5}$-OH

^{1}H NMR (400 MHz, Chloroform-*d*) *δ*(ppm): 5.49 (s, 2H, -CH2-CH-CH-CH2-), 4.12 (h, J = 5.3 Hz, 4H, -CH2-CH2-O-CO-), 3.98 – 3.77 (m, 4H, -CH2-CH-CH-CH2-), 3.58 – 3.13 (m, 132H, -NR-CH2-CH2-NR-), 2.47 – 2.16 (m, 22H,-CO-CH2-CH2), 2.16 – 1.86 (m, 80H, -N-CO-CH3), 1.61 – 1.52 (m, 20H), 1.35 – 1.16 (m, 70H), 0.85 (s, 17H), 0.84 (d, J = 13.0 Hz, 9H, -CO-CH2-CH2- CH2-CH2- CH2-CH2-CH3).

Synthesis of vitamin E with 4-(bromomethyl)benzoyl bromide (VitE-BMB)

In a 250 mL round bottom flask, 5.4 g (19.3 mmol, 1 equiv) of 4-(bromomethyl)benzoyl bromide was dissolved in 50 mL of dry DCM. In a new glass tube, 8.7 mL vitamin E (8.3 g, 19.3 mmol, 1 equiv) and 3 mL triethylamine (21.6 mmol, 1.12 equiv) were dissolved in 50 mL dry DCM. The 50 mL vitamin E - TEA - DCM solution was then added to the 4-(bromomethyl)benzoyl bromide - DCM solution over 30 minutes and stirred at room temperature for 18 hours. The product was purified by column chromatography with the running medium heptane:ethyl acetate (96% : 4%).

^{1}H NMR (500 MHz, CHLOROFORM-d) δ ppm = 0.84 - 0.95 (m, 12 H) 1.07 - 1.21 (m, 5 H) 1.22 - 1.37 (m, 14 H) 1.38 - 1.47 (m, 3 H) 1.53 - 1.67 (m, 2 H) 1.76 - 1.91 (m, 2 H) 2.00 - 2.12 (m, 6 H) 2.12 - 2.21 (m, 3 H) 2.60 - 2.69 (m, 2 H) 4.56 (s, 2 H) 7.54 - 7.61 (m, 2 H) 8.23 - 8.30 (m, 2 H)

5.4 Biological investigations

Determination of the minimum inhibitory concentration (MIC)

This test is performed to determine the lowest or minimum inhibitory concentration (MIC) of a sample sufficient to inhibit 99% of bacteria in growth. Bacterial strain cultures from various freeze-dried bacterial pellets were used for this purpose. To use these, one quarter of a bacterial pellet was swollen with 150 µL of nutrient medium (sterile nutrient medium standard 1, 25 g in 1 L bidest. water) for 30 minutes. Then, 50 µL of each swollen bacterial suspension was dissolved in 25 mL of appropriate culture medium and incubated under optimal growth conditions (Table 5). The following day, the overgrown culture medium was centrifuged (3000 rpm, 10

min), decanted, resuspended in 25 mL of sterile PBS buffer (8.77 g NaCl, 1.56 g $NaH_2PO_4 \cdot 2H_2O$, pH 7.0), and centrifuged again. This procedure was repeated three times. Finally, the bacterial residue was dissolved in 10 mL of PBS buffer and 10 mL of sterile 50% glycerol solution and stored at -20 °C.

Now, precultures can be grown with the prepared bacteria. For this purpose, 50 µL of the corresponding bacterial stock solution was dissolved in 25 mL of culture medium and incubated for 24 h at optimal growth conditions. Before the bacteria can be used, the bacterial count of these was determined by UV/ViS spectroscopy at 541 nm/25 °C and adjusted to ~10^7 bacterial cells per milliliter.

Preparatively, 2-4 mg of the polymer sample was weighed in a 15 mL Falcon tube. A dilution series was prepared with this polymer sample, halving the polymer concentration at each step. For this purpose, the weighed polymer sample was dissolved in 4 mL of culture medium and diluted within 14 steps. In addition, a positive and negative sample was prepared. Now all dilution steps and the positive sample were inoculated with 20 µL of the adjusted preculture (~10^7 bacterial cells per milliliter) and incubated for 24 at optimal growth conditions. To determine the minimum inhibitory concentration, the MIC assay performed was optically evaluated and then 100 µL of an aqueous 2,3,5-triphenyltetrazolium chloride (TTC) solution (1 $mg \cdot mL^{-1}$) was added. After incubating the samples for an additional three hours, dilution step was stained red, which has a bacterial concentration greater than 1%. Thus, the MIC value is determined by the last clear dilution step or the last step not stained red and indicates the value at which 99 % of the bacteria are inhibited in growth.

Table 9: Optimal growth conditions of the bacterial strains used.

Bacterial strain	DSM	ATCC	gram	Growth conditions
Escherichia coli	1103	25922	negative	Nutrient standard 1, pH=6.8, 37 °C
Klebsiella pneumoniae	30104	13883	negative	Nutrient standard 1, pH=7.0, 37 °C
Pseudomonas aeruginosa	50078	17423	negative	Nutrient standard 1, pH=7.0, 30 °C
Staphylococcus aureus	1104	25923	positive	Nutrient standard 1, pH=7.3, 37 °C

Resistance tests

The performance of the resistance tests is based on the procedure for the MIC tests. Initially, the same procedure was followed, a pre-culture was prepared and adjusted to ~10^7 bacterial cells per milliliter, then a dilution series was prepared as described and inoculated with the prepared pre-culture. Now, however, the procedure of the resistance test changes, because after evaluation of the first test series, a new dilution series was prepared with the same polymer sample as before. However, the inoculation was not carried out with newly prepared and adjusted bacteria, but with the bacteria from the previous test series. More precisely, the bacteria of the first turbid dilution step of the first test series were taken to inoculate the second test series. This process was repeated until all dilution series became turbid or more than 15 days had passed. This gave the bacteria time to mutate under evolutionary pressure and build up resistance. In the test with the vitamin E, the PAC was additionally examined with pure CIP in a ratio of 1:1 (mol/mol).

Determination of MIC concentration for loaded particles

In preparation for the assay, the nanoprecipitation method was performed with the duplicate amounts, in which ABA triblock copolymers were loaded with amphiphilic PAHs. After the resulting and loaded particles were stirred in water for 2 h, they were centrifuged at 6000 rpm for 15 min. The supernatant was decanted and the resulting pellet was suspended in 4 mL deionized water and centrifuged again. This procedure was repeated three times. After the last centrifugation, the supernatant was decanted and the resulting pellet was dried under air flow for 3 days. Now the MIC assay was performed as previously described. End group hydrolysis during MIC assay can also be performed. For this purpose, an additional 0.03 M NaOH was added during the MIC test before inoculation with the bacteria to initiate the hydrolysis.

Determination of hemolytic activity (HC_{50} test)

First, the citrate-phosphate-dextrose buffer (CPD buffer) was prepared to determine the hemolytic activity of blood cells. For this purpose, in 1 L bidest. Water 26.3 g

sodium citrate, 3.27 g citric acid monohydrate, 25.5 g glucose monohydrate and 2.51 g sodium dihydrogen phosphate dihydrate, adjusted to pH 7.38 and filtered sterile.

Now fresh, unsalted porcine blood was poured into six 15 mL Falcon tubes and centrifuged at 4000 rpm for 15 minutes. The separating blood plasma was decanted and the erythrocytes were picked up in sterile 150 mM NaCl solution and washed carefully. Increased care must be taken not to swirl the blood cells too much and in no case to vortex them. The washing procedure was repeated three times and subsequently the red cell concentrate was taken up in 10 mL CPD buffer and stored for a maximum of 24 h at 4 °C.

To perform the HC_{50} assays, 40-60 mg of a polymer sample was weighed into 2 mL Eppendorf cups and dissolved in 1.60 mL CPD buffer. A dilution series of eight dilution steps was prepared, halving the polymer concentration in each step. In addition, a positive and negative sample was prepared for each dilution series. In the next step, 200 µL of the red cell concentrate was added to each dilution step and to the positive and negative samples. An erythrocyte concentration of 5-108 blood cells per mL was achieved in each dilution step. An additional 2 µL of Triton X was added to the positive sample, as a hemolytically active component, i.e., for 100% hemolysis. Samples were incubated for 1 h at 37 °C, then centrifuged at 13500 rpm for 5 min, and the release of hemoglobin was examined at UV/ViS at 541 nm/25 °C. The degree of hemolysis of red blood cells is proportional to the hemoglobin concentration and thus to the absorbance measured. The HC_{50} value results from the interpolated concentration at which 50% of the red blood cells were destroyed.

Inhibition of topoisomerase IV and gyrase activity

The activity of gyrase was tested with relaxed pUC18. Negatively supercoiled pUC18 was obtained from E. coli XL1 blue transformed with pUC18 using the QIAprep Spin Miniprep Kit (Qiagen, Hilden, Germany) according to the manufacturer's instructions. Relaxed pUC18 was purified from reactions containing 100 nM negatively supercoiled pUC18. For inhibition reactions, 200 nM GyrA and 800 nM GyrB were incubated with 20 nM pUC18, ciprofloxacine (2.5 µM), synthesized PAC and polymer (500 µM) in buff-er containing 50 mM Tris/HCl, pH 7.5, 10 mM MgCl2, 0.1 M KCl,

10% (v/v) glycerol. After preincubating the samples for 3 min at 37 °C, reactions were started by addition of 1.5 mM ATP and stopped with 0.5% (w/v) SDS and 12.5 mM EDTA, pH 8.0 after 10 min. Reaction products were separated on 1.3% (w/v) agarose gels in TEP buffer (36 mM Tris, 36 mM NaH2PO4, 1 mM EDTA, pH 8.0; 2.6 V/cm, 3 h, 4 °C).

Cell culture cells hMSC

Cryo-preserved bone marrow-derived human mesenchymal stem cells (hMSC; 5^{th} to 10^{th} passage; Lonza, Walkersville Inc., MD, USA) were thawed quickly using a 37 °C water bath (Köttermann 3041; Köttermann GmbH, Uetze, Germany). The thawed cell suspension was added gently to 10 mL pre-warmed cell culture medium RPMI/FCS (RPMI1640 with 0.3 g L^{-1} L glutamine (GIBCO, Invitrogen, Karlsruhe, Germany) and 10% fetal calf serum (FCS, (v/v); GIBCO)), and centrifuged for 5 min at 200 g and RT (Megafuge 1.0R; Thermo Fisher Scientific, Waltham, USA). The obtained cell pellet was re-suspended in 1 mL RPMI/FCS and transferred to a 75 cm^2 cell culture flask (BD Falcon, Becton Dickinson GmbH, Heidelberg, Germany) containing 15 mL pre-warmed RPMI/FCS. Cells were cultured in a humidified atmosphere at 37 °C and 5% CO_2 (Heraeus BB16 CO_2 incubator; Thermo Fisher Scientific) and sub-cultivated every 7 to 14 d. Adherent subconfluently growing hMSC were washed with PBS (GIBCO) and detached from cell culture flasks by addition of 0.2 mL cm^{-2} trypsin/ethylenediaminetetraacetic acid (trypsin/EDTA; 0.25%/0.05% (v/v); Sigma-Aldrich, Taufkirchen, Germany) and incubation at 37 °C for 5 min. Subsequently, detached cells were collected, washed two times with RPMI/FCS (5 min centrifugation, 200 g, RT) and seeded in cell culture plates. All cell culture experiments were performed under sterile conditions using a biological safety cabinet (Herasafe KS18; Thermo Fisher Scientific).

Cell viability and morphology of hMSC

For cell viability experiments hMSC were seeded at a density of 0.75 x 10^4 cells cm^{-2} (1.5 x 10^4 cells mL^{-1}) in 24-well cell culture plates (BD Falcon). After cell adherence different polymer antibiotic conjugates at various concentrations (200, 100, 50 μg

mL^{-1} each) were added, and the cells were incubated for 24 h in RPMI/FCS under cell culture conditions (37 °C, 5% CO_2; Heraeus BB16).

AlamarBlue Assay with hMSC

The cell metabolic activity of hMSC after 24 h of exposure to polymer antibiotic conjugates was analyzed using the AlamarBlue assay. Therefore, hMSC were washed with PBS and incubated with 200 µl of the AlamarBlue reagent (1 + 10 in RPMI1640; GIBCO) for 2 h under cell culture conditions. Subsequently, fluorescence intensity was analyzed at 590 nm by a microplate reader (FLUOstar Optima; BMG LABTECH GmbH, Ortenberg, Germany). The fluorescence intensity of the cell culture incubated without additives was found to be 61748 ± 534 (negative control). When treating the hMSC with 5 $\mu g \cdot mL^{-1}$ silver acetate for 24 h, which kills them, the fluorescence intensity drops below 3000 (positive control). The data are expressed as the mean ± standard deviation (SD) of at least three independent experiments and given as percentage of the untreated hMSC (cells cultured in RPMI/FCS).

Cell culture cells NR8383

Cell experiments were performed with the cell line NR8383 (rat alveolar macrophages, LGC Standards GmbH, Wesel, Germany). Cells cultivation was carried out in Ham's F-12 medium with 15% fetal calf serum (FCS, GIBCO, Invitrogen, Karlsruhe, Germany) in 175 cm2 cell culture flasks (BD Falcon, Becton Dickinson GmbH, Heidelberg, Germany) at standard cell culture conditions (humidified atmosphere, 37 °C, 5% CO2). The NR8383 cells were partly adherent and partly non-adherent, with a ratio between adherent and non-adherent cells about 1:1. For cell experiments, adherent cells were detached from the cell culture flasks with a TPP cell scraper (TPP Techno Plastic Products AG, Trasadingen, Switzerland), combined with non-adherent cells and seeded into 24-well cell culture plates (BD Falcon) at a cell concentration of 5□105 cells mL-1.

AlamarBlue Assay with NR8383

After exposure to polymer antibiotic conjugates for 24 h, the cell metabolic activity of NR8383 was analyzed by the AlamarBlue assay. Therefore, cells were incubated with the AlamarBlue reagent (1 + 10 in Ham's F-12/15% FCS) for 2 h under cell culture conditions. Subsequently, fluorescence intensity was analyzed at 590 nm using a microplate reader (FLUOstar Optima; BMG LABTECH GmbH, Ortenberg, Germany). The fluorescence intensity of the cell culture incubated without additives was found to be 25400 ± 3491 (negative control). After treating NR8383 cells with 5 $\mu g \cdot mL^{-1}$ silver acetate (24 h, toxic conditions), the fluorescence intensity drops below 1000 (positive control). The data are expressed as the mean ± standard deviation (SD) of at least three independent experiments and given as percentage of the untreated cells cultured in Ham's F-12/15% FCS without additives.

6 References

1. Schmidt, M. Synthese von antimikrobiellen Polymer-Antibiotika-Konjugaten und Konjugat-Netzwerken. TU-Dortmund, 19.04.2018.
2. Riley, D. R.; Sieber, K. B.; Robinson, K. M.; White, J. R.; Ganesan, A.; Nourbakhsh, S.; Dunning Hotopp, J. C., Bacteria-human somatic cell lateral gene transfer is enriched in cancer samples. *PLoS computational biology* **2013,** *9* (6), e1003107.
3. Zoetendal, E. G.; Vaughan, E. E.; De Vos, W. M., A microbial world within us. *Molecular microbiology* **2006,** *59* (6), 1639-1650.
4. Drews, G., *Bakterien-ihre Entdeckung und Bedeutung für Natur und Mensch*. Springer: 2015.
5. Dobson, A. P.; Carper, E. R., Infectious diseases and human population history. *Bioscience* **1996,** *46* (2), 115-126.
6. Finlay, B. B.; Falkow, S., Common themes in microbial pathogenicity revisited. *Microbiology and molecular biology reviews* **1997,** *61* (2), 136-169.
7. Alekshun, M. N.; Levy, S. B., Molecular mechanisms of antibacterial multidrug resistance. *Cell* **2007,** *128* (6), 1037-1050.
8. Fleming, A., On the antibacterial action of cultures of a penicillium, with special reference to their use in the isolation of B. influenzae. *Reviews of infectious diseases* **1980,** *2* (1), 129-139.
9. Alanis, A. J., Resistance to antibiotics: are we in the post-antibiotic era? *Archives of medical research* **2005,** *36* (6), 697-705.
10. Boucher, H. W.; Talbot, G. H.; Bradley, J. S.; Edwards, J. E.; Gilbert, D.; Rice, L. B.; Scheld, M.; Spellberg, B.; Bartlett, J., Bad bugs, no drugs: no ESKAPE! An update from the Infectious Diseases Society of America. *Clinical infectious diseases* **2009,** *48* (1), 1-12.
11. Eitinger, T.; Schlegel, H. G., *Allgemeine mikrobiologie*. Georg Thieme Verlag: 2007.
12. America, I. D. S. o., The infectious diseases society of America's 10×'20 initiative (10 new systemic antibacterial agents US food and drug administration approved by 2020): Is 20×'20 a possibility? *Clinical Infectious Diseases* **2019,** *69* (1), 1-11.
13. Woese, C. R.; Kandler, O.; Wheelis, M. L., Towards a natural system of organisms: proposal for the domains Archaea, Bacteria, and Eucarya. *Proceedings of the National Academy of Sciences* **1990,** *87* (12), 4576-4579.
14. Crofts, T. S.; Gasparrini, A. J.; Dantas, G., Next-generation approaches to understand and combat the antibiotic resistome. *Nature Reviews Microbiology* **2017,** *15* (7), 422-434.
15. Schmidt, M.; Romanovska, A.; Wolf, Y.; Nguyen, T.-D.; Krupp, A.; Tumbrink, H. L.; Lategahn, J.; Volmer, J.; Rauh, D.; Luetz, S., Insights into the Kinetics of the Resistance Formation of Bacteria against Ciprofloxacin Poly (2-methyl-2-oxazoline) Conjugates. *Bioconjugate Chemistry* **2018,** *29* (8), 2671-2678.
16. Schmidt, M.; Bast, L. K.; Lanfer, F.; Richter, L.; Hennes, E.; Seymen, R.; Krumm, C.; Tiller, J. C., Poly (2-oxazoline)–antibiotic conjugates with penicillins. *Bioconjugate chemistry* **2017,** *28* (9), 2440-2451.
17. Schmidt, M.; Harmuth, S.; Barth, E. R.; Wurm, E.; Fobbe, R.; Sickmann, A.; Krumm, C.; Tiller, J. C., Conjugation of ciprofloxacin with poly (2-oxazoline) s and polyethylene glycol via end groups. *Bioconjugate Chemistry* **2015,** *26* (9), 1950-1962.

18. Vila, J.; Sanchez-Cespedes, J.; Sierra, J.; Piqueras, M.; Nicolas, E.; Freixas, J.; Giralt, E., Antibacterial evaluation of a collection of norfloxacin and ciprofloxacin derivatives against multiresistant bacteria. *International journal of antimicrobial agents* **2006,** *28* (1), 19-24.
19. Craig, W. A., Overview of newer antimicrobial formulations for overcoming pneumococcal resistance. *The American Journal of Medicine Supplements* **2004,** *117* (3), 16-22.
20. Richter, D. C.; Brenner, T.; Brinkmann, A.; Grabein, B.; Hochreiter, M.; Heininger, A.; Störzinger, D.; Briegel, J.; Pletz, M.; Weigand, M. A.; Lichtenstern, C., Neue Antibiotika bei schweren Infektionen durch multiresistente Erreger. *Der Anaesthesist* **2019,** *68* (11), 785-800.
21. Grün, L., Über die additive Wirkung von ultravioletten Strahlen und Triaethylenglykol bei der Luftdesinfektion. *DMW-Deutsche Medizinische Wochenschrift* **1956,** *81* (31), 1217-1219.
22. Drewelow, B.; Reisinger, E. C., Therapie mit Antibiotika und Chemotherapeutika (Infektionen). In *Pharmakotherapie*, Springer: 2007; pp 119-162.
23. Lemmen, S., Mono-versus Kombinationstherapie bei Antibiotika. *Krankenhaushygiene up2date* **2009,** *4* (01), 65-74.
24. Dickgießer, N.; in der Stroth, S.; Wundt, W., Untersuchungen zum Synergismus von Ciprofloxacin mit β-Laktam-Antibiotika, Gentamicin, Minozyklin und Pipemidsäure. *Infection* **1986,** *14* (2), 82-85.
25. Neu, H. C., Synergy of Fluoroquinolones with Other Antimicrobial Agents. *Reviews of Infectious Diseases* **1989,** *11* (Supplement_5), S1025-S1035.
26. Ewig, S.; Gatermann, S., Antimikrobielle Therapie: Wirkspektrum, Dosierung und Applikation antimikrobieller Substanzen. In *Nosokomiale Pneumonie*, Springer: 2017; pp 137-154.
27. Toniolo, M.; Jetter, A., Methotrexat und Cotrimoxazol bei rheumatologischen Patienten. *Rheuma Schweiz* **2011,** *3* (5), 47-49.
28. Gysling, E., Cotrimoxazol. *pharma-kritik* **1996,** *17* (21).
29. Melhorn, S., Lokale Antibiotika oder Antiseptika in Kombination mit Glukokortikoiden. *Der Hautarzt* **2016,** *67* (10), 850-852.
30. Hübner, N.-O.; Assadian, O.; Sciermoch, K.; Kramer, A., Interaktion von Antiseptika und Antibiotika--Grundlagen und erste Ergebnisse in vitro. *GMS Krankenhaushygiene Interdisziplinaer* **2007,** *2*.
31. Riem, L., Harnwegsinfekt: Es müssen nicht immer Antibiotika sein. *gynäkologie + geburtshilfe* **2017,** *22* (6), 65-65.
32. Todd, P. A.; Benfield, P., Amoxicillin/clavulanic acid. *Drugs* **1990,** *39* (2), 264-307.
33. Nadler, J. P.; Berger, J.; Nord, J. A.; Cofsky, R.; Saxena, M., Amoxicillin-clavulanic acid for treating drug-resistant Mycobacterium tuberculosis. *Chest* **1991,** *99* (4), 1025-1026.
34. Huttner, A.; Bielicki, J.; Clements, M. N.; Frimodt-Møller, N.; Muller, A. E.; Paccaud, J. P.; Mouton, J. W., Oral amoxicillin and amoxicillin–clavulanic acid: properties, indications and usage. *Clinical Microbiology and Infection* **2020,** *26* (7), 871-879.
35. Higgins, P. G.; Wisplinghoff, H.; Stefanik, D.; Seifert, H., In vitro activities of the β-lactamase inhibitors clavulanic acid, sulbactam, and tazobactam alone or in combination with β-lactams against epidemiologically characterized multidrug-

resistant Acinetobacter baumannii strains. *Antimicrobial agents and chemotherapy* **2004,** *48* (5), 1586-1592.
36. Kollef, M. H.; Chastre, J.; Clavel, M.; Restrepo, M. I.; Michiels, B.; Kaniga, K.; Cirillo, I.; Kimko, H.; Redman, R., A randomized trial of 7-day doripenem versus 10-day imipenem-cilastatin for ventilator-associated pneumonia. *Critical Care* **2012,** *16* (6), 1-17.
37. Edwards, S. J.; Emmas, C. E.; Campbell, H. E., Systematic review comparing meropenem with imipenem plus cilastatin in the treatment of severe infections. *Current medical research and opinion* **2005,** *21* (5), 785-794.
38. Rhee, E. G.; Rizk, M. L.; Calder, N.; Nefliu, M.; Warrington, S. J.; Schwartz, M. S.; Mangin, E.; Boundy, K.; Bhagunde, P.; Colon-Gonzalez, F., Pharmacokinetics, safety, and tolerability of single and multiple doses of relebactam, a β-lactamase inhibitor, in combination with imipenem and cilastatin in healthy participants. *Antimicrobial agents and chemotherapy* **2018,** *62* (9), e00280-18.
39. Berglundh, T.; Krok, L.; Liljenberg, B.; Westfelt, E.; Serino, G.; Lindhe, J., The use of metronidazole and amoxicillin in the treatment of advanced periodontal disease: a prospective, controlled clinical trial. *Journal of Clinical Periodontology* **1998,** *25* (5), 354-362.
40. Stein, C.; Makarewicz, O.; Bohnert, J. A.; Pfeifer, Y.; Kesselmeier, M.; Hagel, S.; Pletz, M. W., Three dimensional checkerboard synergy analysis of colistin, meropenem, tigecycline against multidrug-resistant clinical Klebsiella pneumonia isolates. *PloS one* **2015,** *10* (6), e0126479.
41. Rodríguez-Avial, I.; Pena, I.; Picazo, J. J.; Rodríguez-Avial, C.; Culebras, E., In vitro activity of the next-generation aminoglycoside plazomicin alone and in combination with colistin, meropenem, fosfomycin or tigecycline against carbapenemase-producing Enterobacteriaceae strains. *International journal of antimicrobial agents* **2015,** *46* (6), 616-621.
42. Tängdén, T.; Hickman, R. A.; Forsberg, P.; Lagerbäck, P.; Giske, C. G.; Cars, O., Evaluation of double-and triple-antibiotic combinations for VIM-and NDM-producing Klebsiella pneumoniae by in vitro time-kill experiments. *Antimicrobial agents and chemotherapy* **2014,** *58* (3), 1757-1762.
43. Rayaprolu, B. M.; Strawser, J. J.; Anyarambhatla, G., Excipients in parenteral formulations: selection considerations and effective utilization with small molecules and biologics. *Drug development and industrial pharmacy* **2018,** *44* (10), 1565-1571.
44. Li, J.; Zeng, M.; Shan, H.; Tong, C., Microneedle patches as drug and vaccine delivery platform. *Current medicinal chemistry* **2017,** *24* (22), 2413-2422.
45. Tiwari, G.; Tiwari, R.; Sriwastawa, B.; Bhati, L.; Pandey, S.; Pandey, P.; Bannerjee, S. K., Drug delivery systems: An updated review. *International journal of pharmaceutical investigation* **2012,** *2* (1), 2.
46. Panzarini, E.; Inguscio, V.; Tenuzzo, B. A.; Carata, E.; Dini, L., Nanomaterials and autophagy: new insights in cancer treatment. *Cancers* **2013,** *5* (1), 296-319.
47. Weng, M.; Yu, X., Electrochemical oxidation of para-aminophenol with rare earth doped lead dioxide electrodes: kinetics modeling and mechanism. *Frontiers in Chemistry* **2019,** *7*, 382.
48. Bhat, M.; Shenoy, S.; Udupa, N.; Srinivas, C., Optimization of delivery of betamethasone-dipropionate from skin preparation. *Indian Drugs* **1995,** *32* (5), 211-214.

49. Thacharodi, D.; Rao, K. P., Development and in vitro evaluation of chitosan-based transdermal drug delivery systems for the controlled delivery of propranolol hydrochloride. *Biomaterials* **1995,** *16* (2), 145-148.
50. Large, D. E.; Abdelmessih, R. G.; Fink, E. A.; Auguste, D. T., Liposome composition in drug delivery design, synthesis, characterization, and clinical application. *Advanced Drug Delivery Reviews* **2021,** *176*, 113851.
51. Jain, A.; Jain, S. K., Stimuli-responsive smart liposomes in cancer targeting. *Current drug targets* **2018,** *19* (3), 259-270.
52. De Leo, V.; Milano, F.; Agostiano, A.; Catucci, L., Recent advancements in polymer/liposome assembly for drug delivery: From surface modifications to hybrid vesicles. *Polymers* **2021,** *13* (7), 1027.
53. Jain, A.; Jain, S., Advances in tumor targeted liposomes. *Current molecular medicine* **2018,** *18* (1), 44-57.
54. Mu, L.-M.; Ju, R.-J.; Liu, R.; Bu, Y.-Z.; Zhang, J.-Y.; Li, X.-Q.; Zeng, F.; Lu, W.-L., Dual-functional drug liposomes in treatment of resistant cancers. *Advanced drug delivery reviews* **2017,** *115*, 46-56.
55. Park, J. W.; Hong, K.; Kirpotin, D. B.; Colbern, G.; Shalaby, R.; Baselga, J.; Shao, Y.; Nielsen, U. B.; Marks, J. D.; Moore, D., Anti-HER2 immunoliposomes: enhanced efficacy attributable to targeted delivery. *Clinical Cancer Research* **2002,** *8* (4), 1172-1181.
56. Lombardo, G. E.; Maggisano, V.; Celano, M.; Cosco, D.; Mignogna, C.; Baldan, F.; Lepore, S. M.; Allegri, L.; Moretti, S.; Durante, C., Anti-hTERT siRNA-Loaded Nanoparticles Block the Growth of Anaplastic Thyroid Cancer XenograftNanodelivery of Anti-TERT RNAs in Thyroid Cancer Xenograft. *Molecular Cancer Therapeutics* **2018,** *17* (6), 1187-1195.
57. Çağdaş, M.; Sezer, A. D.; Bucak, S., Liposomes as potential drug carrier systems for drug delivery. *Application of nanotechnology in drug delivery* **2014,** *1*, 1-50.
58. Alavi, M.; Karimi, N.; Safaei, M., Application of various types of liposomes in drug delivery systems. *Advanced pharmaceutical bulletin* **2017,** *7* (1), 3.
59. Lamichhane, N.; Udayakumar, T. S.; D'Souza, W. D.; Simone, C. B.; Raghavan, S. R.; Polf, J.; Mahmood, J., Liposomes: clinical applications and potential for image-guided drug delivery. *Molecules* **2018,** *23* (2), 288.
60. Bulbake, U.; Doppalapudi, S.; Kommineni, N.; Khan, W., Liposomal formulations in clinical use: an updated review. *Pharmaceutics* **2017,** *9* (2), 12.
61. Slingerland, M.; Guchelaar, H.-J.; Rosing, H.; Scheulen, M. E.; van Warmerdam, L. J.; Beijnen, J. H.; Gelderblom, H., Bioequivalence of Liposome-Entrapped Paclitaxel Easy-To-Use (LEP-ETU) formulation and paclitaxel in polyethoxylated castor oil: a randomized, two-period crossover study in patients with advanced cancer. *Clinical therapeutics* **2013,** *35* (12), 1946-1954.
62. Meers, P. R.; Pak, C.; Ali, S.; Janoff, A.; Franklin, J. C.; Erukulla, R. K.; Cabral-Lilly, D.; Ahl, P. L., Peptide-lipid conjugates, liposomes and lipsomal drug delivery. Google Patents: 2002.
63. Ling, L.; Ismail, M.; Du, Y.; Yao, C.; Li, X., Lipoic acid-derived cross-linked liposomes for reduction-responsive delivery of anticancer drug. *International Journal of Pharmaceutics* **2019,** *560*, 246-260.
64. Lushchak, V. I., Glutathione homeostasis and functions: potential targets for medical interventions. *Journal of amino acids* **2012,** *2012*.

65. Shim, G.; Kim, D.; Lee, S.; Chang, R. S.; Byun, J.; Oh, Y.-K., Staphylococcus aureus-mimetic control of antibody orientation on nanoparticles. *Nanomedicine: Nanotechnology, Biology and Medicine* **2019,** *16*, 267-277.
66. Urits, I.; Swanson, D.; Swett, M. C.; Patel, A.; Berardino, K.; Amgalan, A.; Berger, A. A.; Kassem, H.; Kaye, A. D.; Viswanath, O., A review of patisiran (ONPATTRO®) for the treatment of polyneuropathy in people with hereditary transthyretin amyloidosis. *Neurology and therapy* **2020,** *9* (2), 301-315.
67. Adams, D.; Gonzalez-Duarte, A.; O'Riordan, W. D.; Yang, C.-C.; Ueda, M.; Kristen, A. V.; Tournev, I.; Schmidt, H. H.; Coelho, T.; Berk, J. L., Patisiran, an RNAi therapeutic, for hereditary transthyretin amyloidosis. *New England Journal of Medicine* **2018,** *379* (1), 11-21.
68. Hasannia, M.; Aliabadi, A.; Abnous, K.; Taghdisi, S. M.; Ramezani, M.; Alibolandi, M., Synthesis of block copolymers used in polymersome fabrication: Application in drug delivery. *Journal of Controlled Release* **2022,** *341*, 95-117.
69. Liu, Z.; Zhou, W.; Qi, C.; Kong, T., Interface engineering in multiphase systems toward synthetic cells and organelles: From soft matter fundamentals to biomedical applications. *Advanced Materials* **2020,** *32* (43), 2002932.
70. Gaitzsch, J.; Huang, X.; Voit, B., Engineering functional polymer capsules toward smart nanoreactors. *Chemical reviews* **2016,** *116* (3), 1053-1093.
71. Egli, S.; Schlaad, H.; Bruns, N.; Meier, W., Functionalization of block copolymer vesicle surfaces. *Polymers* **2011,** *3* (1), 252-280.
72. Gaitzsch, J.; Appelhans, D.; Voit, B., Responsive polymersome. *Nachrichten aus der Chemie* **2012,** *60* (12), 1176-1180.
73. Matoori, S.; Leroux, J.-C., Twenty-five years of polymersomes: lost in translation? *Materials Horizons* **2020,** *7* (5), 1297-1309.
74. Feng, H.; Lu, X.; Wang, W.; Kang, N.-G.; Mays, J. W., Block copolymers: Synthesis, self-assembly, and applications. *Polymers* **2017,** *9* (10), 494.
75. Michler, G. H.; Balta-Calleja, F. J., *Mechanical properties of polymers based on nanostructure and morphology*. CRC Press: 2016.
76. Schöbel, J. Block Copolymer Micelles as Efficient Templates for Mesostructured Hybrid Materials. 2018.
77. Lefley, J.; Waldron, C.; Becer, C. R., Macromolecular design and preparation of polymersomes. *Polymer Chemistry* **2020,** *11* (45), 7124-7136.
78. Škrlová, K.; Rybková, Z.; Stachurová, T.; Zagora, J.; Malachová, K.; Měřinská, D.; Gabor, R.; Havlíček, M.; Muñoz-Bonilla, A.; Fernández-García, M., Long-term antimicrobial effect of polylactide-based composites suitable for biomedical use. *Polymer Testing* **2022,** *116*, 107760.
79. Carvalho, J. R.; Trindade, P. H.; Conde, G.; Antonioli, M. L.; Funnicelli, M. I.; Dias, P. P.; Canola, P. A.; Chinelatto, M. A.; Ferraz, G. C., Facial Expressions of Horses Using Weighted Multivariate Statistics for Assessment of Subtle Local Pain Induced by Polylactide-Based Polymers Implanted Subcutaneously. *Animals* **2022,** *12* (18), 2400.
80. Wang, Z.; Wang, Y.; Ito, Y.; Zhang, P.; Chen, X., A comparative study on the in vivo degradation of poly (L-lactide) based composite implants for bone fracture fixation. *Scientific reports* **2016,** *6* (1), 1-12.
81. Lee, J. S.; Feijen, J., Biodegradable polymersomes as carriers and release systems for paclitaxel using Oregon Green® 488 labeled paclitaxel as a model compound. *Journal of controlled release* **2012,** *158* (2), 312-318.

82. Meng, F.; Hiemstra, C.; Engbers, G. H.; Feijen, J., Biodegradable polymersomes. *Macromolecules* **2003,** *36* (9), 3004-3006.
83. Ayen, W. Y.; Kumar, N., In Vivo Evaluation of Doxorubicin-Loaded (PEG)3-PLA Nanopolymersomes (PolyDoxSome) Using DMBA-Induced Mammary Carcinoma Rat Model and Comparison with Marketed LipoDox™. *Pharmaceutical Research* **2012,** *29* (9), 2522-2533.
84. Ayen, W. Y.; Garkhal, K.; Kumar, N., Doxorubicin-Loaded (PEG)3-PLA Nanopolymersomes: Effect of Solvents and Process Parameters on Formulation Development and In Vitro Study. *Molecular Pharmaceutics* **2011,** *8* (2), 466-478.
85. Romberg, B.; Metselaar, J. M.; Baranyi, L.; Snel, C. J.; Bünger, R.; Hennink, W. E.; Szebeni, J.; Storm, G., Poly(amino acid)s: Promising enzymatically degradable stealth coatings for liposomes. *International Journal of Pharmaceutics* **2007,** *331* (2), 186-189.
86. Abbina, S.; Parambath, A., 14 - PEGylation and its alternatives: A summary. In *Engineering of Biomaterials for Drug Delivery Systems*, Parambath, A., Ed. Woodhead Publishing: 2018; pp 363-376.
87. Liarou, E.; Varlas, S.; Skoulas, D.; Tsimblouli, C.; Sereti, E.; Dimas, K.; Iatrou, H., Smart polymersomes and hydrogels from polypeptide-based polymer systems through α-amino acid N-carboxyanhydride ring-opening polymerization. From chemistry to biomedical applications. *Progress in Polymer Science* **2018,** *83*, 28-78.
88. Oliveira, H.; Pérez-Andrés, E.; Thevenot, J.; Sandre, O.; Berra, E.; Lecommandoux, S., Magnetic field triggered drug release from polymersomes for cancer therapeutics. *Journal of Controlled Release* **2013,** *169* (3), 165-170.
89. Gondi, C. S.; Rao, J. S., Cathepsin B as a cancer target. *Expert Opinion on Therapeutic Targets* **2013,** *17* (3), 281-291.
90. Le Hellaye, M.; Fortin, N.; Guilloteau, J.; Soum, A.; Lecommandoux, S.; Guillaume, S. M., Biodegradable Polycarbonate-b-polypeptide and Polyester-b-polypeptide Block Copolymers: Synthesis and Nanoparticle Formation Towards Biomaterials. *Biomacromolecules* **2008,** *9* (7), 1924-1933.
91. Sanson, C.; Schatz, C.; Le Meins, J.-F.; Brûlet, A.; Soum, A.; Lecommandoux, S., Biocompatible and Biodegradable Poly(trimethylene carbonate)-b-Poly(l-glutamic acid) Polymersomes: Size Control and Stability. *Langmuir* **2010,** *26* (4), 2751-2760.
92. Iatrou, H.; Dimas, K.; Gkikas, M.; Tsimblouli, C.; Sofianopoulou, S., Polymersomes from Polypeptide Containing Triblock Co- and Terpolymers for Drug Delivery against Pancreatic Cancer: Asymmetry of the External Hydrophilic Blocks. *Macromolecular Bioscience* **2014,** *14* (9), 1222-1238.
93. Xu, X.; Wang, Y.; Chen, Z.; Sternlicht, M. D.; Hidalgo, M.; Steffensen, B., Matrix Metalloproteinase-2 Contributes to Cancer Cell Migration on Collagen. *Cancer Research* **2005,** *65* (1), 130-136.
94. Tai, W.; Mo, R.; Di, J.; Subramanian, V.; Gu, X.; Gu, Z., Bio-Inspired Synthetic Nanovesicles for Glucose-Responsive Release of Insulin. *Biomacromolecules* **2014,** *15* (10), 3495-3502.
95. Ramezani, P.; Abnous, K.; Taghdisi, S. M.; Zahiri, M.; Ramezani, M.; Alibolandi, M., Targeted MMP-2 responsive chimeric polymersomes for therapy against colorectal cancer. *Colloids and Surfaces B: Biointerfaces* **2020,** *193*, 111135.
96. Tang, Q.; Hu, P.; Peng, H.; Zhang, N.; Zheng, Q.; He, Y., Near-infrared laser-triggered, self-immolative smart polymersomes for in vivo cancer therapy. *International Journal of Nanomedicine* **2020,** *15*, 137.

97. Canning, S. L.; Smith, G. N.; Armes, S. P., A Critical Appraisal of RAFT-Mediated Polymerization-Induced Self-Assembly. *Macromolecules* **2016,** *49* (6), 1985-2001.
98. Penfold, N. J. W.; Yeow, J.; Boyer, C.; Armes, S. P., Emerging Trends in Polymerization-Induced Self-Assembly. *ACS Macro Letters* **2019,** *8* (8), 1029-1054.
99. Tan, J.; Xu, Q.; Li, X.; He, J.; Zhang, Y.; Dai, X.; Yu, L.; Zeng, R.; Zhang, L., Enzyme-PISA: An Efficient Method for Preparing Well-Defined Polymer Nano-Objects under Mild Conditions. *Macromolecular Rapid Communications* **2018,** *39* (9), 1700871.
100. Li, Q.; Lei Wong, Y.; Yueqi Lee, M.; Li, Y.; Kang, C., Solution structure of the transmembrane domain of the mouse erythropoietin receptor in detergent micelles. *Scientific reports* **2015,** *5* (1), 1-10.
101. Rössler, A.; Skillas, G.; Pratsinis, S. E., Nanopartikel—materialien der zukunft: Maßgeschneiderte werkstoffe. *Chemie in unserer Zeit* **2001,** *35* (1), 32-41.
102. Gao, W.; Thamphiwatana, S.; Angsantikul, P.; Zhang, L., Nanoparticle approaches against bacterial infections. *Wiley interdisciplinary reviews: nanomedicine and nanobiotechnology* **2014,** *6* (6), 532-547.
103. Krumm, C. Endgruppendesign von Poly(2-Oxazolin)en für nanostrukturierte Materialien und schaltbare bioaktive Polymere. Dissertation, TU-Dortmund, 2014.
104. Yan, J.; Su, T.; Cheng, F.; Cao, J.; Zhang, H.; He, B., Multifunctional nanoparticles self-assembled from polyethylenimine-based graft polymers as efficient anticancer drug delivery. *Colloids and Surfaces B: Biointerfaces* **2017,** *155*, 118-127.
105. Li, X.; Iocozzia, J.; Chen, Y.; Zhao, S.; Cui, X.; Wang, W.; Yu, H.; Lin, S.; Lin, Z., From precision synthesis of block copolymers to properties and applications of nanoparticles. *Angewandte Chemie International Edition* **2018,** *57* (8), 2046-2070.
106. Rauner, N.; Mueller, C.; Ring, S.; Boehle, S.; Strassburg, A.; Schoeneweiss, C.; Wasner, M.; Tiller, J. C., A Coating that Combines Lotus-Effect and Contact-Active Antimicrobial Properties on Silicone. *Advanced functional materials* **2018,** *28* (29), 1801248.
107. Orafa, Z.; Bakhshi, H.; Arab-Ahmadi, S.; Irani, S., Laponite/amoxicillin-functionalized PLA nanofibrous as osteoinductive and antibacterial scaffolds. *Scientific Reports* **2022,** *12* (1), 1-12.
108. Sharifi-Rad, J.; Hoseini-Alfatemi, S.; Sharifi-Rad, M.; Iriti, M., Antimicrobial synergic effect of Allicin and silver nanoparticles on skin infection caused by methicillin resistant Staphylococcus aureus spp. *Annals of medical and health sciences research* **2014,** *4* (6), 863-868.
109. Suhail, M.; Rosenholm, J. M.; Minhas, M. U.; Badshah, S. F.; Naeem, A.; Khan, K. U.; Fahad, M., Nanogels as drug-delivery systems: A comprehensive overview. *Therapeutic Delivery* **2019,** *10* (11), 697-717.
110. Akiyoshi, K.; Kobayashi, S.; Shichibe, S.; Mix, D.; Baudys, M.; Kim, S. W.; Sunamoto, J., Self-assembled hydrogel nanoparticle of cholesterol-bearing pullulan as a carrier of protein drugs: complexation and stabilization of insulin. *Journal of Controlled Release* **1998,** *54* (3), 313-320.
111. Sultana, F.; Imran-Ul-Haque, M.; Arafat, M.; Sharmin, S., An overview of nanogel drug delivery system. *Journal of Applied Pharmaceutical Science* **2013,** *3* (8), S95-S105.

112. Yu, S.; Yao, P.; Jiang, M.; Zhang, G., Nanogels prepared by self-assembly of oppositely charged globular proteins. *Biopolymers: Original Research on Biomolecules* **2006,** *83* (2), 148-158.
113. Khalid, Q.; Ahmad, M.; Usman Minhas, M., Hydroxypropyl-β-cyclodextrin hybrid nanogels as nano-drug delivery carriers to enhance the solubility of dexibuprofen: Characterization, in vitro release, and acute oral toxicity studies. *Advances in Polymer Technology* **2018,** *37* (6), 2171-2185.
114. Sarfraz, R. M.; Khan, M. U.; Mahmood, A.; Akram, M. R.; Minhas, M. U.; Qaisar, M. N.; Ali, M. R.; Ahmad, H.; Zaman, M., Synthesis of co-polymeric network of carbopol-g-methacrylic acid nanogels drug carrier system for gastro-protective delivery of ketoprofen and its evaluation. *Polymer-Plastics Technology and Materials* **2020,** *59* (10), 1109-1123.
115. Xiong, M.-H.; Bao, Y.; Yang, X.-Z.; Wang, Y.-C.; Sun, B.; Wang, J., Lipase-sensitive polymeric triple-layered nanogel for “on-demand” drug delivery. *Journal of the American Chemical Society* **2012,** *134* (9), 4355-4362.
116. Jin, S.; Wan, J.; Meng, L.; Huang, X.; Guo, J.; Liu, L.; Wang, C., Biodegradation and toxicity of protease/redox/pH stimuli-responsive PEGlated PMAA nanohydrogels for targeting drug delivery. *ACS applied materials & interfaces* **2015,** *7* (35), 19843-19852.
117. Stefanello, T. F.; Couturaud, B.; Szarpak-Jankowska, A.; Fournier, D.; Louage, B.; Garcia, F. P.; Nakamura, C. V.; De Geest, B. G.; Woisel, P.; Van Der Sanden, B., Coumarin-containing thermoresponsive hyaluronic acid-based nanogels as delivery systems for anticancer chemotherapy. *Nanoscale* **2017,** *9* (33), 12150-12162.
118. Senthilkumar, T.; Lv, F.; Zhao, H.; Liu, L.; Wang, S., Conjugated Polymer Nanogel Binding Anticancer Drug through Hydrogen Bonds for Sustainable Drug Delivery. *ACS Applied Bio Materials* **2019,** *2* (12), 6012-6020.
119. Tao, Q.; Zhong, J.; Wang, R.; Huang, Y. Ionic and Enzymatic Multiple-Crosslinked Nanogels for Drug Delivery *Polymers* [Online], 2021.
120. Atanase, L. I.; Riess, G., Self-assembly of block and graft copolymers in organic solvents: An overview of recent advances. *Polymers* **2018,** *10* (1), 62.
121. Hussein, Y. H.; Youssry, M., Polymeric micelles of biodegradable diblock copolymers: Enhanced encapsulation of hydrophobic drugs. *Materials* **2018,** *11* (5), 688.
122. Muddineti, O. S.; Kumari, P.; Ray, E.; Ghosh, B.; Biswas, S., Curcumin-loaded chitosan–cholesterol micelles: evaluation in monolayers and 3D cancer spheroid model. *Nanomedicine* **2017,** *12* (12), 1435-1453.
123. Li, G.; Zhao, L., Sorafenib-loaded hydroxyethyl starch-TG100-115 micelles for the treatment of liver cancer based on synergistic treatment. *Drug Delivery* **2019,** *26* (1), 756-764.
124. Dong, H.; Dube, N.; Shu, J. Y.; Seo, J. W.; Mahakian, L. M.; Ferrara, K. W.; Xu, T., Long-circulating 15 nm micelles based on amphiphilic 3-helix peptide–PEG conjugates. *ACS nano* **2012,** *6* (6), 5320-5329.
125. Luxenhofer, R.; Schulz, A.; Roques, C.; Li, S.; Bronich, T. K.; Batrakova, E. V.; Jordan, R.; Kabanov, A. V., Doubly amphiphilic poly (2-oxazoline) s as high-capacity delivery systems for hydrophobic drugs. *Biomaterials* **2010,** *31* (18), 4972-4979.
126. Seo, Y.; Schulz, A.; Han, Y.; He, Z.; Bludau, H.; Wan, X.; Tong, J.; Bronich, T. K.; Sokolsky, M.; Luxenhofer, R., Poly (2-oxazoline) block copolymer based

formulations of taxanes: effect of copolymer and drug structure, concentration, and environmental factors. *Polymers for Advanced Technologies* **2015,** *26* (7), 837-850.
127. Wan, X.; Beaudoin, J. J.; Vinod, N.; Min, Y.; Makita, N.; Bludau, H.; Jordan, R.; Wang, A.; Sokolsky, M.; Kabanov, A. V., Co-delivery of paclitaxel and cisplatin in poly (2-oxazoline) polymeric micelles: Implications for drug loading, release, pharmacokinetics and outcome of ovarian and breast cancer treatments. *Biomaterials* **2019,** *192*, 1-14.
128. Zhang, H.; Guo, S.; Fan, W.; Zhao, Y., Ultrasensitive pH-induced water solubility switch using UCST polymers. *Macromolecules* **2016,** *49* (4), 1424-1433.
129. Safwat, M. A.; Mansour, H. F.; Hussein, A. K.; Abdelwahab, S.; Soliman, G. M., Polymeric micelles for the ocular delivery of triamcinolone acetonide: preparation and in vivo evaluation in a rabbit ocular inflammatory model. *Drug Delivery* **2020,** *27* (1), 1115-1124.
130. Duncan, R., Polymer therapeutics: Top 10 selling pharmaceuticals—What next? *Journal of Controlled release* **2014,** *190*, 371-380.
131. Ringsdorf, H. In *Structure and properties of pharmacologically active polymers*, Journal of Polymer Science: Polymer Symposia, Wiley Online Library: 1975; pp 135-153.
132. Veronese, F. M.; Pasut, G., PEGylation, successful approach to drug delivery. *Drug discovery today* **2005,** *10* (21), 1451-1458.
133. Pasut, G.; Veronese, F., Polymer–drug conjugation, recent achievements and general strategies. *Progress in polymer science* **2007,** *32* (8-9), 933-961.
134. Khandare, J.; Minko, T., Polymer–drug conjugates: progress in polymeric prodrugs. *Progress in polymer science* **2006,** *31* (4), 359-397.
135. Li, C.; Wallace, S., Polymer-drug conjugates: recent development in clinical oncology. *Advanced drug delivery reviews* **2008,** *60* (8), 886-898.
136. Radhakumary, C.; Antony, M.; Sreenivasan, K., Functionalized carbon dots enable simultaneous bone crack detection and drug deposition. **2015**.
137. Miller, A.; Shapiro, S.; Gershtein, R.; Kinarty, A.; Rawashdeh, H.; Honigman, S.; Lahat, N., Treatment of multiple sclerosis with copolymer-1 (Copaxone®): implicating mechanisms of Th1 to Th2/Th3 immune-deviation. *Journal of neuroimmunology* **1998,** *92* (1-2), 113-121.
138. Jalilian, B.; Einarsson, H. B.; Vorup-Jensen, T., Glatiramer acetate in treatment of multiple sclerosis: a toolbox of random co-polymers for targeting inflammatory mechanisms of both the innate and adaptive immune system? *International journal of molecular sciences* **2012,** *13* (11), 14579-14605.
139. Aharoni, R.; Teitelbaum, D.; Arnon, R.; Sela, M., Copolymer 1 acts against the immunodominant epitope 82–100 of myelin basic protein by T cell receptor antagonism in addition to major histocompatibility complex blocking. *Proceedings of the National Academy of Sciences* **1999,** *96* (2), 634-639.
140. Piedmonte, D. M.; Treuheit, M. J., Formulation of Neulasta®(pegfilgrastim). *Advanced drug delivery reviews* **2008,** *60* (1), 50-58.
141. Shao, Z. J.; Farooqi, M. I.; Diaz, S.; Krishna, A. K.; Muhammad, N. A., Effects of formulation variables and post-compression curing on drug release from a new sustained-release matrix material: polyvinylacetate-povidone. *Pharmaceutical development and technology* **2001,** *6* (2), 247-254.
142. Kranz, H.; Le Brun, V.; Wagner, T., Development of a multi particulate extended release formulation for ZK 811 752, a weakly basic drug. *International journal of pharmaceutics* **2005,** *299* (1-2), 84-91.

143. Hauschild, K.; Picker-Freyer, K. M., Evaluation of tableting and tablet properties of Kollidon SR: the influence of moisture and mixtures with theophylline monohydrate. *Pharmaceutical development and technology* **2006,** *11* (1), 125-140.
144. Asaduzzaman, M.; Elias-Al-Mamun, M.; Islam, M. S.; Jalil, R.-U., Effect of HPMC 4 Cps and Carbopol 974p NF On Release Kinetics Of Ciprofloxacin From Kollidon® SR Embedded Matrix Tablets. *J Pharm Sci Res* **2009,** *1* (4), 137-45.
145. Suryavanshi, P.; Banerjee, S., Exploration of theoretical and practical evaluation on Kollidon®SR matrix mediated amorphous filament extrusion of norfloxacin by melt extrusion. *Journal of Drug Delivery Science and Technology* **2022,** *67*, 102894.
146. YURTDAŞ-KIRIMLIOĞLU, G.; GÖRGÜLÜ, Ş., Design and characterization of montelukast sodium loaded Kollidon® SR nanoparticles and evaluation of release kinetics and cytotoxicity potential. *Latin American Journal of Pharmacy* **2019,** *38* (7), 1350-60.
147. Fik, C. P.; Krumm, C.; Muennig, C.; Baur, T. I.; Salz, U.; Bock, T.; Tiller, J. C., Impact of functional satellite groups on the antimicrobial activity and hemocompatibility of telechelic poly (2-methyloxazoline) s. *Biomacromolecules* **2012,** *13* (1), 165-172.
148. Milović, N. M.; Wang, J.; Lewis, K.; Klibanov, A. M., Immobilized N-alkylated polyethylenimine avidly kills bacteria by rupturing cell membranes with no resistance developed. *Biotechnology and bioengineering* **2005,** *90* (6), 715-722.
149. Fik, C. P.; Konieczny, S.; Pashley, D. H.; Waschinski, C. J.; Ladisch, R. S.; Salz, U.; Bock, T.; Tiller, J. C., Telechelic Poly (2-oxazoline) s with a Biocidal and a Polymerizable Terminal as Collagenase Inhibiting Additive for Long-Term Active Antimicrobial Dental Materials. *Macromolecular bioscience* **2014,** *14* (11), 1569-1579.
150. Sobczak, M.; Nałęcz-Jawecki, G.; Kołodziejski, W. L.; Goś, P.; Żółtowska, K., Synthesis and study of controlled release of ofloxacin from polyester conjugates. *International journal of pharmaceutics* **2010,** *402* (1-2), 37-43.
151. Namazi, H.; Kanani, A., Investigation diffusion mechanism of β-lactam conjugated telechelic polymers of PEG and β-cyclodextrin as the new nanosized drug carrier devices. *Carbohydrate Polymers* **2009,** *76* (1), 46-50.
152. Greenwald, R. B.; Zhao, H.; Peng, P.; Longley, C. B.; Dai, Q.-H.; Xia, J.; Martinez, A., An unexpected amide bond cleavage: poly (ethylene glycol) transport forms of vancomycin. 2. *European journal of medicinal chemistry* **2005,** *40* (8), 798-804.
153. Pichavant, L.; Bourget, C.; Durrieu, M.-C.; Héroguez, V., Synthesis of pH-sensitive particles for local delivery of an antibiotic via dispersion ROMP. *Macromolecules* **2011,** *44* (20), 7879-7887.
154. Das, D.; Srinivasan, S.; Kelly, A. M.; Chiu, D. Y.; Daugherty, B. K.; Ratner, D. M.; Stayton, P. S.; Convertine, A. J., RAFT polymerization of ciprofloxacin prodrug monomers for the controlled intracellular delivery of antibiotics. *Polymer Chemistry* **2016,** *7* (4), 826-837.
155. Parwe, S. P.; Chaudhari, P. N.; Mohite, K. K.; Selukar, B. S.; Nande, S. S.; Garnaik, B., Synthesis of ciprofloxacin-conjugated poly (L-lactic acid) polymer for nanofiber fabrication and antibacterial evaluation. *International journal of nanomedicine* **2014,** *9*, 1463.

156. Kugel, A.; Chisholm, B.; Ebert, S.; Jepperson, M.; Jarabek, L.; Stafslien, S., Antimicrobial polysiloxane polymers and coatings containing pendant levofloxacin. *Polymer Chemistry* **2010,** *1* (4), 442-452.
157. Yang, H.; Lopina, S. T., Penicillin V-conjugated PEG-PAMAM star polymers. *Journal of Biomaterials Science, Polymer Edition* **2003,** *14* (10), 1043-1056.
158. Harris, J. M.; Bentley, M. D.; Moreadith, R. W.; Viegas, T. X.; Fang, Z.; Yoon, K.; Weimer, R.; Dizman, B.; Nordstierna, L., Tuning drug release from polyoxazoline-drug conjugates. *European Polymer Journal* **2019,** *120*, 109241.
159. Ulbrich, K.; Šubr, V.; Strohalm, J.; Plocova, D.; Jelınková, M.; Říhová, B., Polymeric drugs based on conjugates of synthetic and natural macromolecules: I. Synthesis and physico-chemical characterisation. *Journal of controlled release* **2000,** *64* (1-3), 63-79.
160. Haag, R.; Kratz, F., Polymer therapeutics: concepts and applications. *Angewandte Chemie International Edition* **2006,** *45* (8), 1198-1215.
161. Zhao, Y.-J.; Wei, W.; Su, Z.-G.; Ma, G.-H., Poly (ethylene glycol) prodrug for anthracyclines via N-Mannich base linker: Design, synthesis and biological evaluation. *International journal of pharmaceutics* **2009,** *379* (1), 90-99.
162. Nathan, A.; Zalipsky, S.; Ertel, S. I.; Agathos, S. N.; Yarmush, M. L.; Kohn, J., Copolymers of lysine and polyethylene glycol: a new family of functionalized drug carriers. *Bioconjugate chemistry* **1993,** *4* (1), 54-62.
163. Maeda, H.; Takeshita, J.; Kanamaru, R., A lipophilic derivative of neocarzinostatin a polymer conjugation of an antitumor protein antibiotic. *International journal of peptide and protein research* **1979,** *14* (2), 81-87.
164. Cirillo, G.; Mauro, M. V.; Spizzirri, U. G.; Cavalcanti, P.; Puoci, F.; Giraldi, C.; Vittorio, O.; Picci, N.; Iemma, F., Synthesis, characterization and antimicrobial activity of conjugates based on fluoroquinolon-type antibiotics and gelatin. *Journal of Materials Science: Materials in Medicine* **2014,** *25* (1), 67-77.
165. Du, J.; Bandara, H.; Du, P.; Huang, H.; Hoang, K.; Nguyen, D.; Mogarala, S. V.; Smyth, H. D., Improved biofilm antimicrobial activity of polyethylene glycol conjugated tobramycin compared to tobramycin in pseudomonas aeruginosa biofilms. *Molecular pharmaceutics* **2015,** *12* (5), 1544-1553.
166. Bahamondez-Canas, T. F.; Zhang, H.; Tewes, F.; Leal, J.; Smyth, H. D., PEGylation of tobramycin improves mucus penetration and antimicrobial activity against Pseudomonas aeruginosa biofilms in vitro. *Molecular Pharmaceutics* **2018,** *15* (4), 1643-1652.
167. Lawson, M. C.; Shoemaker, R.; Hoth, K. B.; Bowman, C. N.; Anseth, K. S., Polymerizable vancomycin derivatives for bactericidal biomaterial surface modification: structure− function evaluation. *Biomacromolecules* **2009,** *10* (8), 2221-2234.
168. Degitz, İ. A.; Gazioğlu, B. H.; Aksu, M. B.; Malta, S.; Sezer, A. D.; Eren, T., Antibacterial and hemolytic activity of cationic polymer-vancomycin conjugates. *European Polymer Journal* **2020,** *141*, 110084.
169. Tshweu, L. L.; Shemis, M. A.; Abdelghany, A.; Gouda, A.; Pilcher, L. A.; Sibuyi, N. R.; Meyer, M.; Dube, A.; Balogun, M. O., Synthesis, physicochemical characterization, toxicity and efficacy of a PEG conjugate and a hybrid PEG conjugate nanoparticle formulation of the antibiotic moxifloxacin. *RSC advances* **2020,** *10* (34), 19770-19780.
170. Turos, E.; Shim, J.-Y.; Wang, Y.; Greenhalgh, K.; Reddy, G. S. K.; Dickey, S.; Lim, D. V., Antibiotic-conjugated polyacrylate nanoparticles: new opportunities for

development of anti-MRSA agents. *Bioorganic & medicinal chemistry letters* **2007,** *17* (1), 53-56.
171. Panarin, E. F.; Solovskij, M. V., Polymer derivatives of β-lactam antibiotics of the penicillin series. *Journal of controlled release* **1989,** *10* (1), 119-129.
172. Gonçalves, I.; Abreu, A. S.; Matamá, T.; Ribeiro, A.; Gomes, A. C.; Silva, C.; Cavaco-Paulo, A., Enzymatic synthesis of poly (catechin)-antibiotic conjugates: an antimicrobial approach for indwelling catheters. *Applied microbiology and biotechnology* **2015,** *99* (2), 637-651.
173. He, M.; Xiao, H.; Zhou, Y.; Lu, P., Synthesis, characterization and antimicrobial activities of water-soluble amphiphilic copolymers containing ciprofloxacin and quaternary ammonium salts. *Journal of Materials Chemistry B* **2015,** *3* (18), 3704-3713.
174. Chang, J.; Chen, Y.; Xu, Z.; Wang, Z.; Zeng, Q.; Fan, H., Switchable control of antibiotic activity: a shape-shifting “tail” strategy. *Bioconjugate Chemistry* **2018,** *29* (1), 74-82.
175. Harmuth, S., Masterarbeit. *TU-Dortmund* **2013**.
176. Keil, J. Synthese und Untersuchung des Seitenketteneinflusses amphiphiler Blockcopolymere auf deren antimikrobielle Wirkung. TU-Dortmund, 09.09.2020.
177. Tophoven, J. Synthese und Charakterisierung amphiphiler Blockcopolymere. TU-Dortmund, 03.09.2019.
178. Oruc, M. F. Untersuchung der antimikrobiellen Wirkung von amphiphilen Blockcopolymeren. TU-Dortmund, 18.03.2019.
179. Romanovska, A.; Keil, J.; Tophoven, J.; Oruc, M. F.; Schmidt, M.; Breisch, M.; Sengstock, C.; Weidlich, D.; Klostermeier, D.; Tiller, J. C., Conjugates of ciprofloxacin and amphiphilic block copoly (2-alkyl-2-oxazolines) s overcome efflux pumps and are active against CIP-resistant bacteria. *Molecular Pharmaceutics* **2021,** *18* (9), 3532-3543.
180. Ergene, C.; Yasuhara, K.; Palermo, E. F., Biomimetic antimicrobial polymers: Recent advances in molecular design. *Polymer Chemistry* **2018,** *9* (18), 2407-2427.
181. Palermo, E. F.; Lienkamp, K.; Gillies, E. R.; Ragogna, P. J., Antibacterial activity of polymers: discussions on the nature of amphiphilic balance. *Angewandte Chemie* **2019,** *131* (12), 3728-3731.
182. Bieser, A. M.; Thomann, Y.; Tiller, J. C., Contact-active antimicrobial and potentially self-polishing coatings based on cellulose. *Macromolecular bioscience* **2011,** *11* (1), 111-121.
183. Cheng, G.; Xue, H.; Zhang, Z.; Chen, S.; Jiang, S., A switchable biocompatible polymer surface with self-sterilizing and nonfouling capabilities. *Angewandte Chemie* **2008,** *120* (46), 8963-8966.
184. Ludtke, S. J.; He, K.; Heller, W. T.; Harroun, T. A.; Yang, L.; Huang, H. W., Membrane pores induced by magainin. *Biochemistry* **1996,** *35* (43), 13723-13728.
185. Strassburg, A.; Kracke, F.; Wenners, J.; Jemeljanova, A.; Kuepper, J.; Petersen, H.; Tiller, J. C., Nontoxic, hydrophilic cationic polymers—identified as class of antimicrobial polymers. *Macromolecular bioscience* **2015,** *15* (12), 1710-1723.
186. LeBel, M., Ciprofloxacin: chemistry, mechanism of action, resistance, antimicrobial spectrum, pharmacokinetics, clinical trials, and adverse reactions. *Pharmacotherapy: The Journal of Human Pharmacology and Drug Therapy* **1988,** *8* (1), 3-30.
187. Hooper, D. C., Mechanisms of action and resistance of older and newer fluoroquinolones. *Clinical infectious diseases* **2000,** *31* (Supplement_2), S24-S28.

188. Reece, R. J.; Maxwell, A., DNA gyrase: structure and function. *Critical reviews in biochemistry and molecular biology* **1991,** *26* (3-4), 335-375.
189. Collin, F.; Maxwell, A., The microbial toxin microcin B17: prospects for the development of new antibacterial agents. *Journal of molecular biology* **2019,** *431* (18), 3400-3426.
190. Hijazi, M.; Krumm, C.; Cinar, S.; Arns, L.; Alachraf, W.; Hiller, W.; Schrader, W.; Winter, R.; Tiller, J. C., Entropically driven polymeric enzyme inhibitors by end-group directed conjugation. *Chemistry–A European Journal* **2018,** *24* (18), 4523-4527.
191. Pittenger, M. F.; Mackay, A. M.; Beck, S. C.; Jaiswal, R. K.; Douglas, R.; Mosca, J. D.; Moorman, M. A.; Simonetti, D. W.; Craig, S.; Marshak, D. R., Multilineage potential of adult human mesenchymal stem cells. *science* **1999,** *284* (5411), 143-147.
192. Baksh, D.; Song, L.; Tuan, R. S., Adult mesenchymal stem cells: characterization, differentiation, and application in cell and gene therapy. *Journal of cellular and molecular medicine* **2004,** *8* (3), 301-316.
193. Ullah, I.; Subbarao, R. B.; Rho, G. J., Human mesenchymal stem cells-current trends and future prospective. *Bioscience reports* **2015,** *35* (2).
194. Sisto, F.; Bonomi, A.; Cavicchini, L.; Coccè, V.; Scaltrito, M. M.; Bondiolotti, G.; Alessandri, G.; Parati, E.; Pessina, A., Human mesenchymal stromal cells can uptake and release ciprofloxacin, acquiring in vitro anti-bacterial activity. *Cytotherapy* **2014,** *16* (2), 181-190.
195. Kamocki, K.; Nör, J. E.; Bottino, M. C., Effects of ciprofloxacin-containing antimicrobial scaffolds on dental pulp stem cell viability—In vitro studies. *Archives of oral biology* **2015,** *60* (8), 1131-1137.
196. Ng, V. W. L.; Ke, X.; Lee, A. L. Z.; Hedrick, J. L.; Yang, Y. Y., Synergistic Co-Delivery of Membrane-Disrupting Polymers with Commercial Antibiotics against Highly Opportunistic Bacteria. *Advanced Materials* **2013,** *25* (46), 6730-6736.
197. Szwarc, M., Levy, M., Milkovich R., *J. Am. Chem. Soc.* **1950,** *78*, 2656-2657.
198. Gao, M.; Deng, J.; Chu, H.; Tang, Y.; Wang, Z.; Zhao, Y.; Li, G., Stereoselective stabilization of polymeric vitamin E conjugate micelles. *Biomacromolecules* **2017,** *18* (12), 4349-4356.
199. Huttner, A.; Bielicki, J.; Clements, M. N.; Frimodt-Møller, N.; Muller, A. E.; Paccaud, J.-P.; Mouton, J. W., Oral amoxicillin and amoxicillin–clavulanic acid: properties, indications and usage. *Clinical Microbiology and Infection* **2020,** *26* (7), 871-879.
200. Easton, J.; Noble, S.; Perry, C. M., Amoxicillin/clavulanic acid. *Drugs* **2003,** *63* (3), 311-340.
201. Prasad, K.; Kalra, J., Oxygen free radicals and hypercholesterolemic atherosclerosis: effect of vitamin E. *American heart journal* **1993,** *125* (4), 958-973.
202. Kundu, S.; Sarkar, D., A year away to 100th year of vitamin E synthesis. *Journal of Heterocyclic Chemistry* **2021,** *58* (9), 1741-1748.
203. Fernholz, E., On the constitution of α-tocopherol. *Journal of the American Chemical Society* **1938,** *60* (3), 700-705.
204. Woodle, M. C.; Engbers, C. M.; Zalipsky, S., New amphipatic polymer-lipid conjugates forming long-circulating reticuloendothelial system-evading liposomes. *Bioconjugate chemistry* **1994,** *5* (6), 493-496.
205. Bonné, T. B.; Papadakis, C. M.; Lüdtke, K.; Jordan, R., Role of the tracer in characterizing the aggregation behavior of aqueous block copolymer solutions using

fluorescence correlation spectroscopy. *Colloid and Polymer Science* **2007,** *285* (5), 491-497.
206. Scherbart, A.; Schins, R.; van Berlo, D.; van Schooten, F.; Albrecht, C., Partikel–Makrophagen–Interaktionen: Untersuchungen zu oxidativem Stress und Entzündung. *Pneumologie* **2009,** *63* (S 01), P291.
207. Tophoven, J. Synthese und Charakterisierung von Triblockcopolymeren zur kontrollierten Deaktivierung von Polymer-Antibiotika-Konjugaten. TU-Dortmund, 24.02.2022.
208. Pichavant, L.; Carrié, H.; Nguyen, M. N.; Plawinski, L.; Durrieu, M.-C.; Héroguez, V., Vancomycin functionalized nanoparticles for bactericidal biomaterial surfaces. *Biomacromolecules* **2016,** *17* (4), 1339-1346.
209. Constantinou, A. P.; Zhang, K.; Somuncuoğlu, B.; Feng, B.; Georgiou, T. K., PEG-based methacrylate tetrablock terpolymers: How does the architecture control the gelation? *Macromolecules* **2021,** *54* (13), 6511-6524.
210. Alami-Milani, M.; Zakeri-Milani, P.; Valizadeh, H.; Salehi, R.; Salatin, S.; Naderinia, A.; Jelvehgari, M., Novel pentablock copolymers as thermosensitive self-assembling micelles for ocular drug delivery. *Advanced pharmaceutical bulletin* **2017,** *7* (1), 11.
211. Singh, N. K.; Lee, D. S., In situ gelling pH-and temperature-sensitive biodegradable block copolymer hydrogels for drug delivery. *Journal of Controlled Release* **2014,** *193*, 214-227.
212. Abandansari, H. S.; Aghaghafari, E.; Nabid, M. R.; Niknejad, H., Preparation of injectable and thermoresponsive hydrogel based on penta-block copolymer with improved sol stability and mechanical properties. *Polymer* **2013,** *54* (4), 1329-1340.
213. Steinhaus, A.; Srivastva, D.; Qiang, X.; Franzka, S.; Nikoubashman, A.; Gröschel, A. H., Controlling Janus nanodisc topology through ABC triblock terpolymer/homopolymer blending in 3D confinement. *Macromolecules* **2021,** *54* (3), 1224-1233.
214. Gröschel, A. H.; Walther, A.; Löbling, T. I.; Schacher, F. H.; Schmalz, H.; Müller, A. H., Guided hierarchical co-assembly of soft patchy nanoparticles. *Nature* **2013,** *503* (7475), 247-251.

7 Attachment

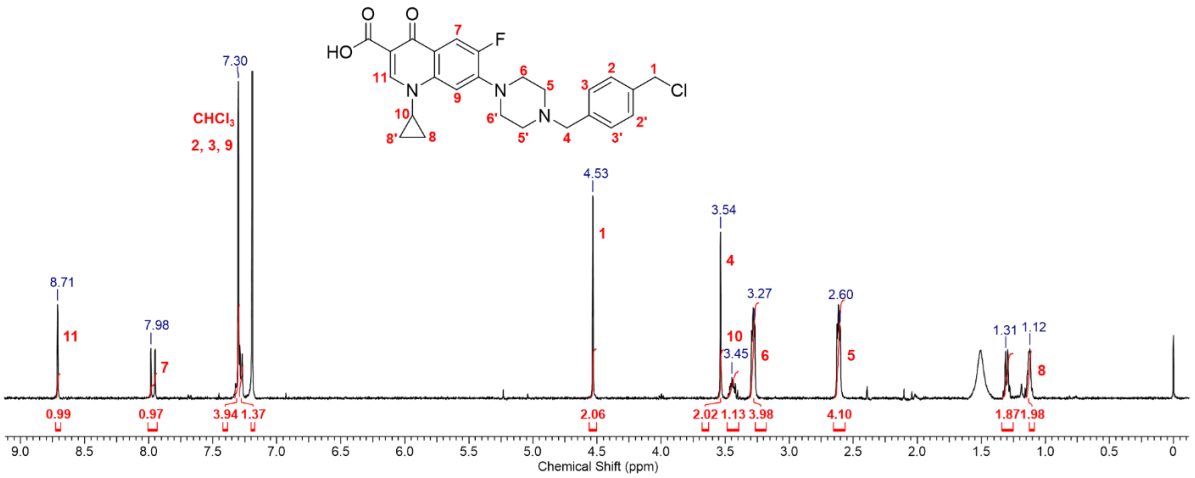

Supp. Fig. 1: *^{1}H NMR spectrum of xCIP.*

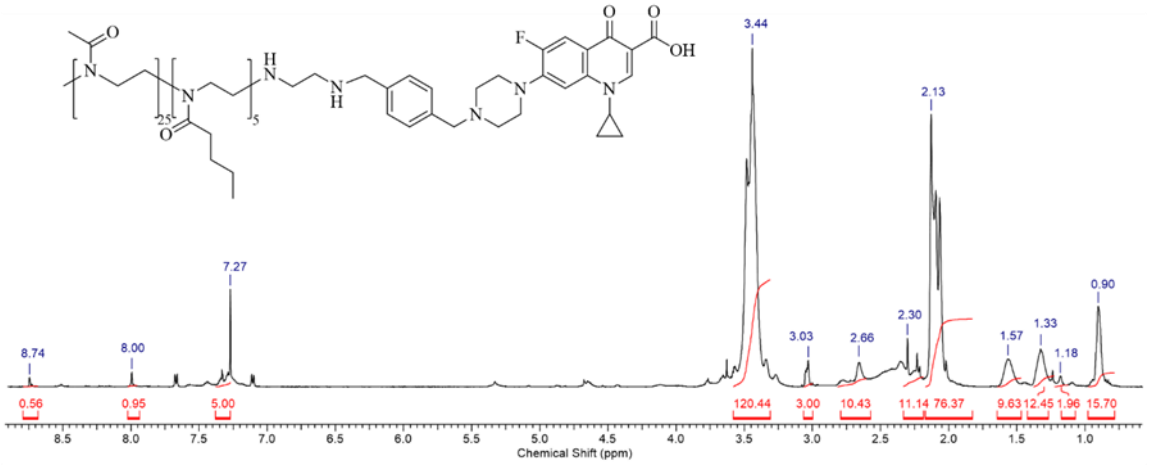

Supp. Fig. 2: *^{1}H NMR spectrum of $PMOx_{25}$-b-$PBuOx_{5}$-EDA-xCIP.*

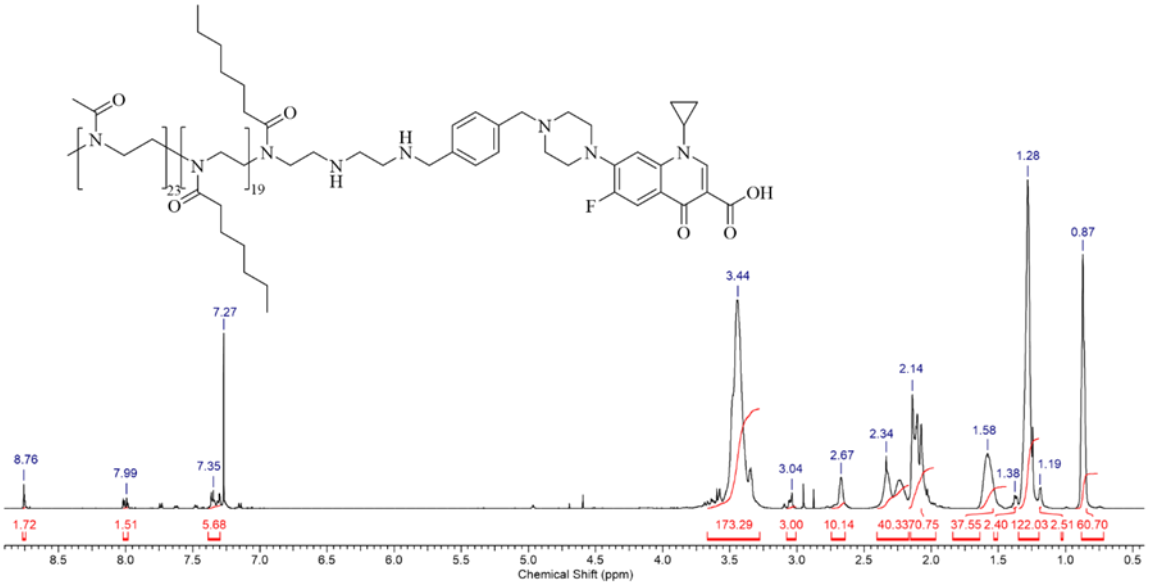

Supp. Fig. 3: *^{1}H NMR spectrum of $PMOx_{23}$-b-$PHexOx_{20}$-EDA-xCIP.*

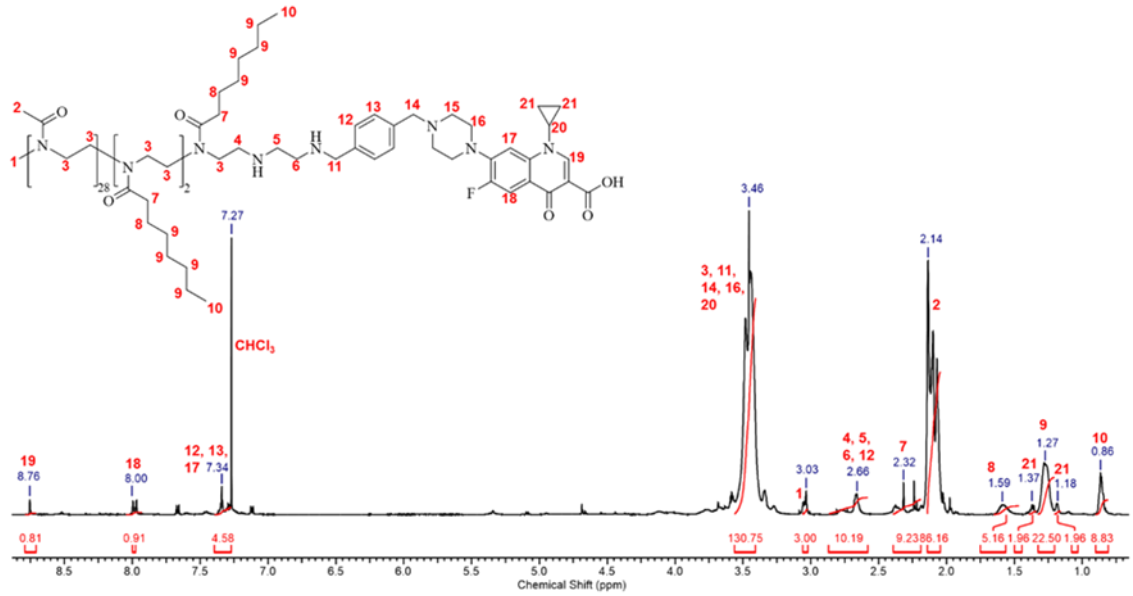

Supp. Fig. 4: *^{1}H NMR spectrum of $PMOx_{28}$-b-$PHeptOx_3$-EDA-xCIP.*

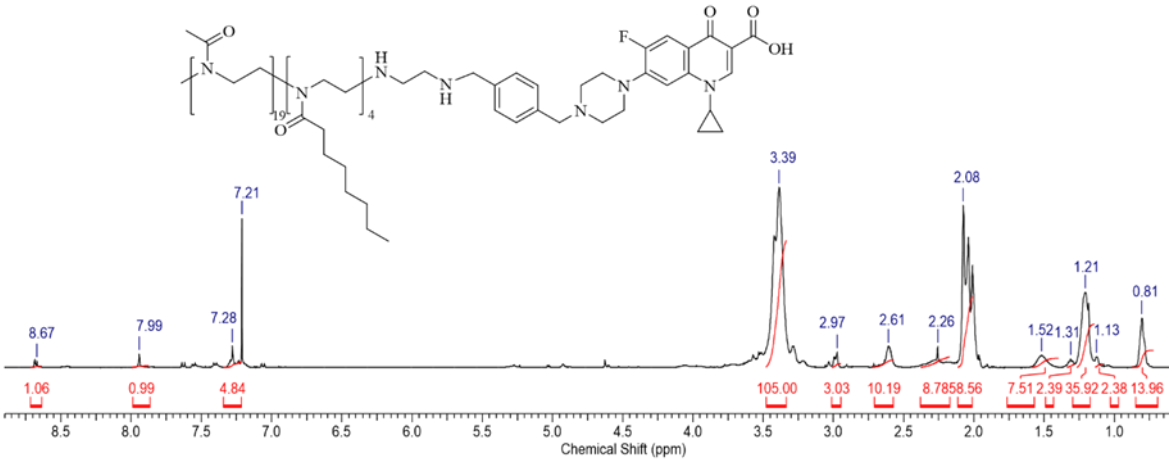

Supp. Fig. 5: *^{1}H NMR spectrum of $PMOx_{19}$-b-$PHeptOx_4$-EDA-xCIP.*

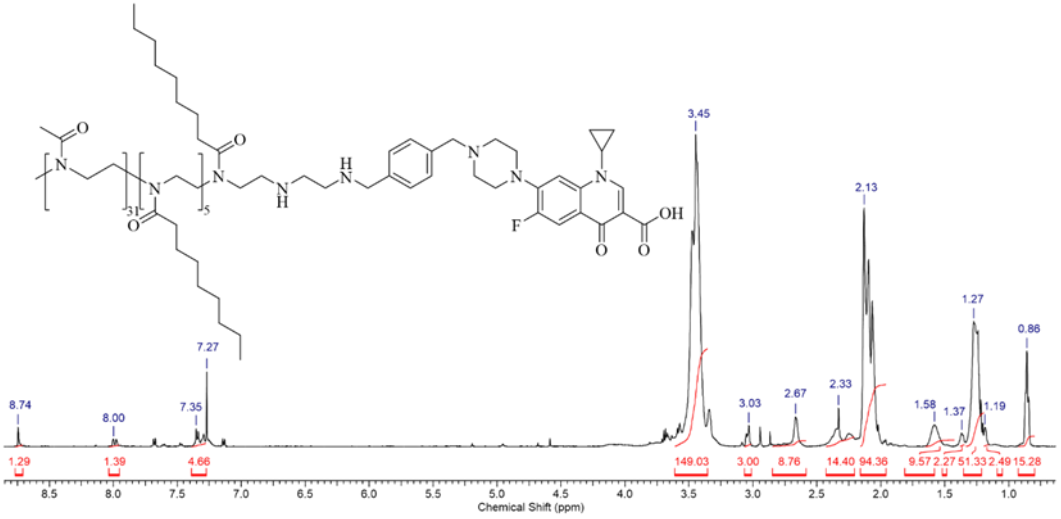

Supp. Fig. 6: *^{1}H NMR spectrum of $PMOx_{31}$-b-$POctOx_6$-EDA-xCIP.*

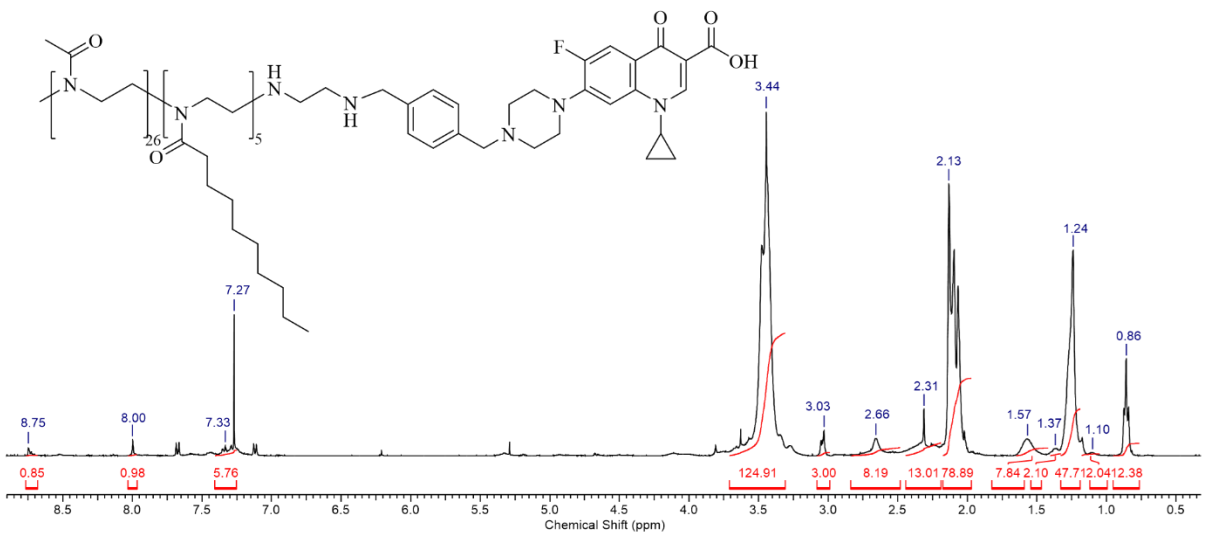

Supp. Fig. 7: *^{1}H NMR spectrum of PMOx$_{26}$-b-PNonOx$_{5}$-EDA-xCIP.*

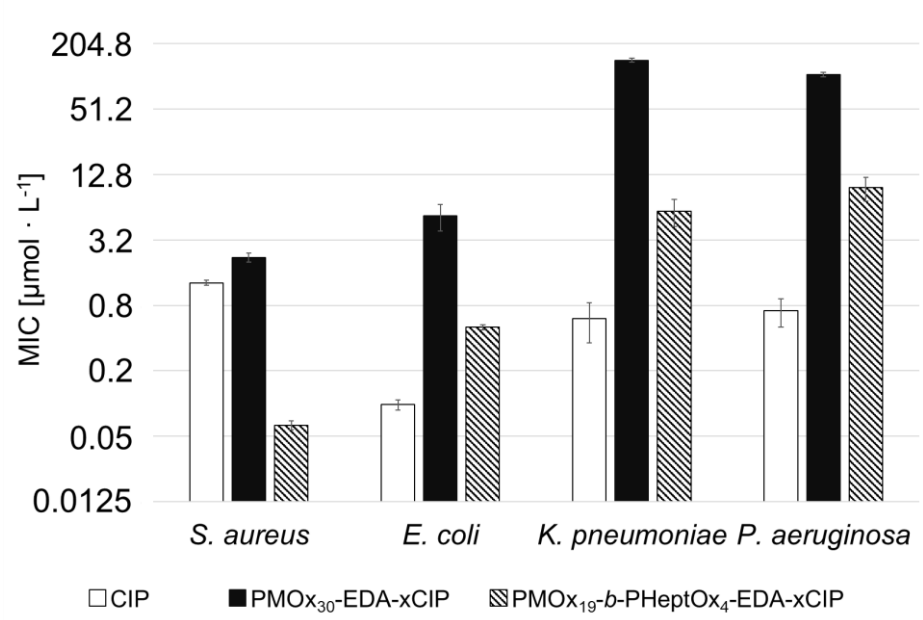

Supp. Fig. 8: *MIC-values of PMOx$_{30}$-EDA-xCIP (black) and PMOx$_{19}$-b-PHeptOx$_{4}$-EDA-xCIP (striped) in comparison to CIP (white).*

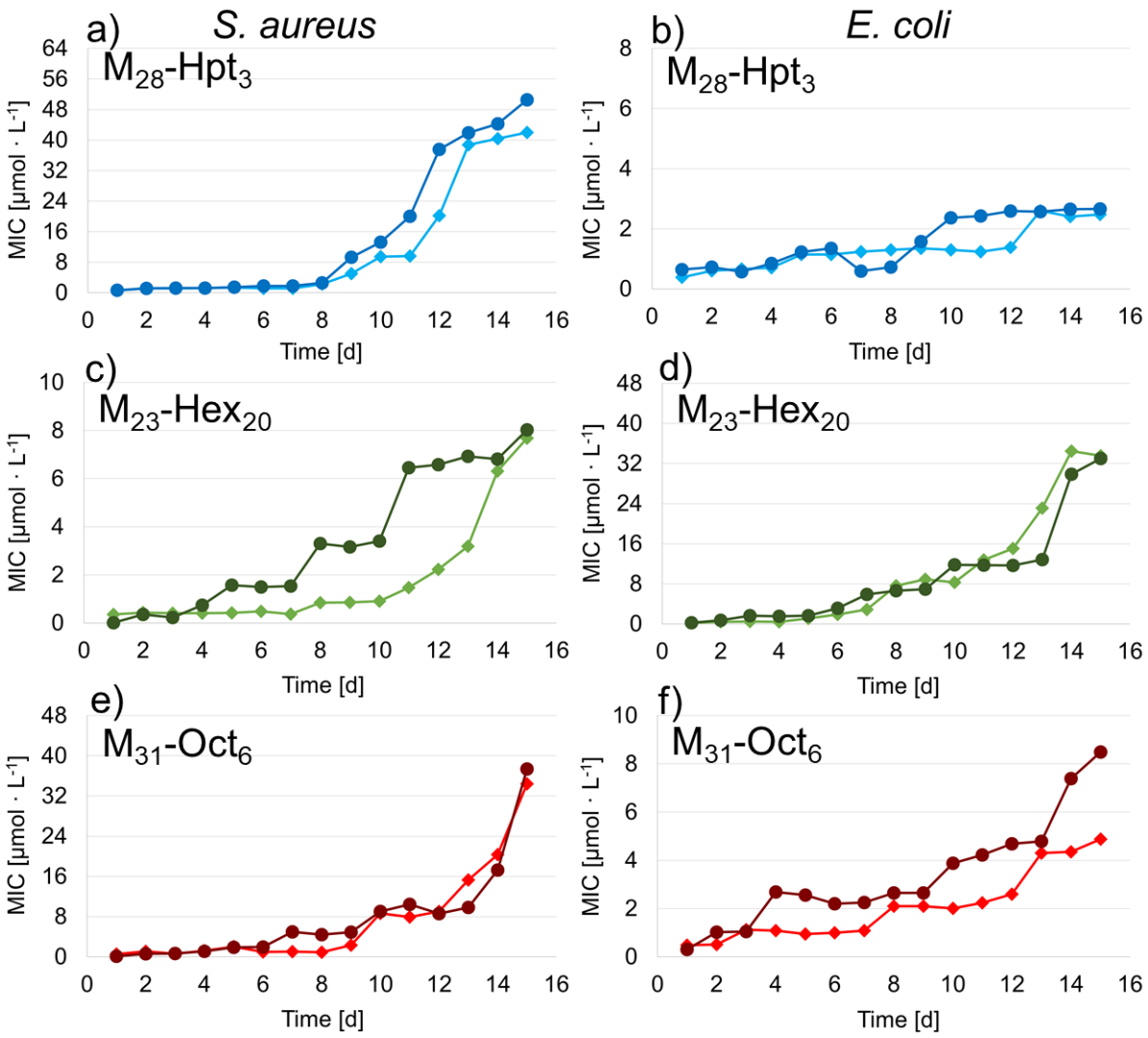

Supp. Fig. 9: *Resistance test for the compounds $PMOx_{23}$-b-$PHexOx_{20}$-EDA-xCIP (green, HHR = 1.15, M_{23}-Hex_{20}), $PMOx_{28}$-b-$PHeptOx_{3}$-EDA-xCIP (blue, HHR = 9.3, M_{28}-Hpt_{3}), $PMOx_{31}$-b-$POctOx_{6}$-EDA-xCIP (red, HHR = 5.2, M_{31}-Oct_{6}) for a), c), e) S. aureus and b), d), f) E. coli, respectively.*

Supp. Table 1: *Hemotoxicity of amphiphilic PACs and DTAC.*

samples	HC_{50} [$\mu g \cdot mL^{-1}$]	HC_{10} [$\mu g \cdot mL^{-1}$]	HC_{5} [$\mu g \cdot mL^{-1}$]
DTAC	564 ± 21	389 ± 35	336 ± 26
$PMOx_{25}$-*b*-$PBuOx_{5}$-EDA-xCIP	17481 ± 501	6248 ± 456	6248 ± 456
$PMOx_{15}$-*b*-$PBuOx_{15}$-EDA-xCIP	146 ± 86	19 ± 3	10 ± 3
$PMOx_{6}$-*b*-$PBuOx_{22}$-EDA-xCIP	-	-	-
$PMOx_{34}$-*b*-$PHexOx_{7}$-EDA-xCIP	200 ± 50	62 ± 22	49 ± 13
$PMOx_{23}$-*b*-$PHexOx_{20}$-EDA-xCIP	-	-	-
$PMOx_{7}$-*b*-$PHexOx_{21}$-EDA-xCIP	-	-	-
$PMOx_{19}$-*b*-$PHeptOx_{4}$-EDA-xCIP	362 ± 154	109 ± 56	75 ± 44
$PMOx_{28}$-*b*-$PHeptOx_{3}$-EDA-xCIP	640 ± 20	298 ± 28	259 ± 24
$PMOx_{34}$-*b*-$PHeptOx_{5}$-EDA-xCIP	641 ± 293	287 ± 184	222 ± 143
$PMOx_{38}$-*b*-$PHeptOx_{6}$-EDA-xCIP	833 ± 278	396 ± 120	294 ± 136
$PMOx_{16}$-*b*-$PHeptOx_{15}$-EDA-xCIP	-	-	-
$PMOx_{14}$-*b*-$PHeptOx_{24}$-EDA-xCIP	-	-	-
$PMOx_{31}$-*b*-$POctOx_{6}$-EDA-xCIP	512 ± 165	297 ± 14	213 ± 8
$PMOx_{21}$-*b*-$POctOx_{16}$-EDA-xCIP	-	-	-
$PMOx_{6}$-*b*-$POctOx_{29}$-EDA-xCIP	-	-	-
$PMOx_{26}$-*b*-$PNonOx_{5}$-EDA-xCIP	4962 ± 910	269 ± 58	189 ± 43
$PMOx_{18}$-*b*-$PNonOx_{18}$-EDA-xCIP	-	-	-
$PMOx_{7}$-*b*-$PNonOx_{26}$-EDA-xCIP	-	-	-

Supp. Table 2: *MIC values of amphiphilic PACs and CIP against Staphilococcus auruginosa, Escherichia coli, Klebsiella pneumoniae, Pseudomonas aeruginosa.*

	MIC [μmol · L^{-1}]			
samples	*S. aureus*	*E. coli*	*K. pneumoniae*	*P. aeruginosa*
CIP	1.29 ± 0.07	0.09 ± 0.01	0.60 ± 0.24	0.71 ± 0.21
xCIP	0.68 ± 0.38	0.17 ± 0.11	6.71 ± 0.11	10.75 ± 3.72
$PMOx_{30}$-EDA-xCIP	2.23 ± 0.21	5.34 ± 1.48	143.12 ± 6.04	105.61 ± 5.02
$PMOx_{25}$-*b*-$PBuOx_5$-EDA-xCIP	0.42 ± 0.02	1.15 ± 0.25	3.73 ± 0.01	19.69 ± 5.32
$PMOx_{15}$-*b*-$PBuOx_{15}$-EDA-xCIP	0.17 ± 0.01	0.36 ± 0.04	1.05 ± 0.28	4.77 ± 0.45
$PMOx_6$-*b*-$PBuOx_{22}$-EDA-xCIP	0.65 ± 0.04	2.25 ± 0.09	8.58 ± 2.51	17.92 ± 6.47
$PMOx_{34}$-*b*-$PHexOx_7$-EDA-xCIP	0.33 ± 0.11	0.48 ± 0.01	2.14 ± 0.34	5.79 ± 1.65
$PMOx_{23}$-*b*-$PHexOx_{20}$-EDA-xCIP	0.09 ± 0.004	0.39 ± 0.02	1.58 ± 0.04	8.91 ± 2.97
$PMOx_7$-*b*-$PHexOx_{21}$-EDA-xCIP	0.73 ± 0.18	1.51 ± 0.49	9.21 ± 1.37	23.13 ± 5.94
$PMOx_{19}$-*b*-$PHeptOx_4$-EDA-xCIP	0.06 ± 0.01	0.50 ± 0.03	5.87 ± 1.63	9.67 ± 2.37
$PMOx_{28}$-*b*-$PHeptOx_3$-EDA-xCIP	0.13 ± 0.02	0.61 ± 0.03	2.56 ± 0.06	14.04 ± 3.10
$PMOx_{34}$-*b*-$PHeptOx_5$-EDA-xCIP	0.29 ± 0.03			
$PMOx_{38}$-*b*-$PHeptOx_6$-EDA-xCIP	0.585 ± 0.003			
$PMOx_{16}$-*b*-$PHeptOx_{15}$-EDA-xCIP	0.34 ± 0.07	1.22 ± 0.01	3.07 ± 0.88	19.71 ± 1.31
$PMOx_{14}$-*b*-$PHeptOx_{24}$-EDA-xCIP	0.64 ± 0.22	1.63 ± 0.09	12.78 ± 0.29	8.33 ± 0.72
$PMOx_{31}$-*b*-$POctOx_6$-EDA-xCIP	0.25 ± 0.02	0.54 ± 0.08	2.14 ± 0.07	5.97 ± 1.72
$PMOx_{21}$-*b*-$POctOx_{16}$-EDA-xCIP	0.59 ± 0.19	0.94 ± 0.11	3.45 ± 0.12	7.07 ± 0.13
$PMOx_6$-*b*-$POctOx_{29}$-EDA-xCIP	3.29 ± 0.33	2.99 ± 0.25	6.66 ± 0.52	32.25 ± 10.36
$PMOx_{26}$-*b*-$PNonOx_5$-EDA-xCIP	0.46 ± 0.08	1.91 ± 0.40	5.34 ± 0.89	30.41 ± 13.06
$PMOx_{18}$-*b*-$PNonOx_{18}$-EDA-xCIP	0.22 ± 0.03	1.16 ± 0.31	2.00 ± 0.003	15.31 ± 0.67
$PMOx_7$-*b*-$PNonOx_{26}$-EDA-xCIP	0.38 ± 0.01	0.61 ± 0.21	3.71 ± 0.19	23.25 ± 2.20

Supp. Table 3: *Analytical data of amphiphilic PACs, characterize by ^{1}H NMR spectroscopy.*

PAC[a]	$M_{n,NMR}$ [g·mol^{-1}]	PDI	F^{d}_{NMR}[b]	HHR[c]	Term
PMOx$_{25}$-*b*-PBuOx$_{5}$-EDA-xCIP	3311	1.27	87%	5	M$_{25}$-Bu$_{5}$
PMOx$_{15}$-*b*-PBuOx$_{15}$-EDA-xCIP	3732	1.26	99%	1	M$_{15}$-Bu$_{15}$
PMOx$_{6}$-*b*-PBuOx$_{22}$-EDA-xCIP	3856	1.24	> 99%	0.3	M$_{6}$-Bu$_{22}$
PMOx$_{34}$-*b*-PHexOx$_{7}$-EDA-xCIP	4527	1.17	> 99%	5	M$_{34}$-Hex$_{7}$
PMOx$_{23}$-*b*-PHexOx$_{20}$-EDA-xCIP	5608	1.19	> 99%	1.2	M$_{23}$-Hex$_{20}$
PMOx$_{7}$-*b*-PHexOx$_{21}$-EDA-xCIP	4402	1.18	> 99%	0.3	M$_{7}$-Hex$_{21}$
PMOx$_{19}$-*b*-PHeptOx$_{4}$-EDA-xCIP	2840	1.15	> 99%	5	M$_{19}$-Hpt$_{4}$
PMOx$_{28}$-*b*-PHeptOx$_{3}$-EDA-xCIP	3437	1.18	92%	9	M$_{28}$-Hpt$_{3}$
PMOx$_{34}$-*b*-PHeptOx$_{5}$-EDA-xCIP	4286	1.26	77%	7	M$_{34}$-Hpt$_{5}$
PMOx$_{38}$-*b*-PHeptOx$_{6}$-EDA-xCIP	4880	1.27	95 %	6	M$_{38}$-Hpt$_{6}$
PMOx$_{16}$-*b*-PHeptOx$_{15}$-EDA-xCIP	4445	1.23	98%	1.1	M$_{16}$-Hpt$_{15}$
PMOx$_{14}$-*b*-PHeptOx$_{24}$-EDA-xCIP	5797	1.23	> 99%	0.6	M$_{14}$-Hpt$_{24}$
PMOx$_{31}$-*b*-PoctOx$_{6}$-EDA-xCIP	4285	1.29	> 99%	5	M$_{31}$-Oct$_{6}$
PMOx$_{21}$-*b*-POctOx$_{16}$-EDA-xCIP	5267	1.20	> 99%	1.3	M$_{21}$-Oct$_{16}$
PMOx$_{6}$-*b*-POctOx$_{29}$-EDA-xCIP	6373	1.17	> 99%	0.2	M$_{6}$-Oct$_{29}$
PMOx$_{26}$-*b*-PNonOx$_{5}$-EDA-xCIP	3746	1.22	94%	5	M$_{26}$-Non$_{5}$
PMOx$_{18}$-*b*-PNonOx$_{18}$-EDA-xCIP	5630	1.28	96%	1	M$_{18}$-Non$_{18}$
PMOx$_{7}$-*b*-PNonOx$_{26}$-EDA-xCIP	6273	1.29	90%	0.3	M$_{7}$-Non$_{26}$

[a]Degree of polymerization determined by ^{1}H NMR spectroscopy via comparison of the respective signals caused by the initiating group and the signals caused by the protons of the polymer backbone.
[b]Degree of functionalization determined by ^{1}H NMR spectroscopy via comparison of the respective signals caused by the initiating and the terminal CIP groups.
[c]The ratio of the hydrophilic and the hydrophobic repeating units of the polymer.

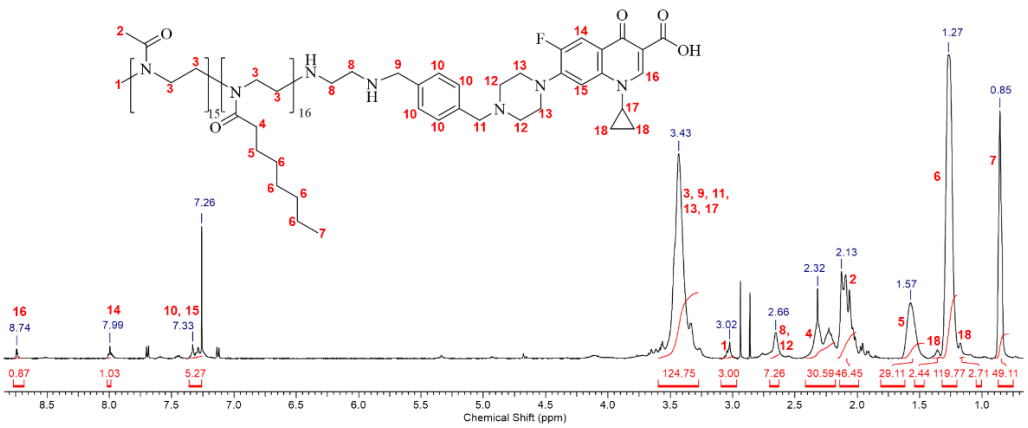

Supp. Fig. 10: *^{1}H NMR spectrum of Me-PMOx$_{15}$-b-PHeptOx$_{16}$-EDA-xCIP.*

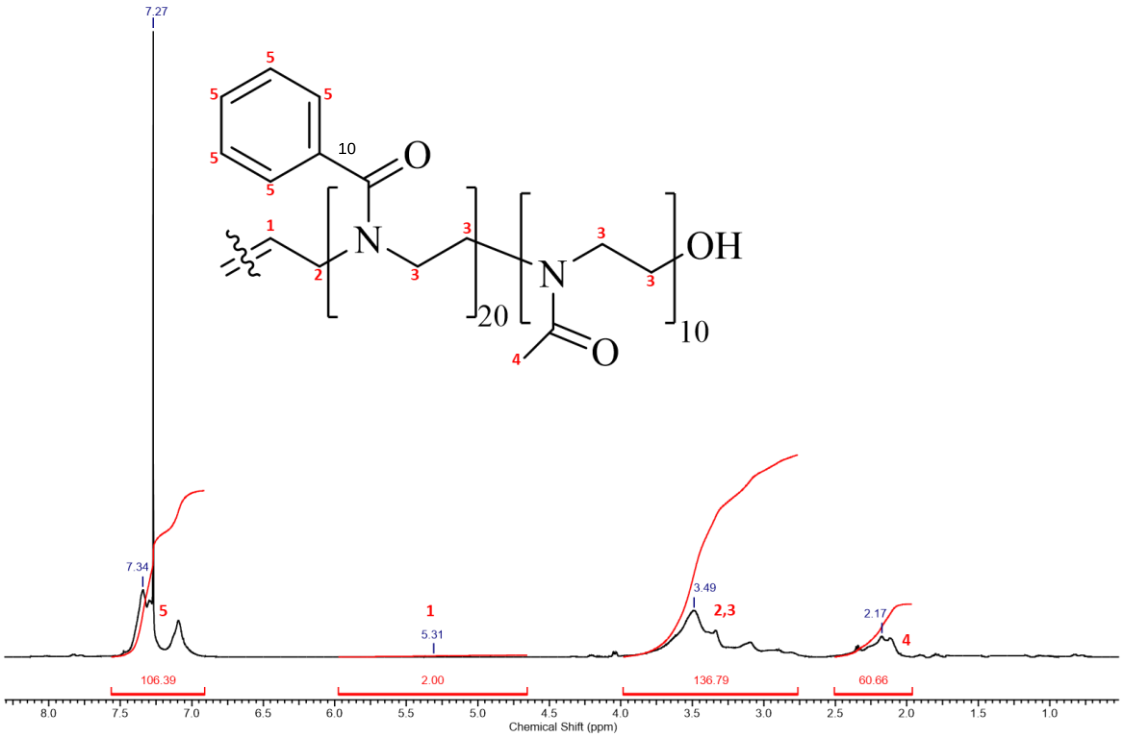

Supp. Fig. 11: *^{1}H NMR spectrum of hydrolysed HO-PMOx$_{10}$-b-PPhOx$_{20}$-b-PMOx$_{10}$-OH.*

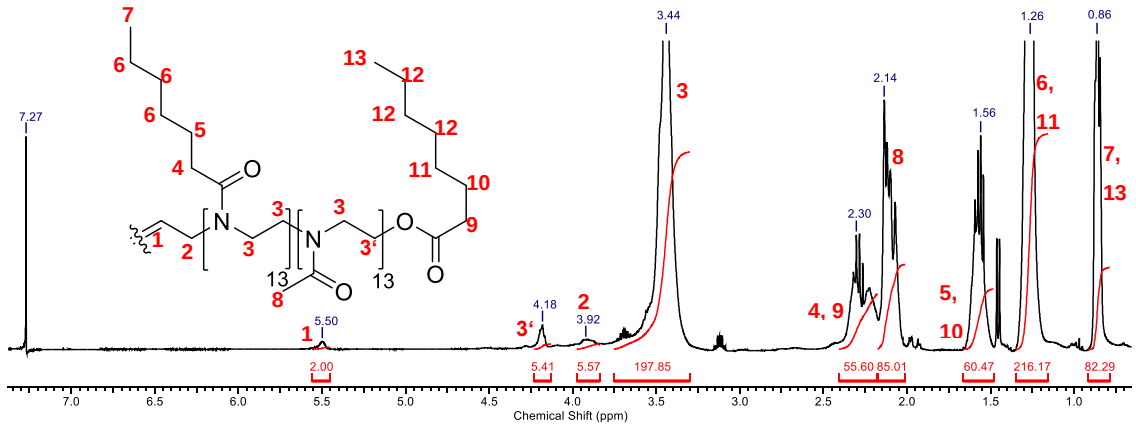

Supp. Fig. 12: *^{1}H NMR spectrum of C$_8$-PMOx$_{13}$-b-PHeptOx$_{26}$-b-PMOx$_{13}$-C$_8$.*

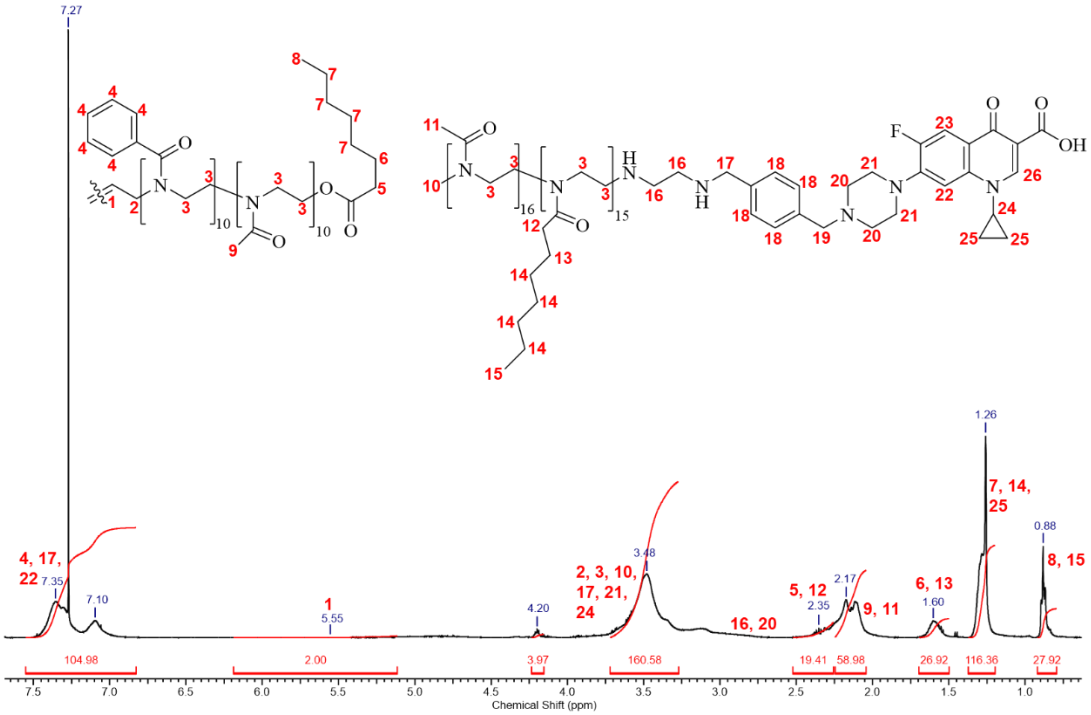

Supp. Fig. 13: *^{1}H NMR spectrum of the ABA triblock copolymer C_8-PMOx$_{10}$-b-PPhOx$_{20}$-b-PMOx$_{10}$-C_8 and the PAC Me-PMOx$_{15}$-b-PHeptOx$_{16}$-EDA-xCIP.*

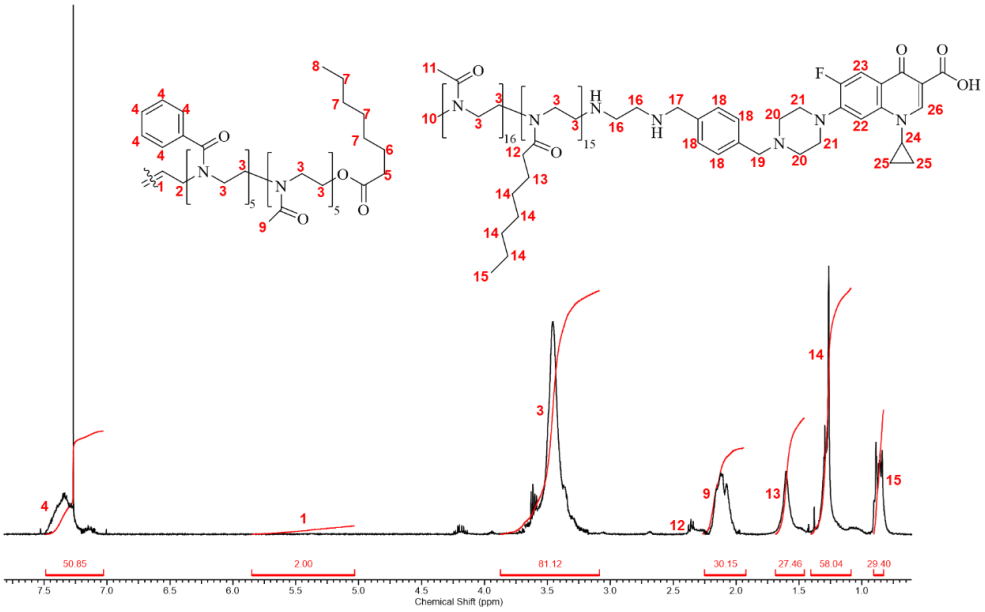

Supp. Fig. 14: *^{1}H NMR spectrum of the ABA triblock copolymer C_8-PMOx$_5$-b-PPhOx$_9$-b-PMOx$_5$-C_8 and the PAC Me-PMOx$_{15}$-b-PHeptOx$_{16}$-EDA-xCIP.*

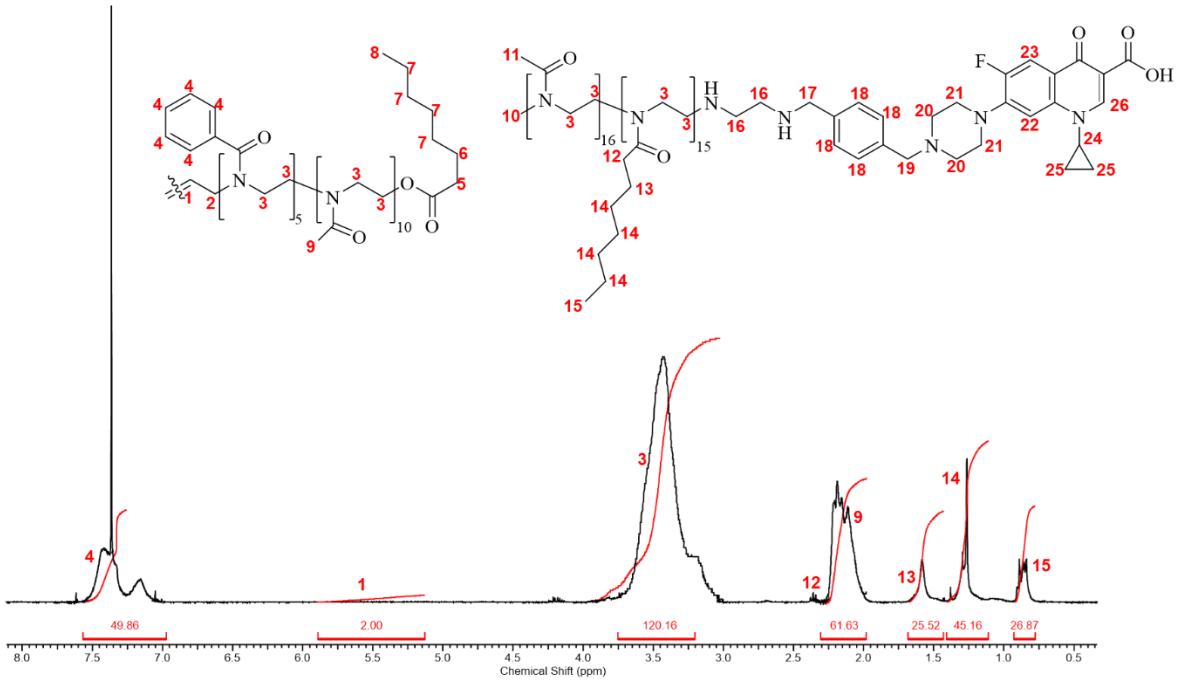

Supp. Fig. 15: *^{1}H NMR spectrum of the ABA triblock copolymer C_8-PMOx$_{10}$-b-PPhOx$_{10}$-b-PMOx$_{10}$-C_8 and the PAC Me-PMOx$_{15}$-b-PHeptOx$_{16}$-EDA-xCIP.*

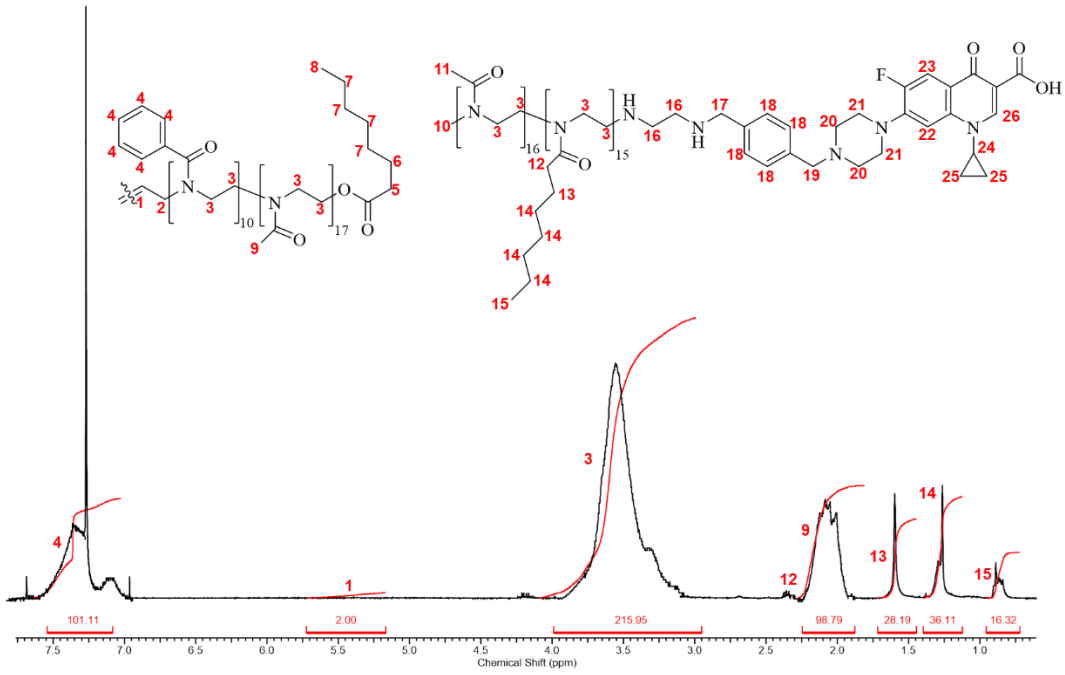

Supp. Fig. 16: ^{1}H NMR spectrum of the ABA triblock copolymer C_8-PMOx$_{17}$-*b*-PPhOx$_{20}$-b-PMOx$_{17}$-C_8 and the PAC Me-PMOx$_{15}$-*b*-PHeptOx$_{16}$-EDA-xCIP.

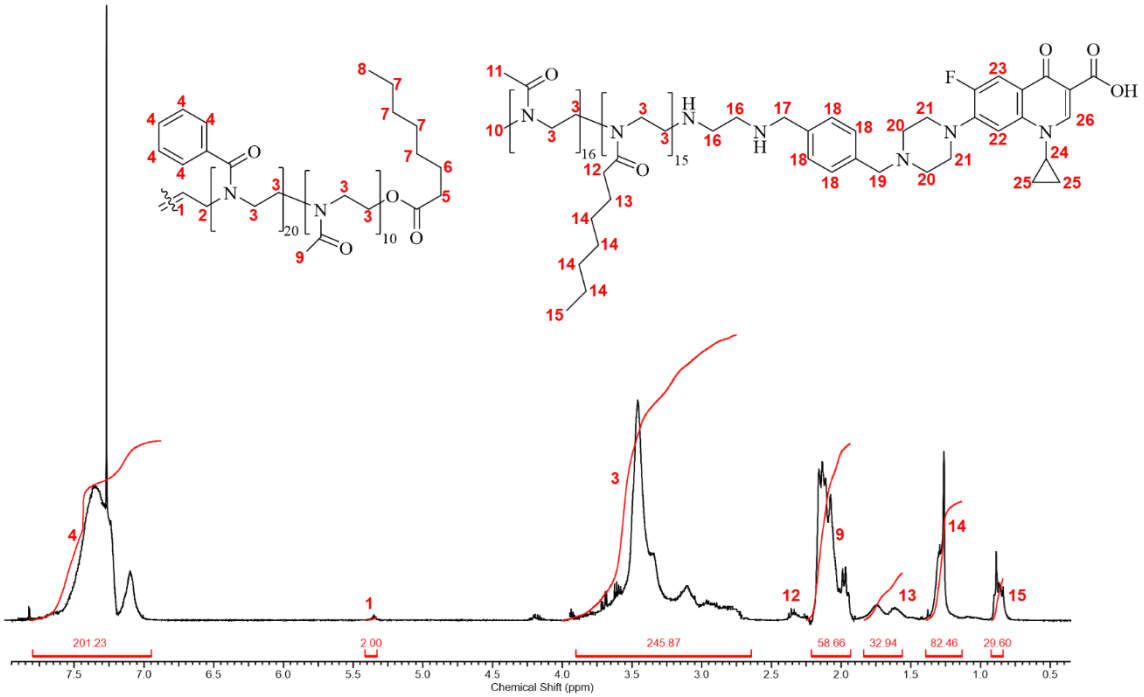

Supp. Fig. 17: *^{1}H NMR spectrum of the ABA triblock copolymer C_8-PMOx$_{10}$-b-PPhOx$_{40}$-b-PMOx$_{10}$-C_8 and the PAC Me-PMOx$_{15}$-b-PHeptOx$_{16}$-EDA-xCIP.*

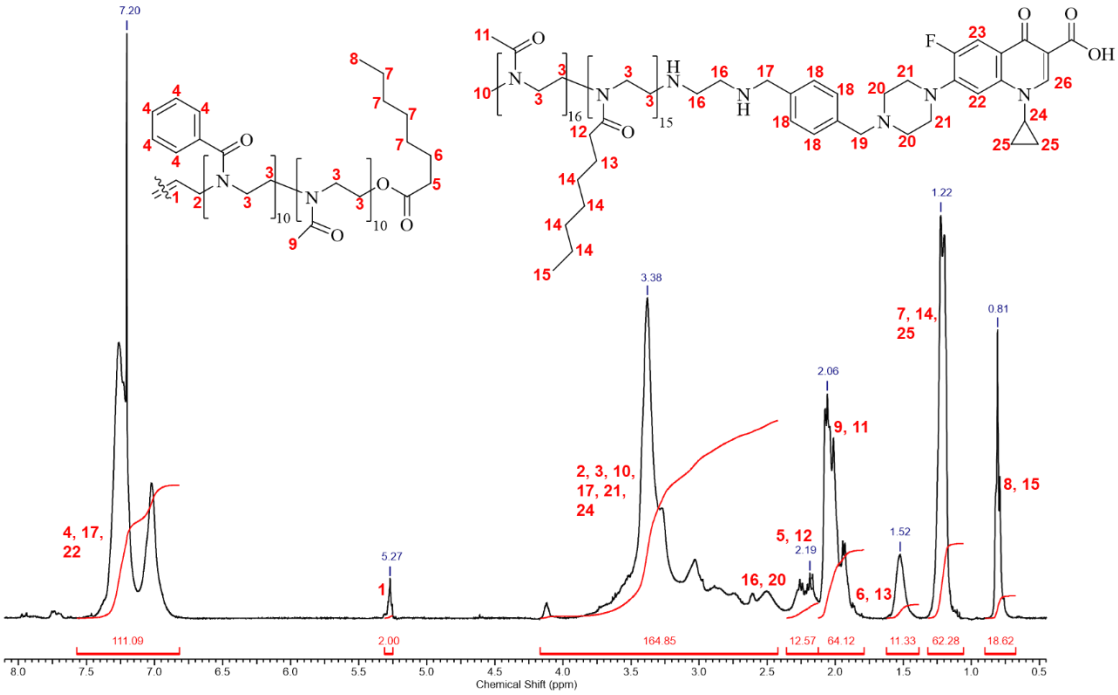

Supp. Fig. 18: *^{1}H NMR spectrum of the ABA triblock copolymer C_8-PMOx$_{10}$-b-PPhOx$_{20}$-b-PMOx$_{10}$-C_8 and the PAC Me-PMOx$_{15}$-b-PHeptOx$_{16}$-EDA-xCIP (2:1 mol/mol).*

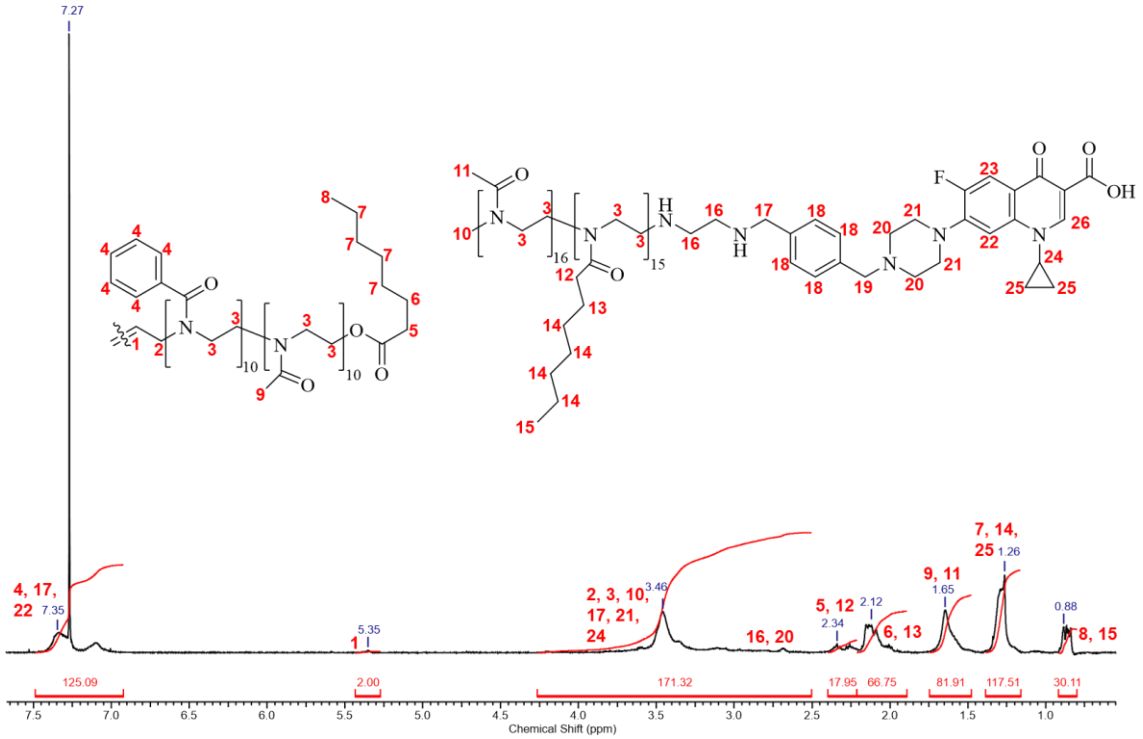

Supp. Fig. 19: *^{1}H NMR spectrum of the ABA triblock copolymer C_8-PMOx$_{10}$-b-PPhOx$_{20}$-b-PMOx$_{10}$-C_8 and the PAC Me-PMOx$_{15}$-b-PHeptOx$_{16}$-EDA-xCIP (1:2 mol/mol).*

Supp. Table 4: *Analytical data of triblock copolymers, characterized by ^{1}H NMR spectroscopy.*

Polymer	$M_{n,NMR}$[a] [g·mol^{-1}]	F^d_{NMR}[b]	Đ[c]
Me-PMOx$_{30}$-EDA-xCIP	3100	96%	1.04
Me-PMOx$_{22}$-*b*-PHeptOx$_8$-EDA-xCIP	3800	98%	1.12
Me-PMOx$_{15}$-*b*-PHeptOx$_{16}$-EDA-xCIP	4500	99%	1.18
C_8-PMOx$_5$-*b*-PPhOx$_9$-*b*-PMOx$_5$-C_8	2700	96%	1.15
C_8-PMOx$_{10}$-*b*-PPhOx$_{10}$-*b*-PMOx$_{10}$-C_8	3500	99%	1.22
C_8-PMOx$_{10}$-*b*-PPhOx$_{20}$-*b*-PMOx$_{10}$-C_8	4500	99%	1.21
C_8-PMOx$_{17}$-*b*-PPhOx$_{20}$-*b*-PMOx$_{17}$-C_8	5700	98%	1.20
C_8-PMOx$_{10}$-*b*-PPhOx$_{40}$-*b*-PMOx$_{10}$-C_8	7900	96%	1.19
C_8-PMOx$_{13}$-*b*-PHeptOx$_{26}$-*b*-PMOx$_{13}$-C_8	5900	99%	1.17

[a] mol% of Me-PMOx$_{15}$-*b*-PHeptOx$_{16}$-EDA-xCIP in the isolated aggregate.
[b] Degree of functionalization determined by ^{1}H NMR spectroscopy via comparison of the respective signals caused by the initiating group *trans*-1,4-dibrom-2-buten and the terminal acid group.
[c] The dispersity was calculated from the GPC: Đ = Mw/Mn.

Supp. Table 5: *MIC values of ABA triblock copolymers and CIP/PAC against Staphylococcus aureus. Values in table S2 are expressed as mean ± SD (n = 3–4).*

samples	MIC [$\mu g \cdot mL^{-1}$]		
	released (calculated)[a]	hydrolysed	encapsulated
$PMOx_{15}$-b-$PHeptOx_{16}$-EDA-xCIP	1.5 ± 0.1		
C_8-$PMOx_{10}$-*b*-$PPhOx_{20}$-*b*-$PPhOx_{10}$-C_8			
Me-$PMOx_{22}$-*b*-$PHeptOx_8$-EDA-xCIP	1.7 ± 0.4	4.2 ± 1	176 ± 16
Me-$PMOx_{15}$-*b*-$PHeptOx_{16}$-EDA-xCIP	1.6 ± 0.3	3.9 ± 0.8	527 ± 25
C_8-$PMOx_5$-*b*-$PPhOx_9$-*b*-$PMOx_5$-C_8			
Me-$PMOx_{15}$-*b*-$PHeptOx_{16}$-EDA-xCIP	1.4 ± 0.4	3.8 ± 1	6 ± 2
C_8-$PMOx_{10}$-*b*-$PPhOx_{10}$-*b*-$PMOx_{10}$-C_8			
Me-$PMOx_{15}$-*b*-$PHeptOx_{16}$-EDA-xCIP	1.4 ± 0.3	3.4 ± 0.8	16 ± 3
C_8-$PMOx_{17}$-*b*-$PPhOx_{20}$-*b*-$PMOx_{17}$-C_8			
Me-$PMOx_{15}$-*b*-$PHeptOx_{16}$-EDA-xCIP	1.9 ± 0.5	7.3 ± 1	102 ± 19
C_8-$PMOx_{10}$-*b*-$PPhOx_{40}$-*b*-$PMOx_{10}$-C_8			
Me-$PMOx_{15}$-*b*-$PHeptOx_{16}$-EDA-xCIP	1.3 ± 0.3	3.6 ± 0.8	88 ± 13

[a] MIC(calculated) = MIC(hydrolysed aggregate)·(mass conjugate)/(mass aggregate) (determined by ^{1}H NMR).

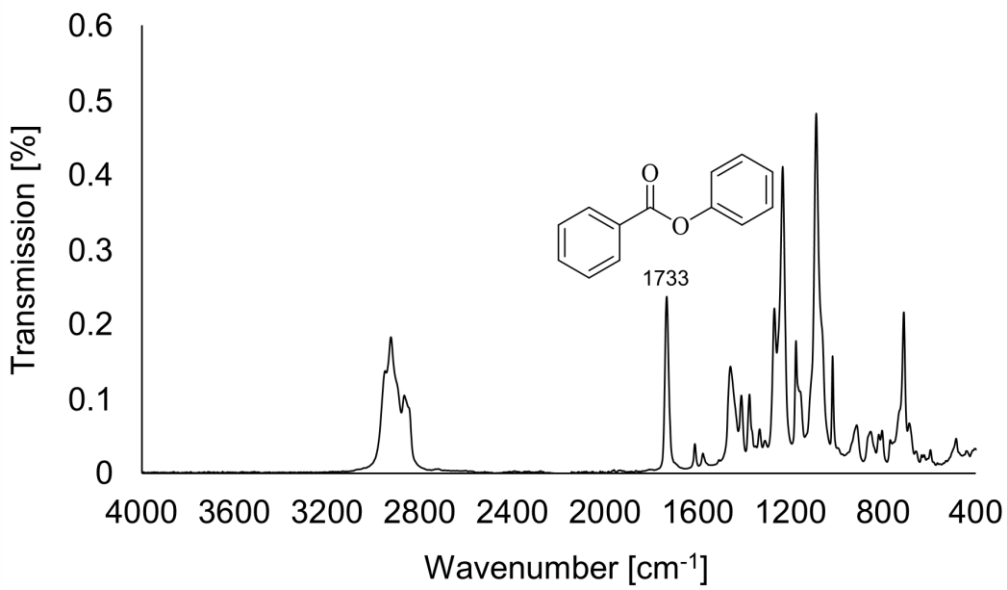

Supp. Fig. 20: *FT-IR of vitamine E 4-(bromomethyl)benzoate (VitE-BMB).*

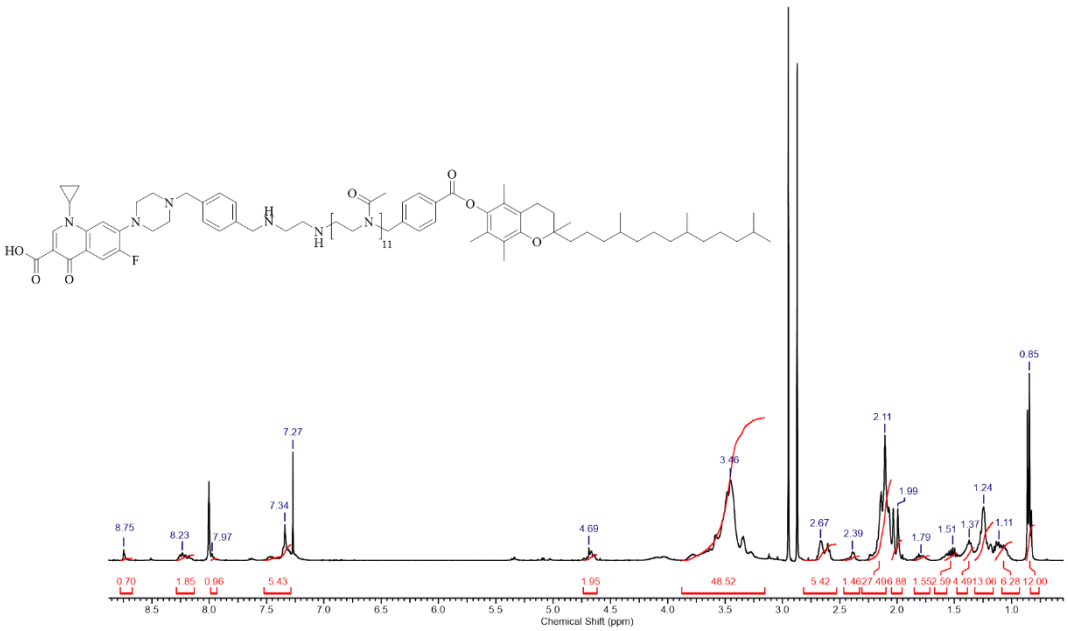

Supp. Fig. 21: *^{1}H-NMR spectrum of VitE-BMB-PMOx$_{11}$-EDA-xCIP.*

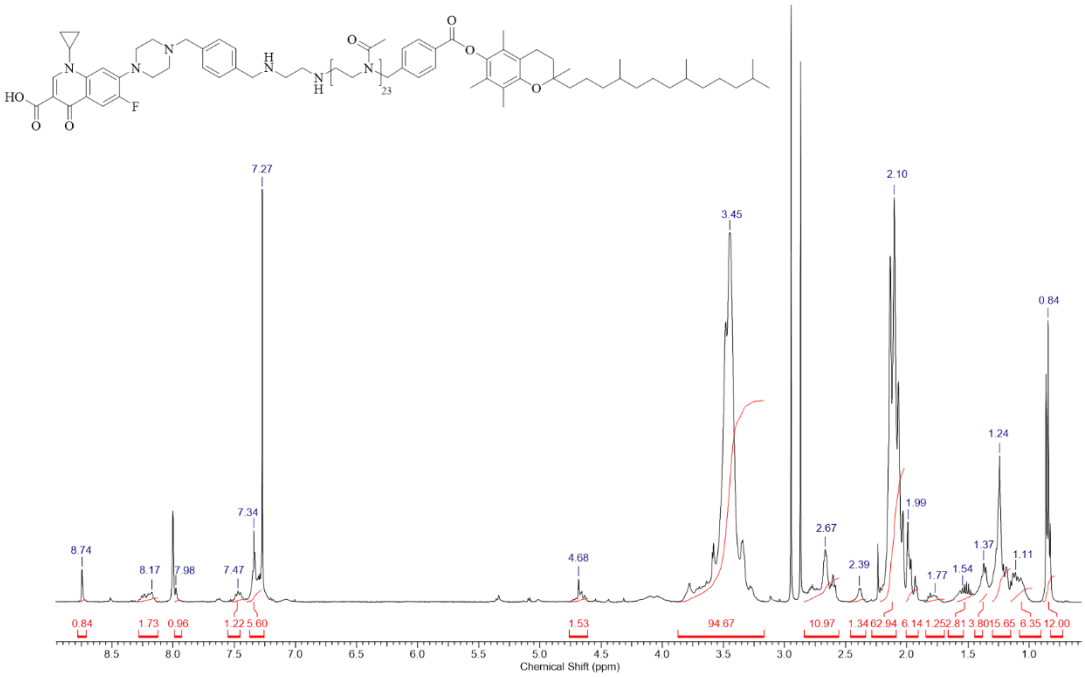

Supp. Fig. 22: *^{1}H-NMR spectrum of VitE-BMB-PMOx$_{23}$-EDA-xCIP.*

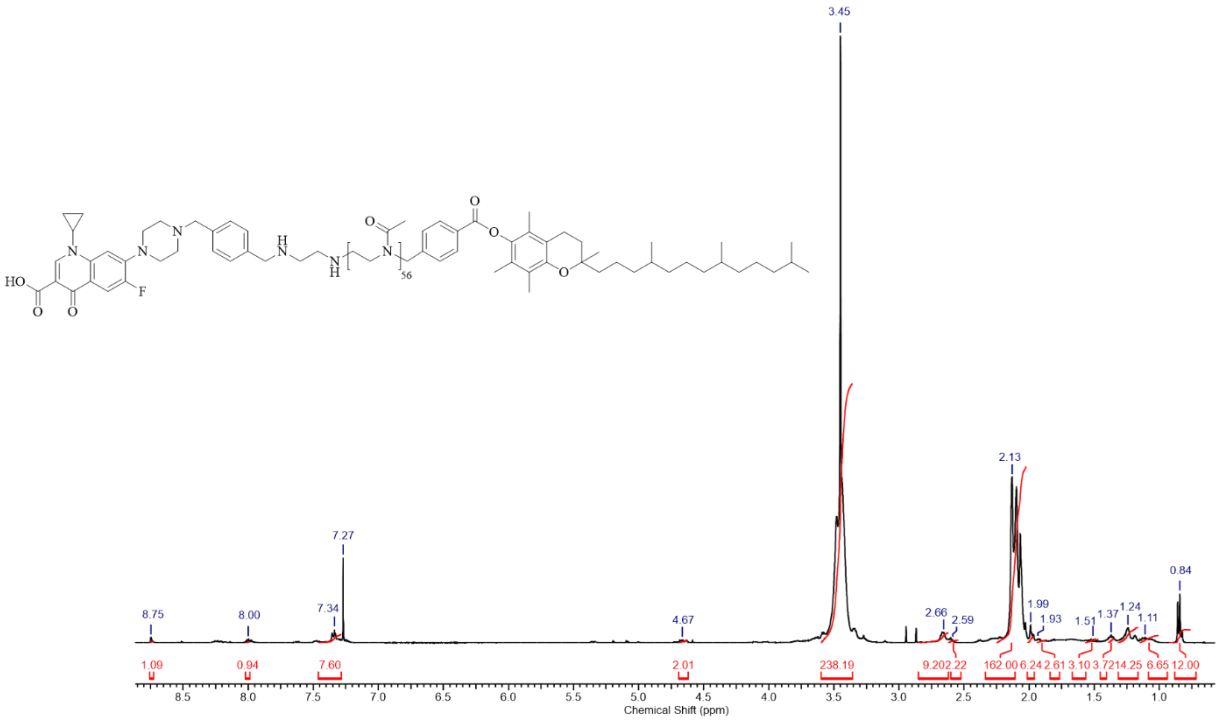

Supp. Fig. 23: *^{1}H-NMR spectrum of VitE-BMB-PMOx$_{56}$-EDA-xCIP.*

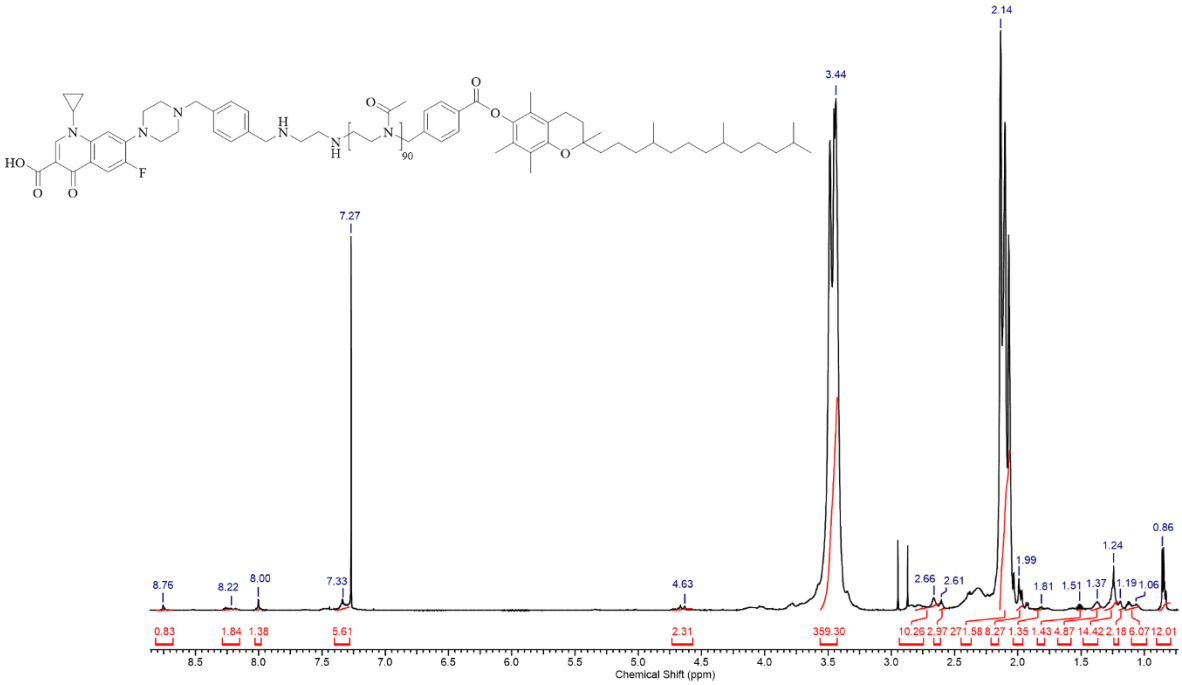

Supp. Fig. 24: *^{1}H-NMR spectrum of VitE-BMB-PMOx$_{90}$-EDA-xCIP.*

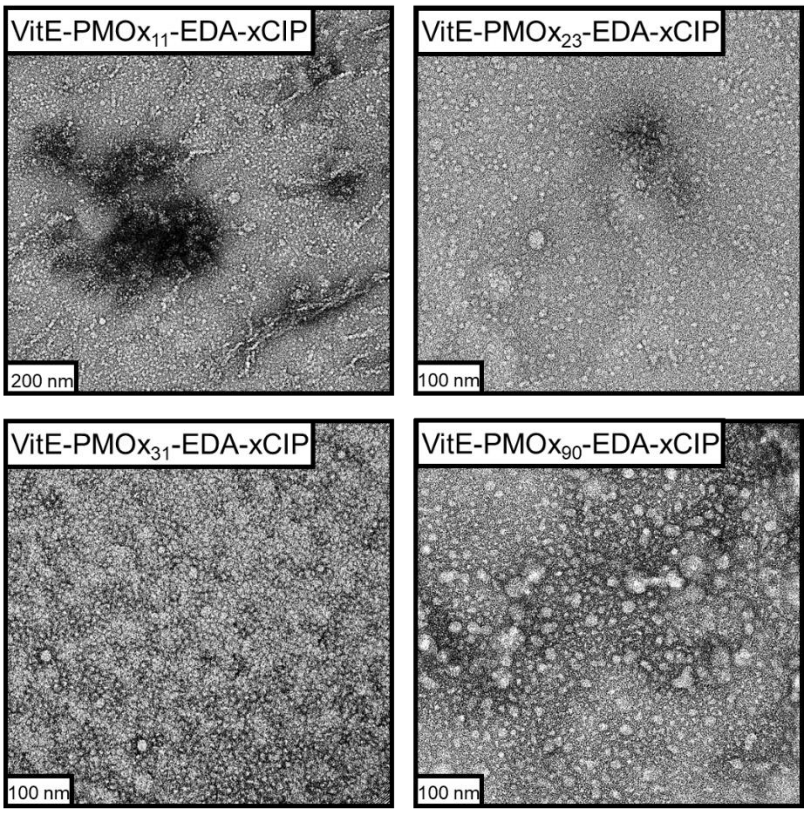

Supp. Fig. 25: *Transmission electron microscopy (TEM) images of the block copolymers VitE-PMOx11-EDA-xCIP, VitE-PMOx23-EDA-xCIP, VitE-PMOx31-EDA-xCIP and VitE-PMOx90-EDA-xCIP.*

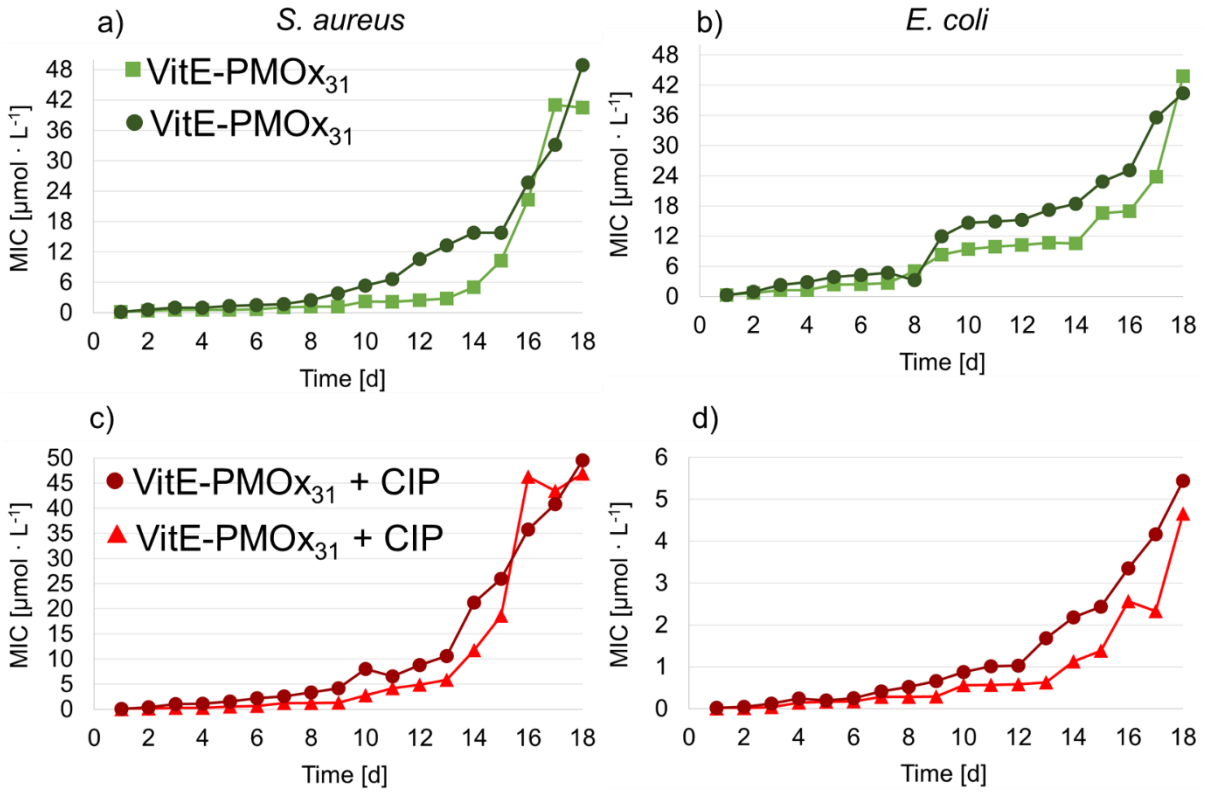

Supp. Fig. 26: *Resistance test for the compounds VitE-BMB-PMOx$_{31}$-EDA-xCIP (green) and VitE-BMB-PMOx$_{31}$-EDA-xCIP with unbound CIP (red) for a), c) S. aureus and b), d) E. coli, respectively.*

Supp. Table 6: *MIC values in [µmol · L^{-1}] of amphiphilic VitE-PACs and CIP against Staphilococcus auruginosa, Escherichia coli, Klebsiella pneumoniae, Pseudomonas aeruginosa. Values are expressed as mean ± SD (n = 3).*

	MIC [μmol · L^{-1}]			
samples	*S. aureus*	*E. coli*	*K. pneumoniae*	*P. aeruginosa*
CIP	1.3 ± 0.1	0.1 ± 0.01	0.6 ± 0.2	0.7 ± 0.2
xCIP	0.7 ± 0.4	0.2 ± 0.1	6.7 ± 0.1	10 ± 4
Me-PMOx_{30}-EDA-xCIP	2.2 ± 0.2	5.3 ± 1.5	143 ± 6.	106 ± 5
VitE-BMB-PMOx_{11}-EDA-xCIP	0.2 ± 0.04	0.4 ± 0.1	1.1 ± 0.1	3.7 ± 1
VitE-BMB-PMOx_{23}-EDA-xCIP	0.4 ± 0.03	0.6 ± 0.1	1.7 ± 0.1	4.6 ± 0.6
VitE-BMB-PMOx_{31}-EDA-xCIP	0.2 ± 0.04	0.3 ± 0.02	0.8 ± 0.2	3.4 ± 0.8
VitE-BMB-PMOx_{56}-EDA-xCIP	0.6 ± 0.1	1.1 ± 0.2	1.9 ± 0.05	8.1 ± 0.3
VitE-BMB-PMOx_{90}-EDA-xCIP	1.2 ± 0.1	1.6 ± 0.3	7.1 ± 2.9	14 ± 2.3

Supp. Table 7: *MIC values in [µg · mL^{-1}] of amphiphilic VitE-PACs and CIP against Staphilococcus auruginosa, Escherichia coli, Klebsiella pneumoniae, Pseudomonas aeruginosa. Values are expressed as mean ± SD (n = 3).*

	MIC [μg · mL^{-1}]			
samples	*S. aureus*	*E. coli*	*K. pneumoniae*	*P. aeruginosa*
CIP	0.4 ± 0.02	0.03 ± 0.01	0.2 ± 0.08	0.2 ± 0.07
xCIP	0.3 ± 0.2	0.08 ± 0.05	3.7 ± 0.05	5.1 ± 1.8
Me-PMOx_{30}-EDA-xCIP	6.9 ± 0.7	17 ± 4.5	444 ± 19	328 ± 13.8
VitE-BMB-PMOx_{11}-EDA-xCIP	0.4 ± 0.1	0.8 ± 0.2	2.4 ± 0.3	7.7 ± 2.1
VitE-BMB-PMOx_{23}-EDA-xCIP	1.2 ± 0.1	1.7 ± 0.3	5.4 ± 0.3	14 ± 1.9
VitE-BMB-PMOx_{31}-EDA-xCIP	0.6 ± 0.2	1.2 ± 0.1	3 ± 0.7	13 ± 3
VitE-BMB-PMOx_{56}-EDA-xCIP	3.8 ± 0.5	6.6 ± 0.9	11 ± 0.3	48 ± 2
VitE-BMB-PMOx_{90}-EDA-xCIP	10 ± 1.2	14 ± 2.4	63 ± 25	122 ± 20